



Letter Report
TLR-RES/DE/CIB-CMB-2021-03

***TECHNICAL ASSESSMENT OF MATERIALS COMPATIBILITY IN
MOLTEN SALT REACTORS***

March 2021

PREPARED FOR:

**U.S. Nuclear Regulatory Commission
TASK ORDER NO. 3131002N0007 (Task 1)**

PREPARED BY:

Oak Ridge National Laboratory
Stephen S. Raiman
Dino Sulejmanovic
J. Matthew Kurley
JoJo Lee
Cory G. Parker
Bruce A. Pint

PROGRAM MANAGERS:

**Office of Nuclear Regulatory Research
U.S. Nuclear Regulatory Commission**
B. Harris
R. Iyengar

DISCLAIMER

This report was prepared as an account of work sponsored by an agency of the U.S. Government. Neither the U.S. Government nor any agency thereof, nor any employee, makes any warranty, expressed or implied, or assumes any legal liability or responsibility for any third party's use, or the results of such use, of any information, apparatus, product, or process disclosed in this publication, or represents that its use by such third party complies with applicable law.

This report does not contain or imply legally binding requirements. Nor does this report establish or modify any regulatory guidance or positions of the U.S. Nuclear Regulatory Commission and is not binding on the Commission.

DOCUMENT AVAILABILITY

Reports produced after January 1, 1996, are generally available free via US Department of Energy (DOE) SciTech Connect.

Website www.osti.gov

Reports produced before January 1, 1996, may be purchased by members of the public from the following source:

National Technical Information Service
5285 Port Royal Road
Springfield, VA 22161
Telephone 703-605-6000 (1-800-553-6847)
TDD 703-487-4639
Fax 703-605-6900
E-mail info@ntis.gov
Website <http://classic.ntis.gov/>

Reports are available to DOE employees, DOE contractors, Energy Technology Data Exchange representatives, and International Nuclear Information System representatives from the following source:

Office of Scientific and Technical Information
PO Box 62
Oak Ridge, TN 37831
Telephone 865-576-8401
Fax 865-576-5728
E-mail reports@osti.gov
Website <http://www.osti.gov/contact.html>

This report was prepared as an account of work sponsored by an agency of the United States Government. Neither the United States Government nor any agency thereof, nor any of their employees, makes any warranty, express or implied, or assumes any legal liability or responsibility for the accuracy, completeness, or usefulness of any information, apparatus, product, or process disclosed, or represents that its use would not infringe privately owned rights. Reference herein to any specific commercial product, process, or service by trade name, trademark, manufacturer, or otherwise, does not necessarily constitute or imply its endorsement, recommendation, or favoring by the United States Government or any agency thereof. The views and opinions of authors expressed herein do not necessarily state or reflect those of the United States Government or any agency thereof.

Materials Science and Technology Division

**TECHNICAL ASSESSMENT OF MATERIALS COMPATIBILITY IN MOLTEN SALT
REACTORS**

Stephen S. Raiman
Dino Sulejmanovic
J. Matthew Kurley
Jo Jo Lee
Cory Parker
Bruce A. Pint

March 2021

Prepared by
OAK RIDGE NATIONAL LABORATORY
Oak Ridge, TN 37831-6283
managed by
UT-BATTELLE, LLC
for the
US DEPARTMENT OF ENERGY
under contract DE-AC05-00OR22725

CONTENTS

LIST OF FIGURES	v
LIST OF TABLES	vii
LIST OF ABBREVIATIONS	ix
EXECUTIVE SUMMARY	xi
1. INTRODUCTION	1
2. BASICS OF CORROSION IN MSRs	1
2.1 THERMODYNAMICS	1
2.1.1 Molten Salt Stability and Redox Potential	2
2.1.2 Reaction of Salts with Multiple Oxidation States Such as Fuels	5
2.2 IMPURITY DRIVEN CORROSION	5
2.3 REDOX CONTROL	7
2.4 NON-REACTING IMPURITIES AND THEIR EFFECT ON EQUILIBRIA	8
2.5 AIR-SIDE OXIDATION	8
2.6 KNOWLEDGE GAPS	8
2.6.1 Behavior and effectiveness of redox control additives	8
2.6.2 Effects of specific impurities	9
2.6.3 Dissimilar material interactions	9
3. EXPERIMENTAL TECHNIQUES	10
3.1 STATIC TESTING	10
3.1.1 Crucible testing	10
3.1.2 Capsule testing	13
3.2 FLOWING SALT TESTING	16
3.2.1 Thermal convection loops	16
3.2.2 Forced convection loops	18
3.3 ELECTROCHEMICAL MEASUREMENTS	18
3.4 KNOWLEDGE GAPS	20
3.4.1 Lack of standardized corrosion tests	20
3.4.2 Lack of recent data in flowing salts	20
3.4.3 Corrosion sensors	20
4. SALT CHEMISTRY AND PHYSICAL PROPERTIES	21
4.1 INTRODUCTION	21
4.2 SELECTION OF CANDIDATE COOLANTS IN MSR APPLICATIONS	21
4.3 HALIDE SALTS PROPERTIES	22
4.4 ACID-BASE CHEMISTRY	24
4.5 IMPURITIES IN MOLTEN SALTS	25
4.6 KNOWLEDGE GAPS	25
4.6.1 Lack of understanding of salt purity	25
4.6.2 Lack of reliable quantification of impurities	25
5. SALT PREPARATION AND PURIFICATION	25
5.1 INTRODUCTION	25
5.2 IMPURITIES IN MOLTEN SALTS	26
5.3 ANALYSIS AND QUANTIFICATION OF IMPURITIES IN MOLTEN SALTS	26
5.3.1 Chemical fluorination for purification of fluoride salts	28
5.3.2 Chemical dehydration for removal of moisture	29
5.4 TECHNICAL GAP ANALYSIS	30
5.4.1 Standards for salt purity at delivery	30
5.4.2 Quantifying impurities in molten salts	31

6.	CORROSION AND MECHANICAL PROPERTIES.....	31
6.1	INTRODUCTION	31
6.2	TELLURIUM EMBRITTLEMENT	31
6.3	ENVIRONMENTALLY ASSISTED CRACKING	33
6.4	POST-CORROSION MECHANICAL TESTING AND MICROSTRUCTURE ANALYSIS.....	34
6.5	CONCLUSIONS.....	34
6.6	KNOWLEDGE GAPS	34
6.6.1	Effects of Te embrittlement	34
6.6.2	Environmentally assisted cracking.....	34
7.	RADIATION EFFECTS.....	34
7.1	OTHER FISSION PRODUCT EFFECTS	37
7.1.1	Knowledge gaps.....	38
8.	GRAPHITE & NON-METALS.....	38
8.1	GRAPHITE CORROSION IN MOLTEN SALT REACTORS (STRUCTURAL GRAPHITE ONLY)	41
8.2	SALT AND GAS PERMEATION OF POROUS GRAPHITE.....	41
8.3	INFILTRATION MITIGATION STRATEGIES	44
8.4	METALLIC ALLOY-GRAPHITE COMPATIBILITY	45
8.5	TRITIUM, FISSION PRODUCTS REACTIVITIES AND OTHER IMPURITIES.....	46
8.6	FLUORINATION.....	47
8.7	RADIATION EFFECTS IN GRAPHITE.....	47
8.8	SIC _F /SIC AND C/C COMPOSITES FOR CORE STRUCTURAL COMPONENTS OF FHR.....	48
8.9	C/C COMPOSITES	50
8.10	KNOWLEDGE GAPS	51
8.10.1	Salt penetration of medium and large grained graphite grades.....	51
8.10.2	Effects of graphite on metal corrosion and vice versa	51
8.10.3	Degradation of structural SiC/SiC and C/C composites	51
9.	CONCLUSIONS	51
9.1	KNOWLEDGE GAPS.....	51
9.1.1	Standards for molten salt corrosion experiments.....	51
9.1.2	Effect of salt impurities and fission products.....	52
9.1.3	Effectiveness of redox control additives.....	53
9.1.4	Graphite compatibility and infiltration	53
9.1.5	Corrosion sensors.....	53
9.1.6	SiC and ceramic components.....	54
9.1.7	Irradiation-corrosion	54
9.1.8	Chloride Salts.....	54
10.	REFERENCES	54

LIST OF FIGURES

Figure 1. Ellingham diagrams of (a) fluoride and (b) chloride species.....	3
Figure 2. (a) Ellingham diagram depicting common fuel salts used in F based chemistries. (b) Ellingham diagram depicting common fuel salts used in Cl based chemistries.	5
Figure 3. Fission-product average valency for $^{239}\text{PuCl}_3$ irradiated with 2-MeV neutrons. Rare gases retained in system.....	7
Figure 4. Schematic of the potentiodynamic experiments used by Vignarooban et al.	11
Figure 5. Calculated corrosion rates from potentiodynamic experiments run by Vignarooban et al.....	12
Figure 6. Measured corrosion rates from immersion experiments run by Vignarooban et al.....	13
Figure 7. Capsule testing apparatus at ORNL.....	14
Figure 8. (Top) Weight loss per area of the alloys tested in graphite capsules by Olson et al at 850°C for 500h.....	14
Figure 9. Light micrograph showing cross-sectional attack of alloy 230 exposed to chloride salt 800°C for 92h in either a Ni or Mo capsule.....	15
Figure 10. SEM and EDS images of alloy 230 exposed in chloride salt at 800°C for 100h, showing O and Na content in the pores of the corrosion area.	15
Figure 11. Schematic drawing of a thermal convection loop used for corrosion studies in molten fluoride at Oak Ridge National Laboratory.	17
Figure 12. Corrosion of Inconel 600 in a thermal convection loop with uranium containing FLiNaK salt at a temperature of 815°C in the hot leg.	18
Figure 13. Schematic of apparatus for potentiodynamic measurements in molten salts, developed at ORNL [Rosenthal 1969].	19
Figure 14. Comparison of free energies of formation between various fluoride and chloride salts including common structural alloy metal fluorides and chlorides.	23
Figure 15. Thermodynamics comparison of HF vs. NF_3 as fluorinating agents for common oxide impurities in fluoride salts.	29
Figure 16. Cracking behavior of Alloy-N exposed 260 hr at 700°C to MSBR Fuel Salt Containing CrTe1.266.	32
Figure 17. Phase diagram at 953 K in the system Zr–Te–F–O with lines from the diagrams for Ni–Te–F–O and Mo–Te–F–O made using Outotec HSC Chemistry v5.1.	33
Figure 18. Drawing of a thermal convection loop that was operated in the ORR.	36
Figure 19. Periodic table with fission products that are soluble in fluoride salts highlighted in green, and fission products that are insoluble in fluoride salts highlighted in yellow.	37
Figure 20. (Left) ZXF-5Q low porosity industrial, non-nuclear grade graphite with ultra-fine pores.....	41
Figure 21. MSRE low porosity graphite CBG.....	44
Figure 22. C-K edge XANES spectra at room temperature: (a) TEY spectra of HOPG graphite, (b) IG-110 and (c) FY spectra of IG-110.....	47
Figure 23. Dimensional change of in neutron irradiated semi-isotropic Gilsocarbon grade graphite, from [1].....	48
Figure 24. Secondary electron image of exposed fiber region of Rolls Royce® CVI SiCf/SiC composite with 2D satin weave SA3 fiber reinforcement (silica polished).....	49
Figure 25. Corrosion of exposed matrix regions around fiber bundles of SiC _f /SiC composite in FLiNaK at 700 °C.....	50

LIST OF TABLES

Table 1. Example chemical composition of typical structural alloys; compositions were measured by inductively coupled plasma and combustion analyses in mass%. Data from various sources.	4
Table 2. Oxidation states of the fission product elements in molten chlorides with ^{239}Pu as the fissile element.	7
Table 3. Compositions and melting points for common fluoride and chloride coolant salts.....	23
Table 4. Elemental impurity analysis by glow discharge mass spectrometry of $\text{BeF}_2\text{-LiF}$ salt purified by HF fluorination.....	27
Table 5. Elemental impurity analysis by glow discharge mass spectrometry in two different batches of LiF-NaF-KF salt purified by HF fluorination.....	27
Table 6. Candidate ceramics and metals considered for reactor components of a pebble-bed FHR.	40
Table 7. Calculated maximum flux and radiation damage estimates for PB-AHTR using an MCNP5-based neutronic model BEAU [Allen 2013b].	40
Table 8. MSRE materials of construction.....	43
Table 9. Tritium production rates in different reactors compared to FHRs [Forsberg 2017a].	46

LIST OF ABBREVIATIONS

ANL	Argonne National Laboratory
ARE	Aircraft Reactor Experiment
ASTM	American Society for Testing and Materials (now ASTM International)
C/C	Carbon fiber/Carbon matrix composite
CSP	Concentrating Solar Power
CTE	Coefficient of Thermal Expansion
CVD	Chemical Vapor Deposition
DCB	Direct Cantilever Beam
EAC	Environmentally Assisted Cracking
FCL	Forced Convection Loop
FHR	Fluoride-salt-cooled High-temperature Reactor
FY	Fluorescence Yield
GDMS	Glow Discharge Mass Spectrometry
HTGR	High-Temperature Gas-cooled Reactor
ICP	Inductively Coupled Plasma
INL	Idaho National Laboratory
LANL	Los Alamos National Laboratory
LWR	Light Water Reactor
MS	Mass Spectrometry
MSBR	Molten Salt Breeder Reactor
MSR	Molten Salt Reactor
MSRE	Molten Salt Reactor Experiment
OES	Optical Emission Spectroscopy
ORNL	Oak Ridge National Laboratory
PNNL	Pacific Northwest National Laboratory
PyC	Pyrolytic Carbon
SEM-EDS	Scanning Electron Microscopy Energy Dispersive x-ray Spectroscopy
SNL	Sandia National Laboratory
SS	Stainless steel
TCL	Thermal Convection Loop

EXECUTIVE SUMMARY

Compatibility of materials with molten salt coolants is one of the more challenging aspects of molten salt reactor (MSR) design. This report outlines relevant knowledge on measurement, management, and mitigation of corrosion in MSRs. The report begins with a discussion of basic concepts. Corrosion in molten salts is largely driven by the redox condition of the salt, which can be described as the F_2 or Cl_2 potential of the salt. The redox potential can be driven upward by the presence of oxidizing impurities such as water, oxygen, and HF. Redox control additives such as Be in F salts and Mg in Cl salts can be used to lower the halogen potential and reduce corrosion. UF_4 and UCl_4 are also particularly oxidizing. The reactions of UF_4 and UCl_4 with structural materials can be controlled by using redox additives to maintain a minimum amount of UF_3 or UCl_3 in the salt melt.

It is important to understand the strengths and weaknesses of various experimental methods, and they are discussed in the third chapter. While experiments with static salt are useful for comparisons and screening tests, flowing salt experiments with a temperature gradient are necessary to truly measure corrosion rates and capture all phenomena accurately. A survey of electrochemical techniques for measuring salt redox is also given. Currently, there are no robust engineering solutions for electrochemical measurements in F or Cl salt, but several studies have reported progress.

In the next chapters, the fundamentals of salt chemistry and salt purification are discussed. Commercially available salts (even reportedly high purity salts) contain levels of moisture that make them unsuitable for use in MSRs and MSR corrosion experiments. Methods for salt dehydration and purification are discussed. The most basic method is drying by simple heating. For more effective purification, salts can be sparged with oxidizing gases such as HF/H_2 or CCl_4 to remove impurities. These methods have been shown to be effective in halide salts. The use of HF in fluoride salts is much more mature, and likely more effective than methods for Cl salts.

Corrosion and mechanical properties are also discussed. Ni-based alloy N, used as a salt-facing structural material in the MSRE, was found to crack in service due to exposure to Te, a fission product. Past work has shown some success at limiting Te-induced cracking by using redox control. More work is necessary to determine if other structural materials are similarly affected. Since Te is more abundant in thermal spectrum reactors, Te cracking is less of a concern in Cl fast reactors.

Irradiation may also affect material corrosion, but work is limited in this area. Different studies show both an acceleration and a deceleration of corrosion due to irradiation, so more work is needed. Fission products are also discussed briefly, but little work exists, aside from research on Te-induced cracking.

Finally, the issues surrounding graphite compatibility are discussed. The most pressing issue is permeation of salts into graphite pores, which may affect the mechanical integrity of the graphite structures, and may also create radiological hot spots and waste disposal issues. Additionally, graphite may accelerate corrosion of metals and vice versa, so experiments are needed in which metals and graphite are simultaneously exposed.

The report concludes with a list of knowledge gaps. The first gap, a lack of standardization for molten salt experimentation, is the most important. It is not currently possible to compare studies performed at different institutions due to a lack of standards for salt purity and experimental setup. To produce meaningful, evidence-based standards, data must be collected in a systematic fashion to determine the effects of specific impurities so standards can be set regarding maximum concentrations. Salt impurities have such a large effect on corrosion rates that small differences in salt impurity concentration can mask other factors and lead to ambiguous conclusions. These knowledge gaps should not be interpreted as absolute barriers to the advancement of molten salt technology. They merely represent guidance for future

research in preparation for upcoming needs. Their relevance and importance is entirely dependent on the design choices made for each particular reactor concept.

1. INTRODUCTION

The first molten salt reactor, the Aircraft Reactor Experiment (ARE), operated for 9 days in November 1954 at Oak Ridge National Laboratory (ORNL) [Rosenthal 1970, Bettis 1957]. It employed a fluoride-based salt consisting of NaF, ZrF₄ and highly enriched UF₄ as its coolant and fuel medium. The knowledge gained from the ARE led to the Molten Salt Reactor Experiment (MSRE), also based at ORNL in the 1960s [Haubenreich 1970]. The MSRE employed a fuel medium and core coolant consisting of LiF-BeF₂-ZrF₄-UF₄ and a secondary coolant consisting of LiF-BeF₂ (commonly referred to as “FLiBe”).

Today, many MSR designs have been proposed, each with a unique combination of construction materials and salt chemistry. Proposed concepts include chloride fast reactors, fluoride-fueled thermal reactors, and fluoride salt cooled reactors. Molten salts have also been used as a heat transfer medium for concentrating solar power, and as a conductive medium in various industrial processes such as actinide recovery, electroplating, and electrowinning.

This work is intended to provide technical information on corrosion of structural materials in MSRs to inform regulatory decisions. For more general information on all materials issues in MSRs, see NRC MSR-2019-03-05, “Technical Gap Assessment for Materials and Component Integrity Issues for Molten Salt Reactors.”

The focus of this work is on the relevant phenomena associated with materials corrosion in molten salts, and not on specific alloys, salts, or combinations thereof. As discussed herein, corrosion rates are highly sensitive to many difficult-to-control variables such as salt purity. Further, the diversity of conditions such as flow rate, experimental volume, and chemical additives renders published corrosion rates for specific salt-material combinations either irrelevant or misleading. Useful comparisons can indeed be made within controlled environments, such as comparing different materials by using the exact same experimental setup and same batch of salt, but comparing corrosion rates across different labs with different methods is not advised, and is avoided in this work.

At the conclusion of each chapter, knowledge gaps are given, and a summary is given at the conclusion of the report. In the opinion of the authors of this report, they represent the most important topics for future research on material compatibility with molten salts.

2. BASICS OF CORROSION IN MSRs

In this chapter, the foundations of alloy corrosion in molten halide salts will be discussed. Foundational thermodynamics will be laid out, along with chemical factors that affect corrosion rates. The discussion in this chapter is limited to uniform corrosion, because localized attack such as pitting has not been found to be a concern in molten salts. Other degradation modes such as environmentally-assisted cracking are discussed in later chapters.

2.1 THERMODYNAMICS

Molten salt corrosion is a process heavily dependent upon complex chemical reactions happening between the salt, the solid materials, and the atmosphere interacting with both. Thermodynamics dictates the chemical equilibria established throughout the system. A volume of salt in a static enclosed system will eventually reach a steady state; that is, none of the key salt parameters change. However, flowing systems create temperature gradients, resulting in a situation unlikely to reach a steady state without

control over the chemistry within the system. Additionally, the chemical composition of the salt varies with function (i.e., coolant versus fuel), temperature range, core design, and many other considerations. All of these factors affect the salt chemistry, changing the overall thermodynamics and subsequent corrosion of the structural material and graphite moderator.

2.1.1 Molten Salt Stability and Redox Potential

In very simplified terms, the reaction of materials with salts can be expressed as:



where M is the metal (Na, K, etc. for $z=1$ and Be, Cr, etc. for $z=2$) and X is the halide (F or Cl) in the metal-halide salt [Edeleanu 1960; Glassner 1957]. The Gibbs free energy of dissociation (ΔG_{dis}), the reverse of formation, influences which side of the equilibrium is favored. A positive value means the left side (MX_z) is the favored state. The equilibrium constant (K_{eq}) relates the relative concentrations of the metal, halogen, and metal halide salt to ΔG_{dis} .

$$e^{-\frac{\Delta G_{dis}}{RT}} = K_{eq} = \frac{a_M a_{X_2}^{\frac{z}{2}}}{a_{MX_z}} \quad 2.2$$

where R is the ideal gas constant, T is the temperature in Kelvin, a_M , a_{X_2} , and a_{MX_z} are the activities of the metal, halogen, and metal halide, respectively. Rearrangement of the equation yields the halogen potential ($\Delta \bar{G}_{X_2}$), the reference point commonly used to relate different systems to one another. [Olander, 2002, Zhang 2018b]

$$\Delta \bar{G}_{X_2} = RT \ln(a_{X_2}) = -\frac{2}{z}\Delta G_{dis} + \frac{2RT}{z} \ln(a_{MX_z}) - \frac{2RT}{z} \ln(a_M) \quad 2.3$$

The halogen potential allows comparison between not only salts in the same group and oxidation state (e.g. NaF and LiF) but salts of different groups (e.g. KF and BeF₂) and oxidation states (e.g. UF₄ and UF₃).

Ellingham diagrams are graphical representations of the stability of species as a function of temperature. They are commonly used, but often misunderstood. Figure 1 shows Ellingham diagrams generated with HSC Chemistry 9 [database sold by Metso Outotec, Finland] for several chloride and fluoride species. In pure salts, the activities of the metal and metal halide are assumed to be unity, effectively removing the last two components in Equation 2.3.

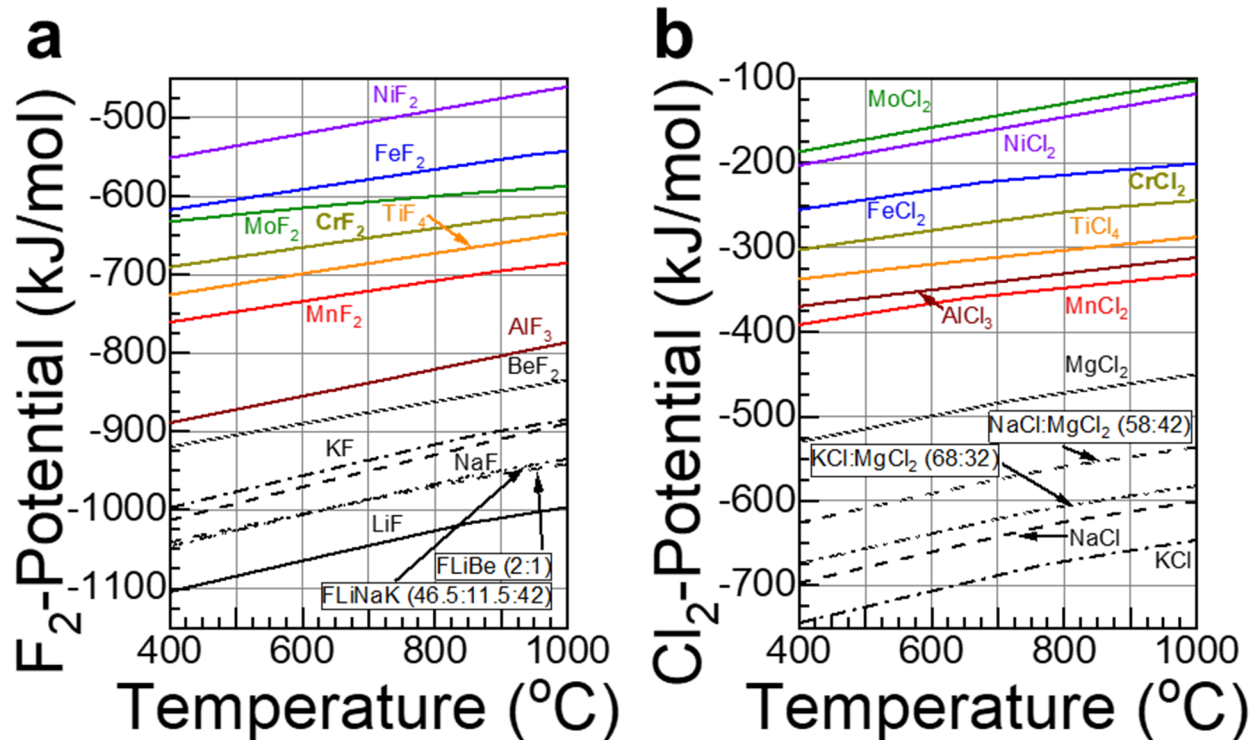


Figure 1. Ellingham diagrams of (a) fluoride and (b) chloride species. All curves were normalized to 1 mole of X_2 . The black lines are for salt components and the colored lines are for structural material components.

The curves for each species on the figure represent the halide potential at which Equation 2.1 is at equilibrium. In other words, the curve represents where $\Delta\bar{G}_{X_2} = 0$ for the reaction. Species that are lower on the Ellingham diagram tend to be more stable as halides, and species higher on the diagram tend to be more stable as metals. Note that the major constituents of common blends such as NaCl and LiF are near the bottom of the diagrams.

The major alloy constituents of salt-facing structural alloys are near the top of the diagram. For reference, typical alloy compositions are shown in Table 1. Most structural alloys made for use with molten salts are mostly a combination of Fe, Cr, Ni, and Mo. Note that the Cr line is the lowest of these on the diagrams, showing that it is the most active, and thus the most susceptible to corrosive attack. For this reason, low Cr alloys are often proposed for use in molten salt applications. When alloys containing a more active alloy constituent are exposed to molten salt, it can be expected that the more active constituent will be attacked preferentially over Cr. Elbakhshwan et al. [2019] exposed a CrMnFeNi high entropy alloy to FLiBe salt, and found that Mn was attacked preferentially before Cr, as predicted in Figure 1.

However, a metal halide with a higher stability (MX_z) will still react with a more noble metal (N) and establish a chemical equilibrium (Equation 2.4).



The above reaction is simply a combination of the individual dissociation reactions for M and N. As such, $\Delta\bar{G}_{X_2}$ between the two reactions will equate when the system has reached equilibrium.

$$\frac{a_{NX_y}}{a_{MX_z}} = \frac{a_M}{a_N} e^{\frac{\frac{2}{y}\Delta G_{N,dis} - \frac{2}{z}\Delta G_{M,dis}}{RT}} \quad 2.5$$

A common misconception is that a reaction will simply not proceed when the halide potential of a system is below the equilibrium potential for a reaction. In actuality, the line represents the point at which the reaction doesn't proceed ($\Delta\bar{G}_{X_2} = 0$) *assuming equal activity* for the reactant and product forms of the species. When the halide potential is well below the line of stability on the diagram, the reaction will still proceed, but will reach equilibrium where the activity of the product form is much less than the activity of the reactant. For example, if the halide potential is well below the line of stability for Cr, it does not mean that Cr will not deplete from alloys into the salt. It means that equilibrium will be reached at a much lower concentration of Cr in the salt, however (perhaps in parts per million or less). In a practical sense, it is often reasonable to assume that reactions do not proceed at potentials below the stability line, since concentrations are low, and often kinetic barriers are sufficient to prevent significant transport. However, in a flowing media with minimal kinetic barrier, it can be assumed that the system will trend toward an equilibrium in which the chemical potential of all the alloy constituents in the salt is equivalent to their chemical potential in the alloy, including the more noble constituents. The equilibrium concentration will be dependent on the redox condition of the salt.

Table 1. Example chemical composition of typical structural alloys; compositions were measured by inductively coupled plasma and combustion analyses in mass%. Data from various sources.

Alloy	Fe	Ni	Cr	Al	Other
<i>Austenitic iron-base chromia-forming stainless steels</i>					
304H*	70.4	8.4	18.4	<	1.6Mn, 0.3Si, 0.3Mo, 0.4Cu, 0.1Co
316L*	66.6	9.6	19.0	0.01	2.4Mo, 1.7Mn, 1.0Si, 0.2Cu, 0.1Co, 0.1W
NF709	49.0	25.0	22.3	0.02	1.5Mo, 1.0Mn, 0.4Si, 0.2Nb, 0.2N
800H	43.2	33.8	19.7	0.7	1.0Mn, 0.5Ti, 0.3Cu, 0.3Si, 0.2Mo
<i>Ni-based low-Cr alloys</i>					
Hastelloy N	3.7	71.9	7.2	<	16Mo, 0.1W, 0.3Mn, 0.3Si, 0.05C, <0.01Ti
244	1.0	62.2	8.1	0.1	22.4Mo, 6W, 0.3Mn, 0.04Si, 0.002C
KhN80MTY u	0.2	77.6	6.8	1.1	13.2Mo, 0.9Ti, 0.1W, 0.01Mn, 0.04Si, 0.03C
<i>Conventional Nickel-base chromia-forming alloys</i>					
C276	5.7	57.7	16.0	0.2	15.3Mo, 3.5W, 0.6Mn, 0.06Si, 0.002C
600	9.4	73.1	16.4	0.3	0.1Mo, 0.2Ti, 0.1Si, 0.2Mn
718	17.6	54.1	18.0	0.5	5Nb, 1Ti, 3.1Mo, 0.3Co, 0.1Mn, 0.1Si, 0.04C
X	17.9	46.8	22.1	0.1	9.5Mo, 1.8Co, 0.6W, 0.7Mn, 0.3Si, 0.07C
C22	3	56	22	<	13Mo, 3W
230	1.5	60.5	22.6	0.3	12.3W, 1.4Mo, 0.5Mn, 0.4Si
617	0.6	55.9	21.6	1.3	11.3Co, 8.6Mo, 0.4Ti, 0.1Si

*< indicates less than 0.01%

*H is high C variant of 304 SS; L is low carbon variant of 316 SS

2.1.2 Reaction of Salts with Multiple Oxidation States Such as Fuels

Fuel salts can contain both fissile and fertile actinides (e.g., U, Pu, and Th) [Serp 2014]. These elements have multiple oxidation states. Uranium and transuranics can exist in oxidation states as high as +6, as low as +3, and everything in between, with certain oxidation states favored for different elements. Thorium is most stable in the +4 state but can reduce to +3 under certain conditions. Ellingham diagrams of fuel-salts are shown in Figure 2, and were generated in a similar manner as Figure 1.

The Molten Salt Reactor Experiment (MSRE) utilized a fuel salt consisting of FLiBe with added ZrF_4 , and UF_4 and/or ThF_4 . U can fluctuate between the +3 and +4 state relatively easily, making Cr oxidation a major concern. Thorium can participate in similar reactions, but ThF_4 is more stable than UF_4 relative to their +3 states. This is exhibited by the vast difference in F-potential between U(III)/U(IV) (black) and Th(III)/Th(IV) (navy). The curve for Th(III)/Th(IV) is far lower, indicating ThF_4 is relatively stable. However, U(III)/U(IV) is higher, indicating UF_4 more easily oxidizes structural alloys than ThF_4 . Chloride based salts will have a similar concern. Fuel salts with UCl_4 are readily reduced to UCl_3 at the expense of the structural alloy. Using a salt with U in the +3 state versus the +4 state is one way to reduce such issues but may substantially change the thermophysical properties of the salt. Another possibility is to adjust the halogen potential with redox control (Section 2.5).

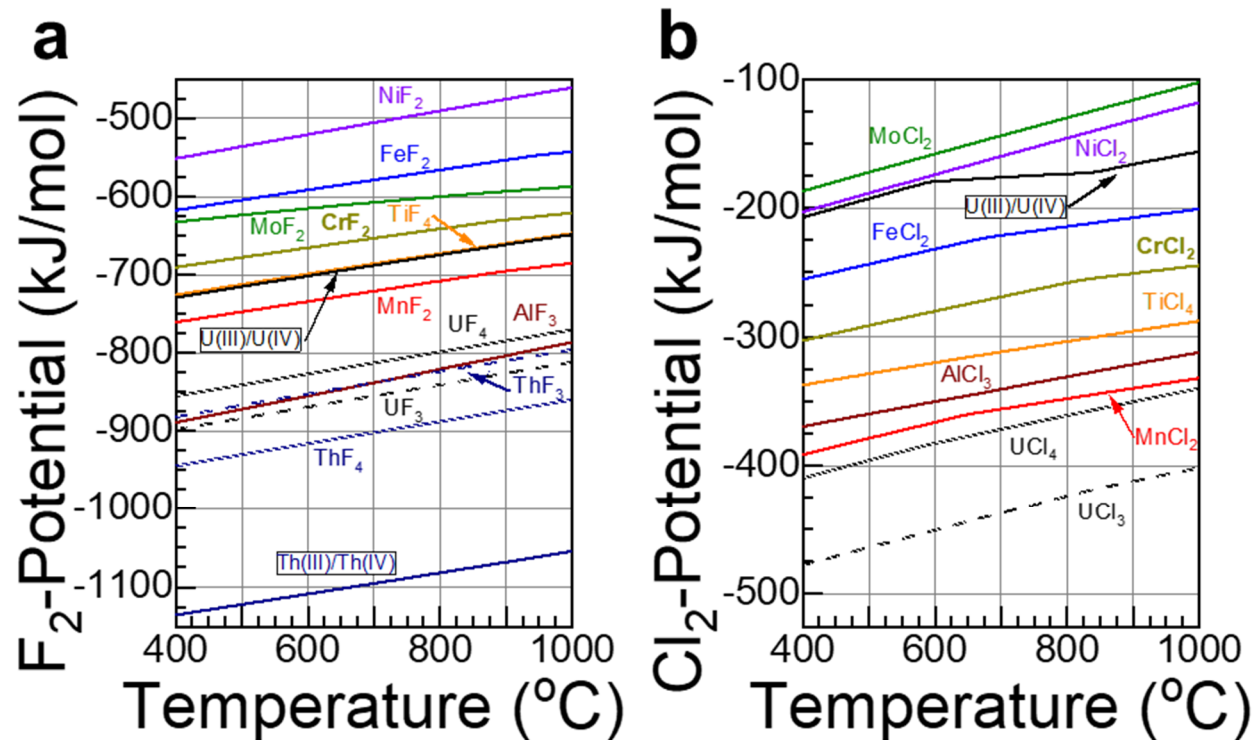


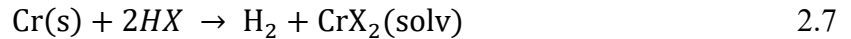
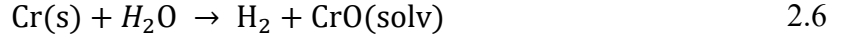
Figure 2. (a) Ellingham diagram depicting common fuel salts used in F based chemistries. (b) Ellingham diagram depicting common fuel salts used in Cl based chemistries. All curves were normalized to 1 mole of X₂.

2.2 IMPURITY DRIVEN CORROSION

Impurity driven corrosion can be divided into three major categories: corrosion products, fission products, and impurities from salt preparation,

The major impurities in molten salts that result from salt synthesis and purification are H₂O, O₂, OH⁻, and O²⁻. [Shaffer 1971, Ding 2018b] Moisture and oxygen can get into the salt during vessel loading, by surface adsorption on the wall of the reactor, and by ingress during system operation. The impurities interact with the containment vessel in two major ways: direct oxidation through impurity reduction and by affecting the equilibria that govern how corrosion progresses, explained in **Section 2.6**. Additional impurities may include residual HX from purification or from salt hydrolysis, residual carbohalide from carbohalogenation, or MX₂ (M=Cr, Ni, etc.) created by corrosion of the purification vessel. Salt purification will be addressed fully in a later chapter.

Proton reduction occurs by reaction with H₂O/OH⁻ or HX, governed by the simplified reactions below:



The above reactions assume Cr is the reacting element, but similar equations can be used for Fe or other active alloy constituents. At low concentrations (less than the solubility limits) corrosion products remain in the melt. However, as corrosion progresses, and reaction products exceed solubility limits, precipitation should be expected in the cold parts of the circulating loop.

In salt-fueled reactors, fission products can be expected to play a role in material degradation. First, the original oxidation state of the fissile material is important. [Chasanov 1965, Robinson 1958a] Using ²³⁵UF₄-containing salts as an example, the oxidation state of U is +4. Since fission produces two atoms for every one that splits, the original average valence state is considered +2. Therefore, if an element in the decay chain is more stable at the same oxidation or with a higher oxidation state (e.g., +3), then the salt becomes more reducing and less likely to corrode the structure. However, if the element is less stable at the same oxidation state or is more stable in a lower oxidation state, then the salt becomes more oxidizing. The decay chain and initial oxidation state must be considered together to fully understand their effect on corrosion. Robinson [1958a] described calculations used to determine the evolution of average valence over time for reactor fuels containing UF₄. He used the following equations in his calculations:

$$U^{+V} \rightarrow 2Fp^{+\bar{V}} + (2\bar{V} - V)e^- \quad 2.8$$

$$\bar{V} = \frac{1}{2} \sum_z y_z V_z \quad 2.9$$

where V is the original oxidation state of U in the fuel, \bar{V} is the average oxidation state of the fission products, and y_z and V_z are the fission yield and oxidation state of the element with atomic number Z, respectively. As mentioned previously, 2 fission products are produced for every atom split (U in this case) and thus requires ½ in front of the average oxidation state (Equation 2.8,2.9). If the difference between twice the average oxidation state of the fission products and the original oxidation state is positive, then the result will likely be reducing in nature. Chasanov [1965] performed the same calculations for (Pu,U)Cl₃ systems and obtained similar results to Robinson. He performed the calculations using the oxidation states shown in Table 2.

Table 2. Oxidation states of the fission product elements in molten chlorides with ^{239}Pu as the fissile element.
Reproduced from Chasanov [1965].

Oxidation State	Elements
-2	Se, Te
-1	I
0	Kr, Xe
+1	Rb, Ag, In, Cs
+2	Sr, Zr, Mo, Pd, Cd, Sn, Ba, Sm, Eu
+3	Y, Tc, Ru, Rh, Sb, La, Ce, Pr, Nd, Pm, Gd
+5	Nb

Using the table as a baseline, Chasanov calculated the average fission product oxidation versus time (Figure 3). However, elements such as Ru, Pd, Tc, and Mo are readily reduced to their metallic state. Curves b, c, and d account for that, and the curve is pushed down, indicating a lower average oxidation state. If the curve is below the dashed line at 1.5 (half of +3, oxidation state of Pu), the salt is oxidizing. The average fission product valency only accounts for the change in valence but does not reflect change in chlorine or fluorine potential as fission progresses. The calculation is more difficult but better represents the change in corrosivity over time. Chasanov does mention the effect the change in salt chemistry as a result of fission has on corrosion of the containment material. However, no solid conclusion was made.

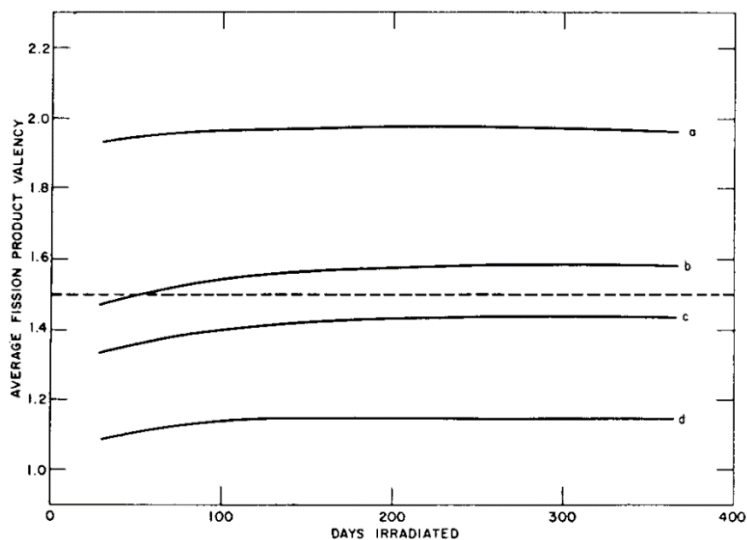


Figure 3. Fission-product average valency for $^{239}\text{PuCl}_3$ irradiated with 2-MeV neutrons. Rare gases retained in system. (a) Valencies as in Table I in Chasanov. (b) Valencies as in Table 2.I in Chasanov, except Ru^0 . (c) Valencies as in Table 2.I in Chasanov, except Ru^0 and Pd^0 . (d) Valencies as in Table 2.I in Chasanov, except Ru^0 , Pd^0 , Tc^0 and Mo^0 . Reproduced from Chasanov [1965].

2.3 REDOX CONTROL

Metallic redox control additives may be used to control the halogen potential of a given salt melt. The metal added typically matches the salt (i.e., Be for FLiBe and Mg for MgCl_2). In the MSRE, the potential of the fuel salt melt was controlled by small additions of Be [Baes 1974]. For candidate concentrated solar

power salts containing MgCl_2 , Mg has been added to reduce the chlorine potential [Ding 2018a]. Full thermodynamic understanding of solvation and salt structure is important for modeling of long-term systems and is a knowledge gap. Additionally, understanding how redox control affects the microstructure of the structural material will be important for lifetime modeling.

Careful control over the U(III)/U(IV) (i.e. $\text{U}^{+3}/\text{U}^{+4}$) was of great concern for the MSRE, as the reduction of U(IV) to U(III) was considered to be the primary mode of material degradation [Baes 1974; Gibilaro 2015]. Small amounts of Be were used to decrease the F potential of the melt, and thus shift the U(III)/U(IV) ratio to greater than 50. This is important for both corrosion of the structural vessel and the effect Te has on the microstructure [Keiser 1977a]. The effect of Te will be discussed in a later chapter. Currently, few such methods for redox control are actively researched for chlorides, but rare earth redox couples are readily studied for electrochemical separations [Guo 2020, Zhang 2018a]. Similar concepts could prove equally effective in chlorides as they are in fluorides.

2.4 NON-REACTING IMPURITIES AND THEIR EFFECT ON EQUILIBRIA

Molten salt corrosion mainly focused on impurity driven corrosion with minimal focus on how impurities not directly reacting affect solubility limits. O^{2-} is the most readily available impurity that is considered non-oxidizing. Little data on its effect on metal cation equilibria in molten salts exists. [Cherginets 2015, Martínez 2000, Suski 1991] Martínez [2000] observed that Cr oxides readily precipitate in the presence of relatively small amounts of O^{2-} in CaCl_2 . In a static environment, the system will reach equilibrium, preventing further materials degradation. However, any system with a temperature gradient will not reach equilibrium because corrosion occurs in the hottest part and precipitation occurs in the coldest part. Any perturbation to the complicated and connected equilibria plays a role on the overall corrosion rate of the containment vessel [Lewis 1971]. Understanding the effect and taking adequate steps to mitigate the impact of O^{2-} will be crucial to increasing the longevity of MSRs and is a knowledge gap that should be addressed. It is particularly important in the fuel salt where UF_x and ThF_x can form their oxides and precipitate out of solution [Baes 1974]. Chlorides should be expected to experience similar phenomena.

2.5 AIR-SIDE OXIDATION

A large body of research into degradation of structural materials in molten salts focuses on the salt-side of corrosion. However, in molten salt reactors, there will be a portion exposed to air at high temperatures. [MacPherson 1957] As established previously, molten salts preferentially remove the most active alloy substituent, which is usually Cr. However, chromium on the air side provides protection from corrosion by forming a passive film. During the development of alloy N (marketed commercially as Hastelloy N) it was found that at least 6 wt.% Cr was required to maintain oxidation resistance to air [Jordan 1957, Koger 1972b].

2.6 KNOWLEDGE GAPS

2.6.1 Behavior and effectiveness of redox control additives

Experimental data shows that redox control additives are effective for mitigating corrosion. However, relatively few additives have been explored outside of Be in fluoride salts and Mg in chloride salts. Further, there is little systematic data providing guidance on ideal concentrations of additives to mitigate corrosion and prevent precipitation in narrow-channel heat exchangers. The performance of redox control additives is a knowledge gap.

2.6.2 Effects of specific impurities

It is well known that more purified salts result in lower corrosion rates, but complete knowledge on the corrosivity of specific impurities is lacking including how redox control may mitigate their effects. This may be important for setting standards regarding maximum concentrations of potentially important impurities such as metals and sulfur. More data on the effects of specific impurities would be beneficial, and the lack of this data is a knowledge gap.

2.6.3 Dissimilar material interactions

A frequent issue in corrosive liquid systems (liquid metals and molten salts) is the possibility that a synergistic reaction will arise because both materials are in contact with the liquid. Koger and Litman [1970] reported catastrophic corrosion of type 304 SS (see Table 1) exposed in a flowing sodium fluoroborate salt loop in which most of the salt-facing metal was alloy 600. They attributed the rapid corrosion to the effect of dissimilar metals. It is not clear if the dissimilar metal effect is due to solid-state electronic transport (galvanic corrosion), or if it is attributable to thermodynamic effects in the salt, such as metallic halides exchanging cations. Olson et al. [2009, 2015] reported a galvanic effect when structural alloys were exposed in molten salts along with graphite, but the work describes a non-galvanic mechanism involving Cr dissolving from metallic coupons and reacting with the graphite container to form chromium carbides. By removing the Cr reaction product from the salt, this accelerates the dissolution of the metallic specimen—a classic dissimilar materials effect. In general, the lack of sufficient data, and unclear mechanistic explanation suggests a knowledge gap.

3. EXPERIMENTAL TECHNIQUES

Before presenting the results of corrosion studies in molten salts, it is worth discussing the main experimental techniques used in these studies. Corrosion testing in molten salts can be grouped into three categories—static tests, thermal convection loops, and pumped loops. Electrochemical testing during these tests is an important characterization technique for monitoring the status of experiments.

Static testing in molten salts is widely employed [Zheng 2016, Olson 2009, Gomez-Vidal 2016, Ambrosek 2011]. Static tests can be conducted in an open crucible with a (usually inert) cover gas, or in a sealed capsule. Unless a thermal gradient is imposed on flowing salt, the specimen and the salt will approach equilibrium, so static tests are less predictive than loop experiments. However, capsule and crucible experiments are a useful and economical way to conduct initial screening experiments, compare alloys, and conduct targeted corrosion studies to investigate specific phenomena in salt and alloys.

The chemical compatibility of the specimens and containers is vitally important for accurate measurements of corrosion rates. Material differences between the specimen and container can drive increased corrosion.

3.1 STATIC TESTING

3.1.1 Crucible testing

One common approach is to expose samples in an open crucible containing molten salt, under an inert cover gas. Unfortunately, tests in open capsules, even in highly pure atmospheres, are susceptible to impurity-driven corrosion. Crucible testing is useful for cheaper and easier to set up experiments that use in situ diagnostics such as electrochemistry [Gomez-Vidal 2016, Feng, 1982, Vignarooban 2014, 2015]. Gomez-Vidal et al. [2016] used an open crucible with nitrogen as a cover gas to conduct electrochemical experiments in a KCl-LiCl melt. Platinum reference and counter electrodes were used to measure polarization plots for various alloys. The researchers recorded relatively high corrosion rates, in excess of a few mm/year for stainless steels (SSs) and Ni-based alloys (Table 1) at 650 °C. The researchers did not attempt to purify the salts in their liquid state, so the polarization data likely reflected an initial period of very aggressive impurity-driven corrosion that could be expected to slow with exposure time as impurities are “consumed.” Later work by Gomez-Vidal et al. [2017], using similarly unpurified chloride salt, recorded corrosion rates of less than 0.25 mm/year for aluminum-forming alloys at 700 °C.

Electrochemical measurements were also performed by Vignarooban et al. [2014, 2015]. The NaCl, KCl, ZnCl₂ salts used in these experiments were commercially purchased salts and were not purified except by heating to 200 °C before testing. Testing was done at 250 and 500 °C in quartz containers for Ni-based alloys C276, C22, and N (Table 1) in three eutectic salt mixtures. Two types of tests were run, potentiodynamic and immersion, to prove potentiodynamic measurements are reliable in predicting corrosion rates. A schematic of the potentiodynamic set-up is given in Figure 4.

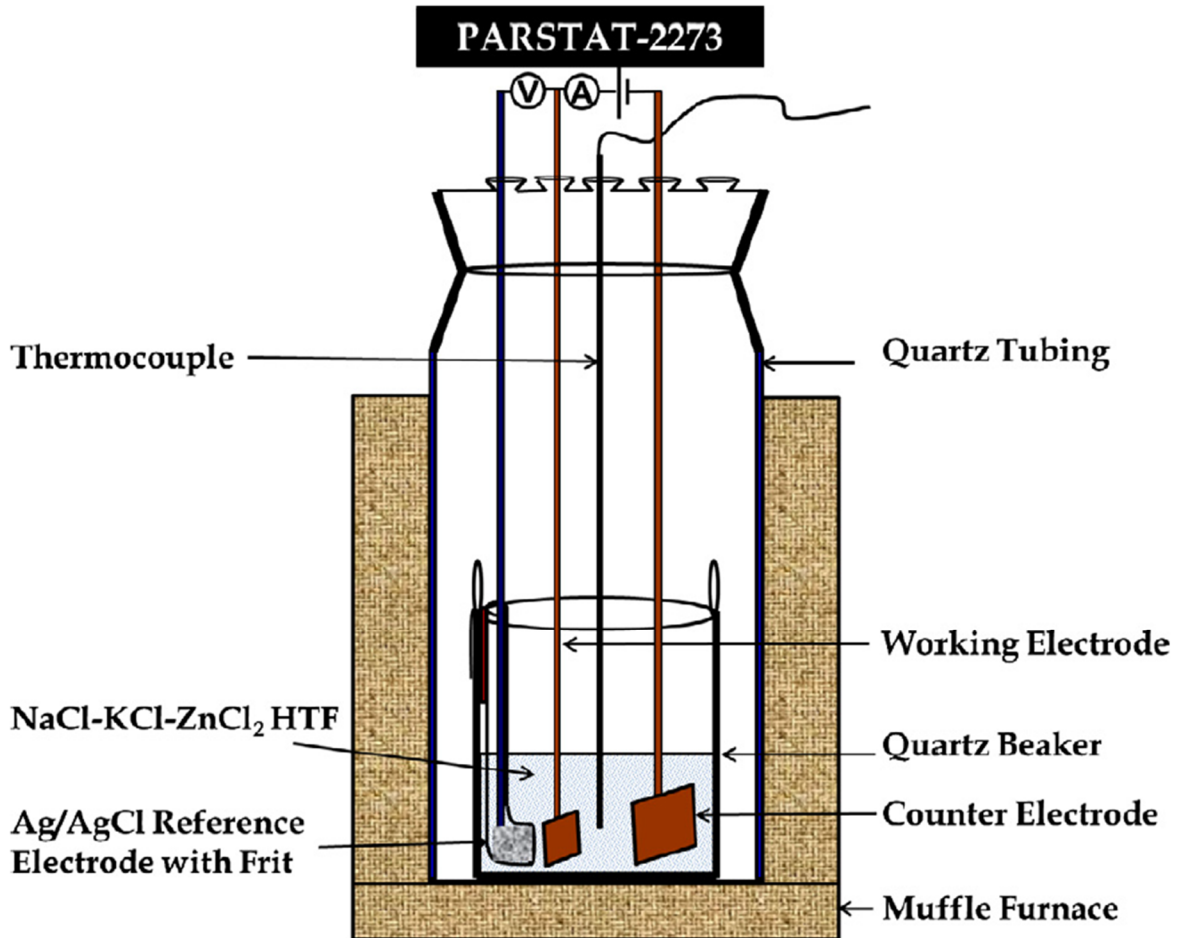


Figure 4. Schematic of the potentiodynamic experiments. A small volume of molten salt is used in these experiments. Reproduced from Vignarooban et al. [2014].

Rather than reporting the mass change, all of the immersion exposure data were converted to corrosion rates without providing the assumptions for that calculation, e.g. 10-25 $\mu\text{m}/\text{yr}$ for C276 and C22 at both 250 and 500 $^{\circ}\text{C}$ versus 40-50 $\mu\text{m}/\text{yr}$ for alloy N at 250 $^{\circ}\text{C}$ and 180 $\mu\text{m}/\text{yr}$ at 500 $^{\circ}\text{C}$ from the potentiodynamic experiments. Detailed results are shown in Figure 5. Only results for immersion exposures of Ni-based alloy C276 at 500 $^{\circ}\text{C}$ were reported, with the longest exposure being 42 days. High corrosion rates of $\sim 110 \mu\text{m}/\text{yr}$ were measured after one week, with corrosion rates stabilizing around 50 $\mu\text{m}/\text{yr}$ after 42 days. These values are much higher than calculated from the potentiodynamic experiments, Figure 6. Ultimately these results point out a few key factors for experimental rigor. Because the potentiodynamic experiments were done over a period of several minutes, while immersion tests were done over weeks, the results do not ultimately compare to one another. The immersion testing data show similar increased initial corrosion rates as those reported by Gomez-Vidal [2017] when the salt was not properly purified. Ultimately, it is important to report analytical measurements of salt composition before and after testing to ensure that the static nature of the tests were not saturating the salt melt with corrosion products, and for a better understanding of impurities. The potentiodynamic principles used for measurement of corrosion rate are used elsewhere in the literature, however they do not seem suited to the experimental set-up used here and this set of experiment failed to establish a correlation between immersion test results and potentiodynamic experiments, which is a knowledge gap.

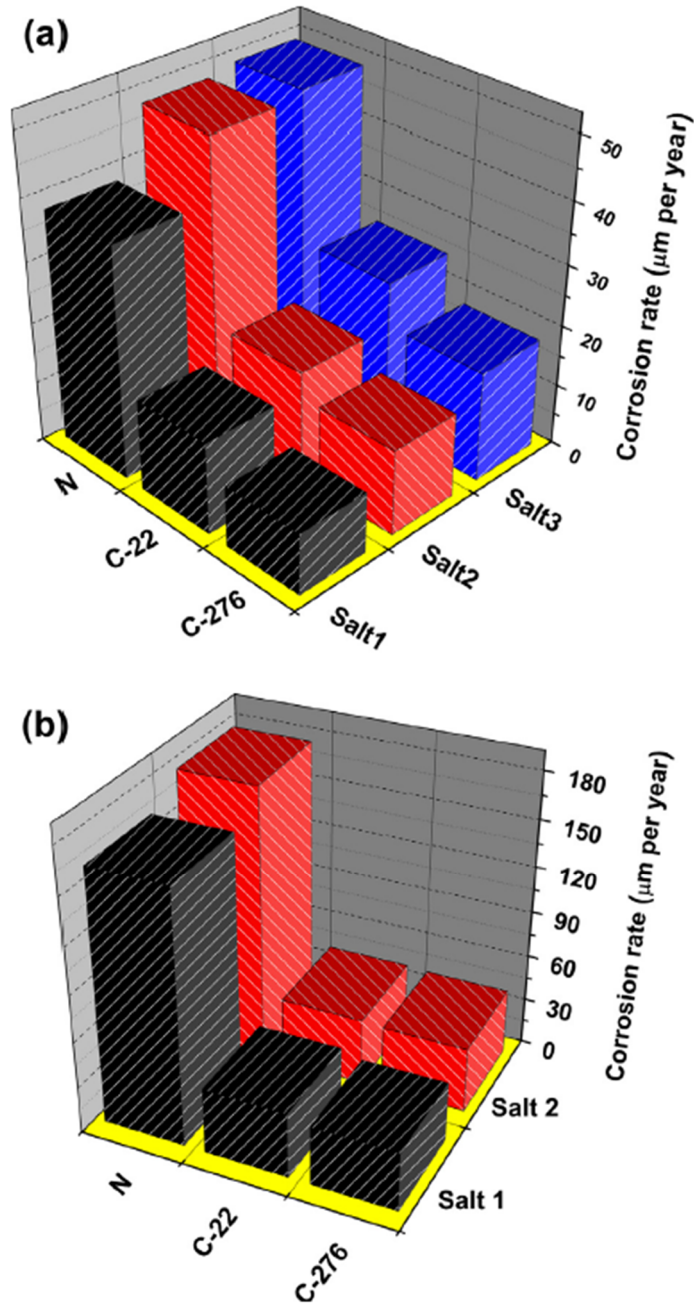


Figure 5. 3D histograms of calculated corrosion rates from potentiodynamic experiments performed on 3 alloys in NaCl-KCl-ZnCl₂ salt at (a) 250°C and (b) 500°C Alloy N with the lowest Cr content had the highest rates in all cases. Reproduced from Vignarooban et al. [2014].

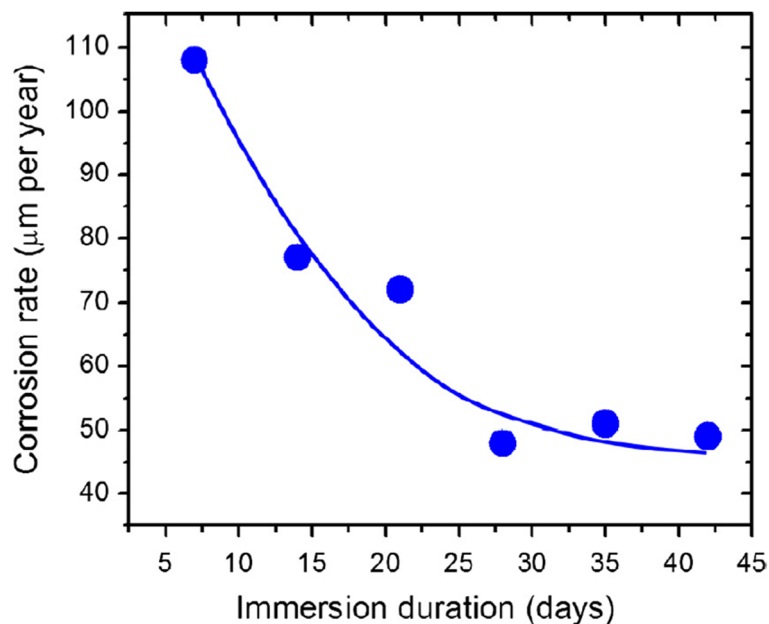


Figure 6. Calculated corrosion rates from immersion experiments for six C276 specimens exposed at 500°C as a function of exposure time. Rates reported here are much higher than any calculated rate from the potentiodynamic experiments. Reproduced from Vignarooban et al. [2014].

3.1.2 Capsule testing

To eliminate the effect of impurities in the cover gas, corrosion tests can be conducted in sealed capsules, a method employed by the University of Wisconsin [Olson 2009, Ambrosek 2011, Sabharwall 2010, Cheng 2017] the Chinese Academy of Sciences [Hou, 2016, Yang 2016a, Qiu, 2014] and ORNL [Raiman, 2019, Pint 2019]. Researchers at ORNL have used Mo capsules, owing to its inertness in molten fluoride salts and welded the capsules shut. The design of the capsules is shown in Figure 7. Capsules are filled in an inert atmosphere glovebox to 2/3 capacity and ideally welded shut in the glovebox. The Mo capsules are sealed within SS outer capsules to prevent atmospheric degradation and then heated in high-temperature box furnaces. At the end of the exposure, the capsules with the specimen attached at one end, are flipped upside down to allow the salt to drain from the sample surface for easier removal.

Testing by Olson [2009] involved purified FLiNaK salt (with reported purity levels) that had been sparged with Argon H_2/HF and then H_2 gas mixtures. Graphite was used as the inner container material for all tests in this study due to its assumed inert behavior in fluoride salts and to save cost. Type 316 SS was used as the outer container. To maintain purity, salt was introduced into the capsules in a controlled Ar environment through a small hole in the containers. Nickel-based alloys with varying Cr contents were tested, alloys N, X, 617 and 230 (Table 1), along with Fe-based 800H, Nb-1Zr and Nickel 201 which contains no Cr. Each tested capsule contained three samples. Results show a spread of 100 ppm Cr measured in the salt after exposure between alloys X and 800H, despite having a difference in Cr content of about 1%. Alloy 230 showed the most weight loss per area of the alloys at 50 mg/cm^2 after exposure at 850°C for 500h. These results are shown in Figure 8. The researchers do note, however, that Cr-carbides were formed in samples that were high in Cr content and Zr-carbides formed on Nb-1Zr. This suggests that the capsule material played a large role in these results, as carbide formation would bring corrosion products out of solution, possibly allowing for more selective corrosion of these elements to occur.

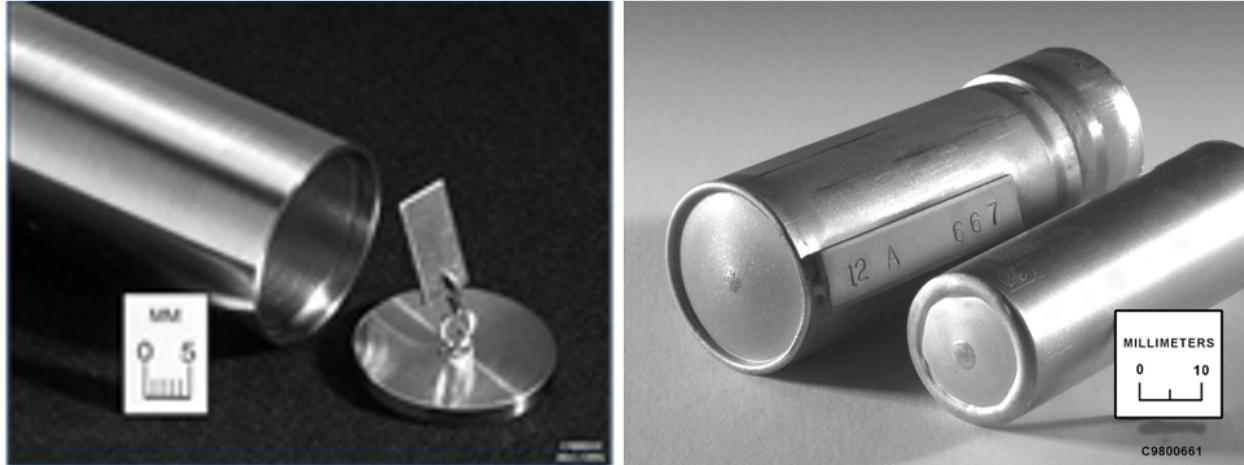


Figure 7. Capsule testing apparatus at ORNL. (L) A sample attached to the lid of the inner capsule and (R) an inner capsule and outer capsule.

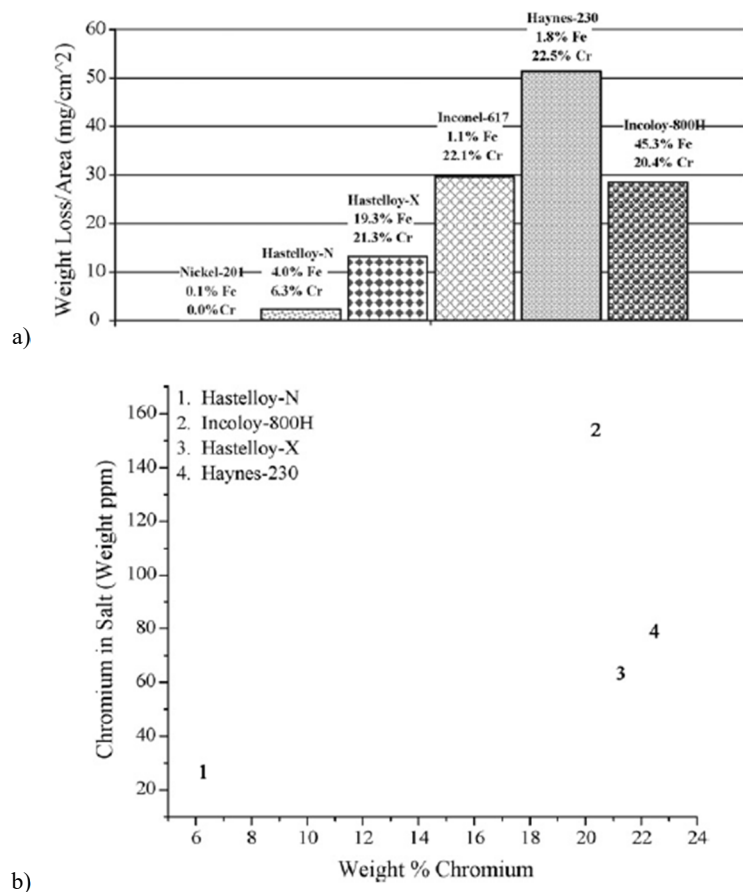


Figure 8. (a) Specific mass loss for alloys tested in graphite capsules at 850°C for 500h in purified FLiNaK (b) Cr alloy content vs. Cr measured in the salt after exposure. In (b), a large spread in salt Cr content was measured despite little difference in alloy Cr content. Reproduced from Olson, et al. [2009].

More recent testing at ORNL has utilized either Mo capsules due to the relative inert behavior of Mo in molten salts, or capsules made of the same material as the sample being tested [Pint et al., 2019]. KCl-NaCl-MgCl₂ salt was used in these experiments, purified using the carnalite method and sparging [Mayes

2018, Kurley 2019]. Capsules were electron-beam welded shut with salt added to the capsules under a controlled Ar glovebox atmosphere. Exposure times ranged from 100-1000 h. These experiments are based on techniques developed at ORNL in the 1950's that were used for a wide range of molten salt and liquid metal experiments. Ultimately these tests reinforce the importance of the selection of inert container materials, salt purification, impurity control during the experiment and challenge the use of mass change data as a direct correlation to corrosion rate (such as $\mu\text{m}/\text{yr}$, which assumes a linear reaction rate). Figure 9 shows polished cross sections of alloy 230 specimens exposed in either Ni or Mo capsules at 800 °C for 92 h to a commercial (K, Mg, Na) Cl salt used for concentrating solar power (CSP) applications. The porosity resulted from selective Cr removal and clear differences in corrosion behavior can be observed, with the Ni capsules showing increased intergranular attack. Figure 10 shows EDS images of alloy 230 exposed at 800 °C for 100 h in a Ni capsule with O and Na trapped in pores that formed during corrosion in the same commercial Cl salt without O purification (salt #2). This shows that the mass change for these specimens was a combination of mass loss from selective attack and mass gain from the salt that infiltrated the porous microstructure. This means that mass change in static tests cannot always be extrapolated to meaningful corrosion rates.

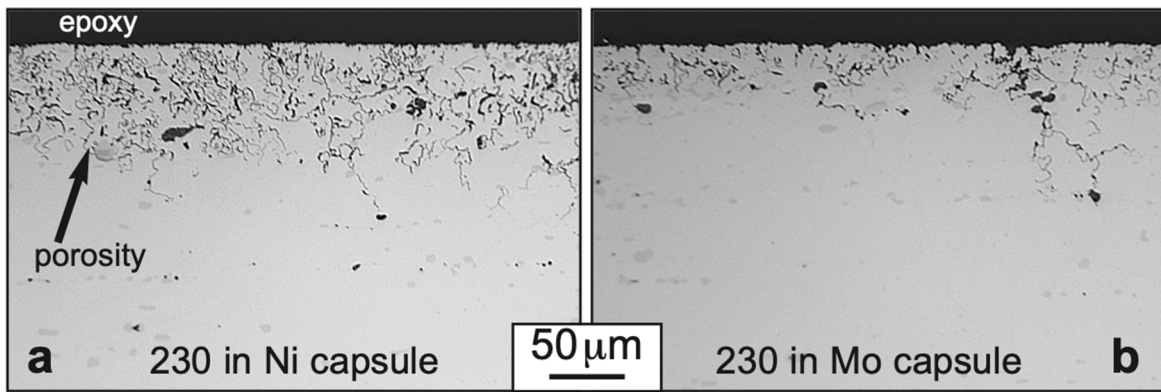


Figure 9. Light micrographs showing cross-sectional attack of alloy 230 exposed to chloride salt at 800°C for 92 h in (a) Ni or (b) Mo capsule. Much more intergranular attack was observed in the sample exposed in the Ni capsule. Extracted from Pint, et al. [2019].

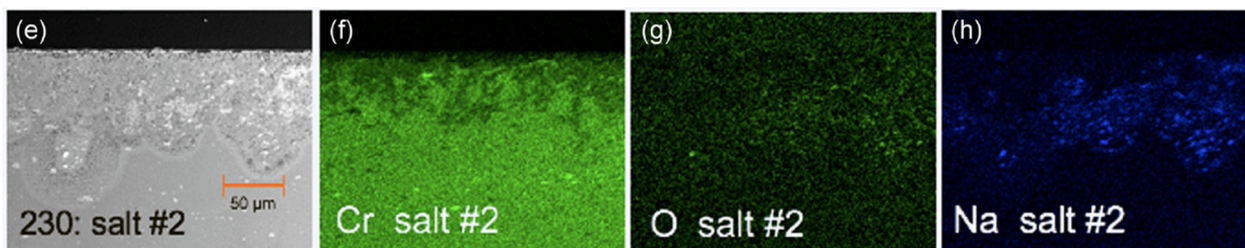


Figure 10. SEM and EDS images of alloy 230 exposed in chloride salt at 800°C for 100h, showing O and Na content in the pores of the corrosion area. These images suggest that mass gain in the form of trapped salt or possibly oxides can form during testing. This calls into question the validity of extrapolation of mass change to corrosion rate directly. Reproduced from Pint, et al. [2019].

Dissimilar container and specimen materials can cause large changes in corrosion behavior during testing. Guo, et al. [2018] found the corrosion rate of alloy 800H exposed in FLiNaK salt at 800 °C for 500 h varied from 4.4 to 727.2 $\mu\text{m}/\text{yr}$ depending on the container used. In the higher corrosion rate experiments Cr was selectively leached from the specimen and deposited on the container material, forming carbides with graphite crucibles and a Ni-Cr alloy layer on a Ni crucible. (A similar effect was reported for Figure

9 [Pint 2019].) Similar effects were reported with specimens of alloy N, pure Cr, and a 9Cr-2W steel (JFL-1). These results are important for interpretation of data using different procedures and help guide future experimental design. Data on corrosion rates for specimens exposed in crucibles, capsules, or flowing salt loops made of dissimilar material are unlikely to be representative of behavior in a reactor scenario. A standard of matching alloys for both specimen and container is ideal, even if this makes experimentation more difficult due to fabrication concerns.

3.2 FLOWING SALT TESTING

3.2.1 Thermal convection loops

Thermal convection loops (TCLs) use flowing salt in a thermal gradient to more accurately measure material corrosion rates. Extensive work was done at ORNL in the 1950s through the 1970s using TCLs to study corrosion of various structural materials in fluoride salts [DeVan, 1962, Keiser, 1976, 1977, 1979, Distefano, 1995] and has resumed recently [Pint 2019]. To support the MSRE, alloy N was the most common material of construction, although others, notably 316 stainless steel, were also used. More recent TCLs have been constructed of type 316H SS and Ni-based alloys 600 and C276. The TCLs employed a design (an example shown schematically in Figure 11) in which one side of the TCL was heated and the other side was not. This served to both drive the flow in the TCL and to more accurately recreate the conditions in a reactor. The work is well summarized by Koger [1972b], Ignatiev and Surenkov [2013], and Sridharan and Allen [2013]. ORNL researchers (as well as others [Zheng 2016, Olson 2009, Liu 2013]) reported that the primary mechanism of alloy degradation in molten fluoride salts was selective dissolution of Cr from the alloy into the salt. It was found during TCL testing that samples in the hot side of the loop lost mass as a result of Cr dissolution, while samples in the cold side gained mass because of Cr deposition of from the hot side. Rather than the salt saturating in a static, isothermal experiment, mass transfer can occur in the $\sim 100^\circ\text{C}$ TCL temperature gradient. The thermal gradient in the TCL experiments is important because the solubility of Cr is dependent on the temperature of the salt. This dependence creates a situation in which Cr tends to dissolve in the hot part of the loop where solubility is high, and precipitate in the cold part of the loop where solubility is lower.

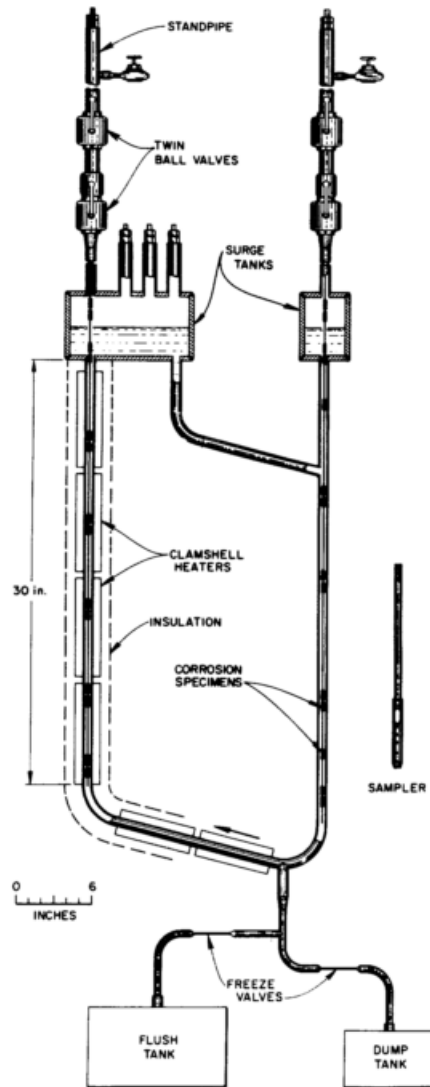


Figure 11. Schematic drawing of a thermal convection loop used for corrosion studies in molten fluoride at ORNL. Reproduced from Keiser [1977c]

Figure 12 shows corrosion (as depth of attack) of Ni-based alloy 600 (Table 1) in a thermal convection loop, in an experiment conducted by Manly [1957] at ORNL. After an initial stage of impurity-driven degradation, corrosion slows to a steady state rate determined by the precipitation and dissolution of species due to the thermal gradient in the TCL where the peak temperature was 815°C.

This steady state corrosion rate likely mimics the conditions in a reactor, as species are expected to dissolve in the reactor core. Thermal gradient loop experiments have also been conducted extensively by researchers at the Kurchatov Institute [Ignatiev, 2008, 2013a, 2013b].

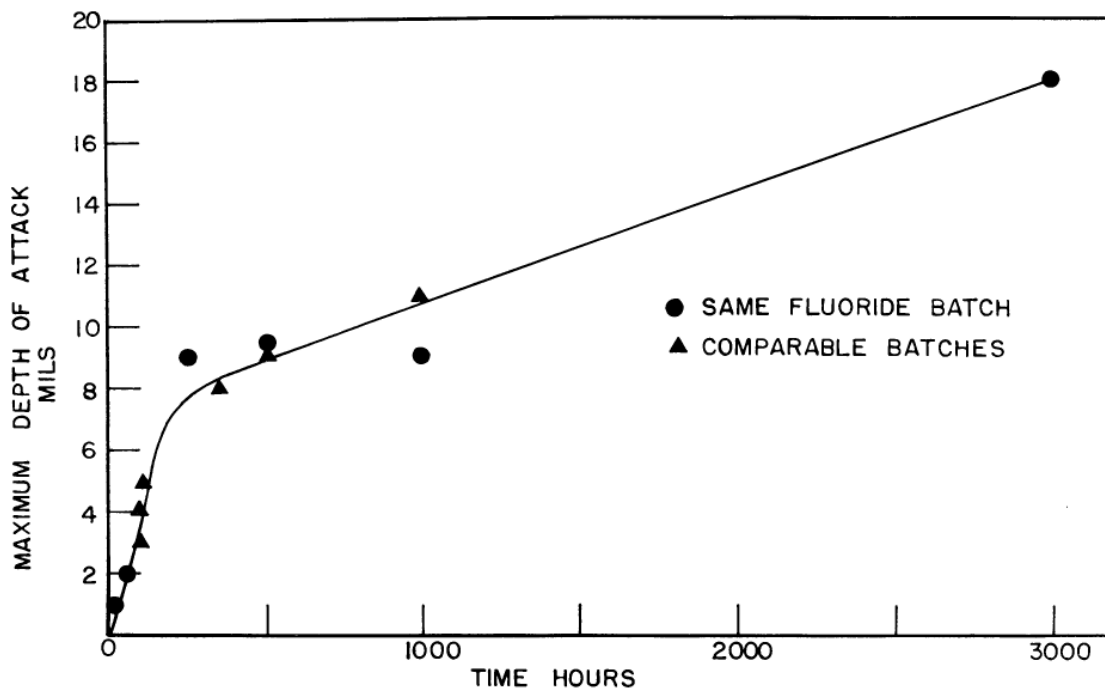


Figure 12. Corrosion of alloy 600 in a thermal convection loop with uranium containing FLiNaK salt at a temperature of 815°C in the hot leg. Depth of attack in mils (0.001" = 25µm). Reproduced from Manly [1957].

3.2.2 Forced convection loops

Studies at Brookhaven National Laboratory [Susskind, 1960] and ORNL [Macpherson 1959, Manly 1957, Koger 1972b] have examined corrosion in pumped loops, sometimes referred to as "forced convection loops." Tests at ORNL included thermal gradients, similar to the natural convective loops. These loops showed the same chromium depletion in the hot section and deposition in the cold section [DeVan, 1962]. No new corrosion mechanisms were discovered using pumped loops. However, pumped loops could produce prototypic conditions and more design relevant information than thermal convection loops. Because of the great expense involved with building and operating pumped loops, they are the final step in conducting corrosion experiments with prototypic materials and reactor conditions including quantifying the effects of velocity and thermal gradient on corrosion rates. Typically at this stage of development, corrosion testing was not the primary focus. Other experiments, such as thermal hydraulics (e.g. heat transfer and fluid mechanics), were emphasized.

3.3 ELECTROCHEMICAL MEASUREMENTS

Electrochemical measurements were used in molten salt experiments carried out at ORNL in the early 1960's to measure salt level in vessels [Hyland, 1962]. These early measurements had sensitivity of 1.3 mm (0.05") and used a single electrode contacting the salt. Electrochemical measurements have become more sophisticated in recent years, allowing for measurement of concentration of fission products as well as structural alloying elements [Mamantov 1966, Jenkins 1969, Tylka 2015a]. Electrochemical measurements were also used at ORNL to measure the U^{3+}/U^{4+} ratio in a salt melt [Rosenthal, 1972]. Measurements made at the time required insertion of the electrode when a measurement was desired to be made, and then removed afterward [Rosenthal, 1969]. A schematic of an electrode used to measure the U^{3+}/U^{4+} ratio is given in Figure 13. Platinum electrodes were used, with boron nitride spacers to avoid electrical contact.

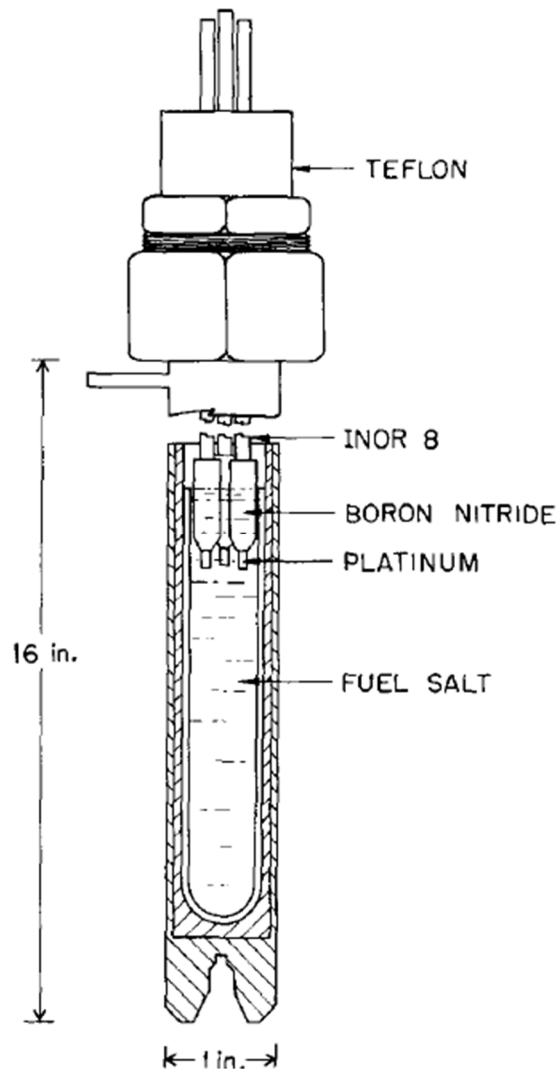


Figure 13. Schematic of apparatus for potentiodynamic measurements in molten salts, developed at ORNL [Rosenthal 1969].

A mathematical relation was determined for calculation of the uranium ratio using the $E_{1/2}$, or standard potential, value for the U^{3+}/U^{4+} couple, given as

$$E_{eq} - E_{1/2} = \frac{2.3RT}{nF} - \log \frac{U^{(IV)}}{U^{(III)}} \quad 3.1$$

In situ electrochemical measurements made this way rely on the fact that the redox reactions occurring for dissolution of metal ions into the molten salt have a characteristic potential. Such measurements were made at ORNL in $LiF-BeF_2-ZrF_4$ and $NaF-NbF_4$ salts. These techniques were accurate to the ppm range, verified through comparison to spectrographic data. One strength of these measurements is that they do not require a standard because the oxidation and reduction reactions measured have well known potentials. Wetting behavior of the salts to the electrodes was noticeably different in the ORNL studies, requiring different approaches in each salt.

Development of reference electrodes was attempted at ORNL in 1970. The primary thrust of the development was around the use of a single crystal LaF_3 as the ionic conductor between the reference and the melt. The single crystal was chosen due to its stability at temperatures above 500 °C, in which boron nitride was not stable. This allowed for ionic conductance through the mobile fluoride ions. However, this approach had unknown sources of extra potential and lost weight rather rapidly [Rosenthal 1970]. Further developments of electrodes in this era are outlined by Bamberger [1975]. Electrochemical measurements were also used at this time to screen for the presence of tellurium, a known agent of intergranular cracking [Keiser 1977a].

Extracting concentration data of individual species from these electrochemical measurements requires knowledge of the diffusion coefficient of the species being measured, an accurate area of the electrode, temperature of the melt, and the potential of the redox reaction being observed [Tylka 2015b]. This method showed precision within hundredths of wt.% when compared to ICP-AES.

Construction of the electrodes and understanding of how these measurements are made are critical in the accurate interpretation of the results yielded by these techniques.

3.4 KNOWLEDGE GAPS

3.4.1 Lack of standardized corrosion tests

Variability in corrosion experiments across different laboratories can lead to inconsistent and contradictory results. For example, inconsistencies in purification of salts, containment material and cover gases can result in vastly different outcomes. It is difficult to compare materials, salts, additives, etc. when the differences in outcomes associated with these variables are masked by uncontrolled variability in salt condition and test methodology.

3.4.2 Lack of recent data in flowing salts

Conducting experiments in flowing salts is much more difficult and costly than experimentation in static salts. While static experiments are useful, many phenomena such as mass transfer can only be recreated in flowing salt experiments. Further, if salt flow rates are high enough to prevent local equilibria at material-salt interfaces, pumped experiments that accurately mimic flow conditions may be important for accurately creating the thermodynamic conditions in MSR. Flowing experiments are especially important for fully understanding the behavior of salt additives, which may have temperature-dependent solubilities.

3.4.3 Corrosion sensors

Knowledge of the salt redox condition is a key input for understanding the conditions in an MSR and in a salt-corrosion experiment. Currently, electrochemical redox measurement is an immature technology. While solutions are in various stages of development, they must be considered research projects themselves, and not yet mature engineering solutions. Addressing this knowledge gap can lead to a better link between performance and salt conditions by linking redox measurements to specific corrosion rates

4. SALT CHEMISTRY AND PHYSICAL PROPERTIES

4.1 INTRODUCTION

Molten salts can be composed of a wide range of mixtures of simple, binary, stable compounds of alkali, alkaline-earth, and rare-earth cations that form mostly ionic interactions with halide and other anions. The term ‘molten’ refers to the liquid state of the salt at elevated temperatures; and much like water, molten salts flow and behave like liquids at liquidous temperatures.

4.2 SELECTION OF CANDIDATE COOLANTS IN MSR APPLICATIONS

The criteria for the selection of molten salt coolants was established by Grimes [1970]. He developed a set of screening criteria for both primary and secondary coolants and although published in the late 1960s and early 1970s, Grimes’ molten salt coolant selection criteria still apply today. Based on these criteria the salt coolant candidates must:

- 1) Exhibit chemical stability above 800 °C,
- 2) Be stable under irradiation conditions (primary coolants),
- 3) Have a useful melting point (less than 525 °C) and have low volatility,
- 4) Be compatible with alloys and graphite (graphite is only present in thermal reactors),
- 5) Have low capture neutron cross section, less than 1 barn (primary coolants), and
- 6) Dissolve useful amounts of fertile and fissile material (fuel salts).

Several fluoride and chloride salt compositions meet the above criteria and are discussed below.

Fluorides

Three basic systems which have favorable neutronic and thermophysical properties as well as compatibility with Ni-based alloys are: 1) alkali fluorides, 2) ZrF₄ salt mixtures and 3) BeF₂ salt mixtures [Williams 2006]. For fluoride-salt-cooled high-temperature reactors (FHRs) the preferred primary coolant is the peritectic LiF-BeF₂ (FLiBe) composition with the relative molar ratio of 2 to 1, respectively. FLiBe is the top candidate as a primary coolant due to its low neutron cross section, chemical stability, thermophysical properties and low corrosion rates with Ni-based alloys [Kato 1983, Benes 2009]. Another potential candidate for primary cooling in FHRs is the NaF-ZrF₄ with the molar composition 59.5 % of NaF and 40.5 % ZrF₄ [Williams 2006]. Advantages of using NaF-ZrF₄ over FLiBe include no beryllium toxicity, no tritium production and lower cost. However, it has less attractive neutronic and thermophysical properties and a higher vapor pressure when compared to FLiBe. For secondary loop coolants, neutronic properties are not a concern since these fluids are only used for their thermal transport properties. FLiNaK, which is a composition containing LiF, NaF and KF in 46.5-11.5-42 mol.% ratio, respectively, is a potential candidate for secondary cooling in FHRs. FLiNaK has a melting point similar to FLiBe, relatively large heat capacity, comparable corrosion rates to those of FLiBe salt, low vapor pressure and high stability at elevated temperature. Chloride and nitrate salts are also candidates for secondary salts.

Chlorides

As is the case with fluoride salts, most chloride-containing molten salts have favorable properties such as low melting point (less than 550 °C), large CTE, good solvent properties for fissile materials, thermal and radiolytic stability, low vapor pressure, and excellent heat transfer properties. Due to its favorable nuclear, chemical and physical properties, NaCl has been studied in the past with actinide chlorides such as UCl_{4/3} and PuCl₃ [Bulmer 1956, Harder 1969].

Both CaCl_2 and MgCl_2 form eutectic melts with NaCl that have significantly lower melting points than do the individual salts. CaCl_2 - NaCl eutectic melting point is around 507°C and that of MgCl_2 - NaCl is 445°C . KCl - MgCl_2 , NaCl - MgCl_2 , and KCl - NaCl - MgCl_2 are commonly discussed coolant salts for CSP and/or MSR secondary loops.

In terms of material compatibility with chloride salts, limited literature reports suggest that the chloride salts are not particularly aggressive to structural materials such as stainless steel without the presence of oxygen and/or water. However, in practice, chloride salts are usually shown to be more aggressive to alloys than fluoride salts [Raiman 2018], likely due to the greater difficulty in removing impurities. Most of this data, however, is based on chloride salts containing MgCl_2 , a particularly hygroscopic species. Little data is available on chloride-based fuel salts [Harder 1969].

4.3 HALIDE SALTS PROPERTIES

Stability

Alkali and alkaline-earth halide salts are thermodynamically stable ionic compounds. Standard Gibbs free energy of formation, shown in Table 3, is a useful comparison of the relative stabilities of these ionic compounds [Glassner 1957]. In general, the trend is that with increasing anion size, standard Gibbs free energy of formation becomes more positive, and the relative stability of halide salts decreases. Among the Group 1 halide salts, fluorides are the most stable followed by chlorides, bromides and iodides.

In terms of the thermochemical stability of fluorides, the general trend is that pre-transition metal fluorides and tetravalent actinides (*e.g.*, UF_4) have enthalpies of formation more negative than -420 kJ mol^{-1} and are more stable compared to fluorides of transition metals which have enthalpies of formation in the range of -330 to -420 kJ mol^{-1} [Baes, 1974; Köhler, 2014]. The relatively lower stability of transition metal fluorides is beneficial since most structural materials are made of transition metals. The greater stability of Groups I - IV and actinide fluorides compared to transition metal fluorides means that the exchange of the fluoride anion between the salt and alloy metals in molten fluoride coolant and fuel salts will be minimal. The Gibbs free energy of formation illustrates the key driving force for corrosion in structural alloys. Table 3 shows the Gibbs free energy of formation for some common salt constituents as well as fluorides and chlorides of common alloying elements [Grimes 1967, Forsberg 2004, Olson 2009, Sohal 2010]. Alloy-metal halides have free energies of formation more positive compared to coolant salt halide constituents. This means that the formation of halides with alloying elements is not spontaneous in common coolant salts and therefore thermodynamic-driven corrosion caused by pure salts should be minimal. However, in the presence of impurities such as HCl or HF , the corrosion of structural alloys proceeds with increasing nobility of the alloy metal constituents. For example, Figure 14 shows that CrF_2 (and CrCl_2) have ΔG values that are more negative compared to NiF_2 (and NiCl_2 , respectively) which indicates that Cr is most prone to corrosion attack. Previous experimental data obtained from exposing Cr- and Ni-containing alloys to molten fluoride and chloride environments confirm the preferential leaching of Cr from the alloy [DeVan 1962; Raiman 2018].

Table 3. Compositions and melting points for common fluoride and chloride coolant salts. Adapted from [Forsberg, 2004; Williams, 2008]

Fluoride Coolants	Composition (mol%)	Melting point (°C)	Chloride Coolants	Composition (mol%)	Melting point (°C)
LiF-KF	50-50	492	LiCl-KCl	59.5-40.5	355
LiF-RbF	44-56	470	LiCl-RbCl	58-42	313
LiF-NaF-KF (FLiNaK)	46.5-11.5-42	454	NaCl-MgCl ₂	58-42	445
LiF-NaF-RbF	42-6-52	435	NaCl-MgCl ₂	63-37	475
LiF-BeF ₂ (FLiBe)	67-33	460	KCl-MgCl ₂	68-32	426
LiF-BeF ₂ -ZrF ₄	64.5-30.5-5	428	NaCl-KCl-MgCl ₂	30-20-50	396
NaF-BeF ₂	57-43	340	LiCl-KCl-MgCl ₂	55-40-5	323
LiF-NaF-BeF ₂	31-31-38	315			
LiF-ZrF ₄	51-49	509			
NaF-ZrF ₄	59.5-40.5	500			
LiF-NaF-ZrF ₄	42-29-29	460			
NaF-RbF-ZrF ₄	33-24-43	420			
RbF-ZrF ₄	58-42	410			
KF-ZrF ₄	58-42	390			

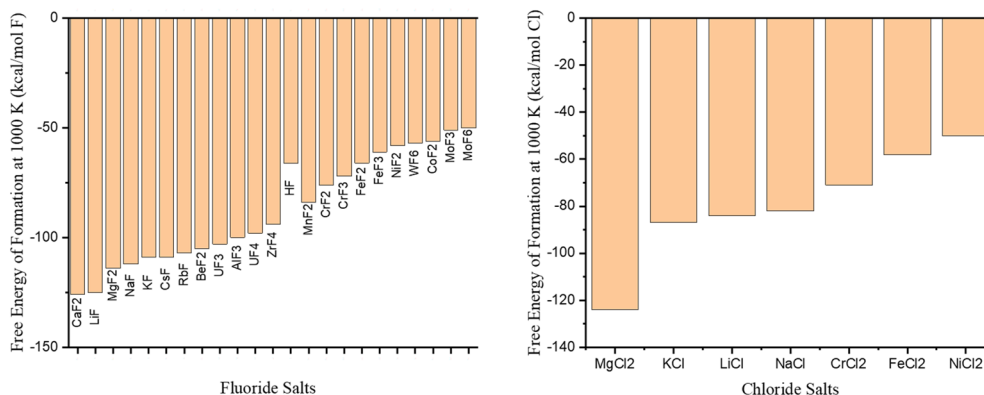


Figure 14. Comparison of free energies of formation between various fluoride and chloride salts including common structural alloy metal fluorides and chlorides. Compiled from [Chase 1985, Gurvich 1994]

Melting Points and Eutectic Mixtures

Melting or freezing point of a coolant material is one of its most important thermophysical properties. Individual alkali and alkaline-earth halides in their pure forms melt at temperatures that are, in most cases, too high for their use as coolants in nuclear reactors. This is especially true for alkali fluorides which melt above 800 °C. However, selective addition of a secondary component can result in a binary mixture

where the freezing point is significantly depressed. When pure salts are combined in a molar ratio such that a minimum freezing point is reached, these mixtures of two or more salts are called eutectic points. Typically, binary mixtures can lower the freezing point by up to 500 °C compared to their pure salt components. Further, addition of a third salt can lower the freezing point by up to another 50 °C. Binary alkali and alkaline-earth halide mixtures have been thoroughly explored by construction of phase diagrams that illustrate their melting properties. Ternary phase diagrams of group I and II halides also exist but are not as explored as the binary mixtures. Less common, a fourth or fifth component is added to the salt mixture, but this is usually done to alter certain chemical or physical properties of the salt rather than to lower the freezing point.

Vapor Pressure

In most cases, molten fluoride and chloride salts have very low vapor pressures (far less than 1 bar) below 900 °C [Williams 2008]. However, even with such low vapor pressures, it is beneficial to use salts with vapor pressures below 0.2 kPa (0.002 bar) to simplify design and prevent loss of salt through cover-gas exhaust. Mixtures of salts containing high compositions of BeF₂ and ZrF₄ can have vapor pressures greater than 0.2 kPa at 900 °C as is the case with LiF-ZrF₄, NaF-ZrF₄ with vapor pressures 10.3 and 0.67 kPa at 900 °C, respectively. Borofluoride salts such as NaF-NaBF₄ are impractical as a coolant due to their high vapor pressure (1270 kPa at 900 °C). Chloride salts containing MgCl₂ have vapor pressures slightly higher than 0.2 kPa (0.3 kPa for NaCl-MgCl₂) but this does not restrict their use as coolant salts [Williams 2008].

Density and Viscosity

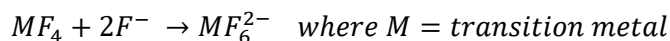
Density and viscosity values of fluoride and chloride molten salts are not particularly restrictive. These values are only considered when discussing heat transfer properties of the salts. Exceptions are BeF₂- and ZrF₄-containing salts as they tend to be more viscous. Viscosity of LiF-BeF₂ (FLiBe) is 5.6 mPa·s compared to LiF-NaF-KF (FLiNaK) 2.9 mPa·s. For BeF₂ salts, compositions with greater than 45% BeF₂ form extremely viscous mixtures and their use should be avoided due to their poor fluid dynamics properties [Cohen, 1957, Williams 2006, 2008].

Heat Transfer: Heat Capacity and Thermal conductivity

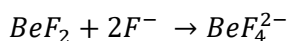
Both fluoride and chloride molten salts are excellent heat transfer media with large specific heat and large CTE. Lighter alkali metal-containing halide salts are somewhat better heat transfer media, but these differences are not limiting factors for the use of heavier alkali halide counterparts.

4.4 ACID-BASE CHEMISTRY

One of the commonly overlooked topics in molten salt chemistry is the Lewis acid-base behavior of salt species. A Lewis acid is simply a species that can accept an electron pair while a Lewis base is an electron pair donor. Acidic salts are typically composed of di-, tri- or multi-valent metal ions that can easily form complexes with Lewis bases such as F⁻. [Baes, 1974]



Because of their relatively high charge, alkaline-earth metals such as Be are also considered Lewis acids and can form complexes with Lewis bases according to the chemical equation below.



The Lewis acidity of these salts impacts their physical properties such as density and viscosity as discussed above. Similar effects can be expected when transition metal (alloy corrosion products) fluorides or chlorides are present in the molten salt. However, the effect of corrosion products on molten salt properties are not well known and require further investigation.

4.5 IMPURITIES IN MOLTEN SALTS

Fluoride and chloride salts are typically obtained through commercial salt providers as individual binary salts (e.g., NaF, NaCl, etc.). While certain manufacturers provide salts that are relatively pure, they are still unusable as coolant salts in their raw form due to detrimental effects of chemical corrosion on container materials by trace impurities. Fluoride and chloride salts generally contain water, oxides, HF/HCl, sulfates, sulfides and bromides as impurities. Among these, water and oxygen have been given the most attention due to their relative persistence and corrosiveness at elevated temperatures. Halide salts are ionic compounds and are very hygroscopic. In their dry form, halide salts are considered some of the best desiccants. They readily form hydrates and hydroxides at room temperature and oxides upon heating. Stability of oxygen-containing species varies with temperature and environmental conditions. For this reason, purification of halide salts with respect to removal of oxygen-containing species (water, hydroxide, oxide, etc.) requires understanding of chemistries and stabilities of hydrates, hydroxides, oxyhalides, hydroxyhalides and oxides within a given halide salt matrix. Purification of halide salts will be discussed in greater detail in chapter 5. Corrosion issues due to salt impurities are discussed further in Chapter 6.

4.6 KNOWLEDGE GAPS

4.6.1 Lack of understanding of salt purity

Pure alkali and alkaline-earth halides are thought to be compatible with structural materials with low corrosion rates especially with Ni-based alloys. However, impurities such as oxygen and moisture significantly increase corrosion rates in structural materials. One of the biggest gaps in knowledge is the lack of reliable studies that correlate specific impurity species and concentration corrosivity. This knowledge is required for setting data-informed limits on impurity concentrations.

4.6.2 Lack of reliable quantification of impurities

Related to the previous gap, there is a need for a reliable method for quantification of impurities in molten salts. Especially important are corrosive impurities. Trace metals impurities can be quantified reliably by inductively coupled plasma (ICP) methods. However, methods for quantification of anionic impurities such as oxides, hydroxides, oxyhalides, etc. are not well developed. Standardizing the quantification of corrosive anionic impurities would allow for better understanding of corrosion mechanism of alloys in molten salts by linking the findings from corrosion studies to relevant salt properties.

5. SALT PREPARATION AND PURIFICATION

5.1 INTRODUCTION

The level of impurities present in halide salts largely influences their thermophysical and chemical properties such as heat capacity, heat conductivity and corrosivity towards containment materials. Halide salts have been purified by various methods depending on the nature and stability of impurities [Shaffer 1971], including controlled heating to vaporize water [White 1983], vacuum techniques [White 1983], chemical drying agents [White 1983], fluorination and chlorination methods [Ingersoll 2006, Olander

2002, Olson 2009], ammonium bifluoride reaction for fluorides [White, 1983] and physical filtration to remove undissolved solids.

For the most part, dehydration and deoxygenation of fluoride and chloride salts can be achieved by sequential slow heating up to the melting point under continuous flow of an inert gas. However, stable oxide solid impurities are typically not removed by simple heating. In addition, hydrolysis products such as oxychlorides and oxyfluorides can be formed in the presence of water. When chloride and fluoride salts hydrolyze, they release corrosive hydrochloric (HCl) or hydrofluoric (HF) acid byproducts, respectively [Mathews 1967, Kurley 2019]. When in contact with alloy containment materials, HCl and HF react with the alloy surfaces causing depletion of the least noble transition metal constituents of the alloy (Mn, Al, Cr, Fe, Ni, in order of reactivity). Over time, the rate of corrosion can be sustained as long as the corrosive impurities are present in the molten salt. The effect of sustained impurity-driven corrosion can lead to buildup of corrosion products on the surfaces of alloys and can be detrimental to the properties of the alloys. The corrosion of alloys can cause possible blockage in piping and can weaken the strength of alloys. These risks are particularly exacerbated at high temperatures due to increased reaction kinetics between corrosive impurities and alloy constituents. In addition to corrosion effects, impurities can significantly affect thermophysical properties of molten salts.

5.2 IMPURITIES IN MOLTEN SALTS

Commercial chloride salts such as NaCl, KCl and MgCl₂ are sourced from salt mines around the world. Sea water, which contains about 35 g of salt per liter (mostly NaCl), is an important source of chloride salts. Manufacturers produce salts in various levels of purities which are typically measured on the basis of metallic impurities only, and can range from low to ultra-high, 99.999% purity. The high purity salts are typically produced on smaller scales and are not economically viable for large scale uses including their use as heat transfer media in next generation MSR or CSP thermal storage. Moreover, since the purity is measured in metals basis, it provides no information on the level of water present in the salts. Because of its high corrosivity to alloys at high temperatures, water is the main corrosion concern in molten salts. The level of moisture present in salts varies based on the identity of the salt, purity level and the amount of time the salt is exposed to air or other wet environments prior to being used. As an example, if left on a bench, anhydrous magnesium chloride will gradually absorb water from the air resulting in the formation of hydrates that vary from one water molecule (monohydrate) per MgCl₂ to up to 12 water molecules per mole of MgCl₂. Fluoride salts such as LiF, NaF, KF, BeF₂ are generally less hygroscopic compared to chloride salts but impurity water is still one of the main concerns [Punwani 1968] Other impurities that are commonly present in both fluoride and chloride salts are bromides and iodides (NaBr, NaI, KBr, KI, etc.), oxides (MgO, BeO, Na₂O, Li₂O, etc.), hydroxides (NaOH, LiOH, KOH, Mg(OH)₂, etc.), sulfates (Na₂SO₄, Li₂SO₄, MgSO₄, etc.) and transition metals (Fe, Cr and others). The effect of these impurities on molten salt properties including corrosivity and thermophysical properties is, for the most part, unknown.

5.3 ANALYSIS AND QUANTIFICATION OF IMPURITIES IN MOLTEN SALTS

Because impurities can negatively affect molten salt properties, quantification and characterization of impurities in molten salts is important. Several traditional analytical methods can be used to quantify various impurities in molten salts.

Elemental composition

For elemental composition, bulk methods such as ICP with mass spectrometry (MS) or optical emission spectroscopy (OES) detection can be used to quantify trace alkali, alkaline-earth, transition and rare-earth metals. In addition, some main group elements can also be quantified using ICP-MS and/or ICP-OES.

Low-level, parts per million (< 20) detection is common but detection down to parts per billion can be achieved in some cases with both ICP methods. The strength of these techniques is their low-level detection and the ability to analyze a wide range of elements. The main drawback of ICP methods is sampling, matrix effects and the requirement of standards.

Another complimentary method that can be used to analyze various elemental impurities in salts is glow discharge mass spectrometry (GDMS). As an example, GDMS analysis of fluoride salts is shown in Tables 4 and 5. The advantage of this method is that little or no sample preparation is needed and the detection of low-level impurities, down to low parts per million concentrations. However, because the analysis of impurities depends on what portion of the sample was used during the measurement, some compositional inconsistencies can arise compared to the bulk analysis methods such as ICP.

Table 4. Elemental impurity analysis by glow discharge mass spectrometry of BeF₂-LiF salt purified by HF fluorination*

(ppm wt.)	Li	Be	B	O	F	Na	Mg	Al	Si	P	S	Cl	K
FLiBe	Matrix	Matrix	< 0.1	-	Matrix	130	15	4.9	0.75	< 0.5	< 0.5	< 0.5	8.7
	Ca	Sc	Ti	V	Cr	Mn	Fe	Co	Ni	Cu	Zn	Ga	Ge
FLiBe	14	< 0.05	< 0.5	< 0.1	2.4	1	1.2	< 0.5	< 1	< 1	< 5	< 0.5	< 1
	As	Se	Br	Rb	Sr	Y	Zr	Nb	Mo	Ru	Rh	Pd	Ag
FLiBe	< 1	< 5	< 5	< 0.5	< 0.5	< 1	< 1	< 20	< 10	< 0.5	< 0.1	< 0.5	< 0.5
	Cd	In	Sn	Sb	Te	I	Cs	Ba	La	Ce	Pr	Nd	Sm
FLiBe	< 1	< 1	< 1	< 1	< 1	< 10	< 0.5	0.72	< 0.1	< 0.1	< 0.1	< 0.1	< 0.1
	Eu	Gd	Tb	Dy	Ho	Er	Tm	Yb	Lu	Hf	Ta	W	Re
FLiBe	< 0.1	< 0.1	< 0.1	< 0.1	< 0.1	< 0.1	< 0.1	< 0.1	< 0.1	< 1	Electrode	< 2	< 0.5
	Os	Ir	Pt	Au	Hg	Tl	Pb	Bi	Th	U			
FLiBe	< 0.1	< 0.1	< 0.5	Interference	< 1	< 0.5	< 0.5	< 5	< 0.1	< 0.1			

*Research funded by DOE Nuclear Energy, Advanced Reactor Campaign

Table 5. Elemental impurity analysis by glow discharge mass spectrometry in two different batches of LiF-NaF-KF salt purified by HF fluorination.*

(ppm wt.)	Li	Be	B	C	N	O	F	Na	Mg	Al	Si	P	S
FLiNaK-1	Matrix	< 0.05	4.9	-	-	-	Matrix	Matrix	36	12	190	3.4	2.5
FLiNaK-2	Matrix	< 0.05	0.15	-	-	-	Matrix	Matrix	19	10	1.9	< 0.05	< 0.5
	Cl	K	Ca	Sc	Ti	V	Cr	Mn	Fe	Co	Ni	Cu	Zn
FLiNaK-1	87	Matrix	21	< 0.05	3.1	< 0.05	24	7.6	66	3.5	230	< 1	< 1
FLiNaK-2	6.1	Matrix	48	< 0.05	24	< 0.05	3.6	0.7	1	< 1	1.9	< 1	< 1
	Ga	Ge	As	Se	Br	Rb	Sr	Y	Zr	Nb	Mo	Ru	Rh
FLiNaK-1	< 0.1	< 0.5	< 5	< 5	< 5	28	0.5	< 0.1	< 0.1	< 10	< 5	< 0.1	< 1
FLiNaK-2	< 0.1	< 0.5	< 5	< 5	< 5	6.1	1.4	< 0.1	230	25	< 5	< 0.1	< 1
	Pd	Ag	Cd	In	Sn	Sb	Te	I	Cs	Ba	La	Ce	Pr
FLiNaK-1	< 0.5	< 0.5	< 1	< 1	< 0.5	< 0.5	< 5	< 10	< 0.5	0.82	< 0.5	< 0.1	< 0.1
FLiNaK-2	< 0.5	< 1	< 1	< 1	< 0.5	< 0.5	< 5	< 10	< 0.5	110	< 0.5	< 0.1	< 0.1
	Nd	Sm	Eu	Gd	Tb	Dy	Ho	Er	Tm	Yb	Lu	Hf	Ta
FLiNaK-1	< 0.1	< 0.1	< 0.1	< 0.1	< 0.1	< 0.1	< 0.1	< 0.1	< 0.1	< 0.1	< 0.1	< 1	Electrode
FLiNaK-2	< 0.1	< 0.1	< 0.1	< 0.1	< 0.1	< 0.1	< 0.1	< 0.1	< 0.1	< 0.1	< 0.1	< 1	Electrode
	W	Re	Os	Ir	Pt	Au	Hg	Tl	Pb	Bi	Th	U	
FLiNaK-1	< 5	< 0.5	< 0.1	< 0.1	< 5	Interference	< 1	< 1	< 0.5	< 0.5	< 0.01	< 0.01	
FLiNaK-2	< 5	< 0.5	< 0.1	< 0.1	< 5	Interference	< 1	< 1	< 0.5	< 0.5	< 0.01	< 0.01	

*Research funded by DOE Nuclear Energy, Advanced Reactor Campaign

Scanning electron microscopy coupled to energy-dispersive x-ray spectroscopy (SEM-EDS) can be used to identify impurities in salt samples. However, this technique is not convenient for bulk analysis and is not considered fully quantitative, especially for light elements.

Oxygen, hydrogen and sulfur

Water is an ever-present impurity in salts and because of its corrosivity towards salt-facing alloys, it is one of the most important impurities to quantify and remove from salts. Analyzing oxygen and hydrogen in molten salts can provide information on the levels of water present. In the late 1960s and 1970s, oxygen was quantified by the reaction of bromofluorides, BrF₃ and KBrF₄, and the oxides present in the

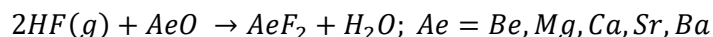
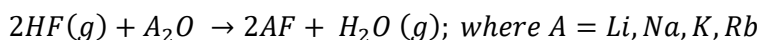
salt [Kirtchik 1965, Goldberg 1960]. However, the use of BrF_3 is extremely dangerous due to its explosiveness, and therefore it is not an ideal method for quantification of oxygen. Currently, combustion analysis is routinely used to quantify O, H, C, N and S in organic and inorganic samples. This technique is not commonly applied to molten salt samples due to instrument limitations. Current research at ORNL and ANL aims to qualify this emerging tool for oxygen analysis in molten salts.

Despite some recent progress in analysis of impurities in molten salts, further research is still needed to develop new and robust methods to analyze corrosive impurities in molten salts.

5.3.1 Chemical fluorination for purification of fluoride salts

Fluorination by HF

Oxide impurities in salts are common. Given their refractory nature and high melting points, oxides cannot be removed easily by controlled heating and vacuum techniques. For fluoride salts, chemical fluorination by dry HF/H_2 gas flow at melt temperatures can effectively convert alkali and alkaline-earth oxides to alkali fluorides with water vapor as the only by-product [Shaffer 1971]. The water vapor is flushed by a continuous flow of an inert gas such as argon. Fluorination of oxide impurities by HF gas at melt temperatures is shown by the two reactions below.



Alternative fluorination routes

Though widely used, HF is a highly toxic and corrosive gas at room temperature. Special care during transportation and handling is required for safe operation with HF. In addition, costly laboratory safety engineering is necessary to prevent accidents and reduce risks associated with the use of HF. Given the high toxicity of HF, alternative routes of purification with lower toxicity chemicals are desired.

Fluorination by NF_3

Nitrogen trifluoride (NF_3) has recently been proposed as an alternative fluorine source for purification of fluoride salts [Scheele 2010]. NF_3 has been used in the past in the semiconductor industry as an etchant and cleaning agent of various parts and chambers. It is listed as an oxidant; it is only mildly toxic, non-corrosive and non-reactive at room temperature. Because of its relatively lower toxicity compared to HF, NF_3 is easier to manage from an engineering and hazards standpoint.

In terms of its viability as a fluorinating agent towards common impurities in alkali and alkaline-earth fluorides, NF_3 seems to be much more favorable compared to HF [Scheele 2010]. Thermodynamics (Gibbs free energy of formation, kJ/mol F) comparison of HF and NF_3 for the fluorination reactions are illustrated in Figure 15 below. From the thermodynamics perspective, the more negative ΔG values for reactions involving NF_3 show that NF_3 is a stronger fluorinating agent at all temperatures. With an increase in temperature HF tends to be less favorable as a fluorinating agent while NF_3 shows the opposite trend. Additionally, NF_3 may be more effective at temperatures around the melting points of the common fluoride salt eutectic mixtures between 300 and 500 °C. These possible strengths have not yet been supported by experimental evidence, and the fact that ORNL researchers chose H_2/HF as a purifying agent over NF_3 suggests there may be some disadvantages that are not available in literature such as reactions with the container vessel.

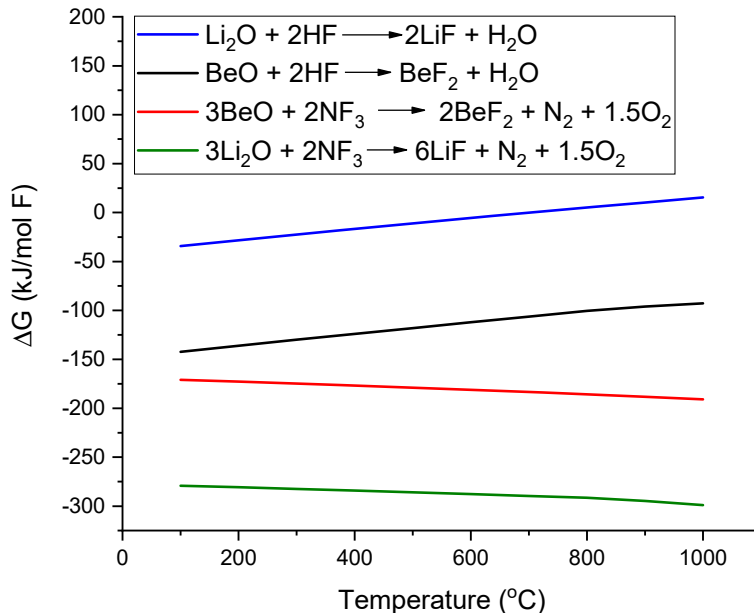


Figure 15. Thermodynamics comparison of HF vs. NF₃ as fluorinating agents for common oxide impurities in fluoride salts. Reproduced from Scheele and Casella [2010].

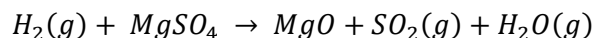
Ammonium bifluoride

While fluorination by hydrofluoric acid has been the preferred purification method of fluoride salts, its use requires special monitoring equipment and safety engineering that oftentimes is not economically viable on smaller laboratory scales. Ammonium bifluoride as a fluorinating agent has been used at ORNL for fluoride salt purification [Long 1948, Friedman 1963, Afonichkin 2011, O’Hara 2017] Ammonium bifluoride (NH₄HF₂) has intrinsic safety advantages over HF gas. NH₄HF₂ is a solid at room temperature (T_m=125 °C) and as such is convenient and safer to use for the conversion of oxides such as UO₂ to anhydrous fluoride UF₄.



Sulfur, sulfates and halide impurities

Sulfur is typically found in the form of sulfates (SO₄²⁻) in chloride and fluoride salt melts. Alkali and alkaline-earth sulfates are relatively stable compounds. Apart from beryllium sulfate (BeSO₄), all alkali and alkaline-earth sulfates melt at temperatures above 800 °C and have boiling points that are above 1000 °C [Chase 1985]. In addition to their high temperature stability, they are readily soluble in molten salt media which precludes their separation by physical filtration. To get rid of sulfate impurities, chemical sparging of the melt is necessary. Conveniently, during the oxide removal via chemical fluorination and chlorination, sulfates are also converted to fluorides and chlorides, respectively. The byproducts of the reaction are gaseous SO₂ and H₂O.



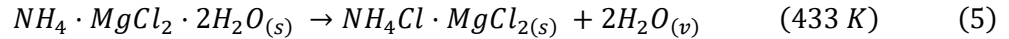
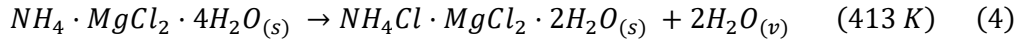
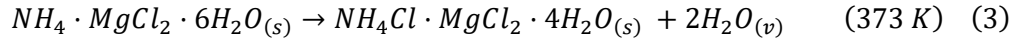
5.3.2 Chemical dehydration for removal of moisture

Most alkali metal halides are relatively easily dehydrated by sequential heating and vacuum drying methods. However, some alkaline-earth metals, such as Mg, form stable oxyhalide species up to the

melting temperatures which precludes sequential drying and vacuum techniques as means of oxide impurity removal. $MgCl_2$ is very hygroscopic and forms multiple hydrates ($MgCl_2 \cdot nH_2O$, $n = 1, 2, 4, 6, 8, 12$) [Kipouros 2001]. During the sequential thermal dehydration, the last monohydrate, $MgCl_2 \cdot H_2O$ decomposes to magnesium hydroxylchloride at temperatures up to 527 °C according to equation 1 below.



At higher temperatures, the hydroxylchloride is converted to the oxide with HCl as a byproduct, equation 2. According to Le Chatelier's principle, avoiding the formation of oxychlorides and oxides would require high vapor pressure of HCl or other chlorinating agents. To help drive the dehydration of magnesium chloride with minimal oxychloride and oxide formation, the $NH_4Cl \cdot MgCl_2$ carnallite double salt method was used [Kipouros 2001, Kurley 2019, Mayes 2018]. The dehydration of the ammonium double salt occurs according to the following reactions.



Upon complete removal of water from ammonium carnallite, the dehydrated double salt is then heated above 573 K (300 °C) to yield dehydrated $MgCl_2$.



In addition to oxygen and water impurities, the as-received salt contains hydroxide, oxychloride and oxide impurities. To get rid of these impurities the purification requires the use of strong chlorinating agents such as Cl_2/CO , $SOCl_2$ or CCl_4 at elevated temperatures. While Cl_2/CO chlorination is more economical and suitable on an industrial scale, CCl_4 chlorination offers a more practical approach on lab scale. The process of chlorination of MgO by CCl_4 has shown recent success [Mayes 2018, Kurley 2019, Pint 2019].

5.4 TECHNICAL GAP ANALYSIS

Coolant/heat transfer salt candidates contain impurities that significantly affect their usability in molten salt reactors. The main concern with impurities is their reactivity (both corrosion and possible thermal embrittlement) towards containment materials. Corrosive impurities such as water, oxyfluorides, oxychlorides, HF and HCl attack structural materials by reacting with the least noble alloying elements (Cr, Mn, Fe) and thereby significantly affecting their performance. In addition to the above-mentioned corrosive impurities, other impurities that may affect the integrity of structural materials are oxides, sulphates, carbonates, bromides, iodides, transition metals, etc. Control of these impurities from molten salts is imperative before their use in nuclear reactors. We identified a few technical knowledge gaps related to salt purity and purification process that should be considered.

5.4.1 Standards for salt purity at delivery

In addition to the standardization of salt purity in operation mentioned in the previous chapter, standards should be set for salt purity upon delivery. To decide "how pure is pure enough", one must consider corrosivity of impurities contained in molten salts. Designed corrosion experiments probing the

correlation between the type and level of impurities present in salts and the attack on structural alloy specimens are critical to addressing this knowledge gap. This data can then inform salt purity standards.

5.4.2 Quantifying impurities in molten salts

Traditional methods to quantify low level impurities are not well suited for molten salt applications because of the reactivity and harsh nature of molten salt environments which are damaging to instruments. Common techniques are available for finding metallic impurities, but no well-qualified standard solutions exist for quantifying anionic impurities

6. CORROSION AND MECHANICAL PROPERTIES

6.1 INTRODUCTION

Corrosion and mechanical properties are closely linked, since the loss of component integrity due to material loss is one of the primary negative consequences of corrosion. Most of this report has focused on non-localized corrosion, but environmentally assisted cracking also must be addressed. As noted in the Introduction, specific alloy corrosion rates are not summarized here because of the difficulty in comparing data between laboratories (all using different test conditions and salt purities) and the limited data available under prototypic flowing conditions.

6.2 TELLURIUM EMBRITTLEMENT

Post-exposure analysis of salt-facing materials from the MSRE identified Te in the grain boundaries of salt-facing alloy N structures. [McCoy 1972a] Te was generated as a fission product during the experiment. The observed combination of Te exposure and applied stress simultaneously worsened the extent of intergranular cracking when compared to the same materials without Te penetration.

To effectively simulate the effects of Te in the MSRE, Keiser et al. [1977a, 1976] exposed alloy N coupons to FLiBe-based salts with added Cr_3Te_4 or $\text{CrTe}_{1.266}$. Alloying elements, such as Nb or Ti, were added to the material to mitigate the effects. Ti appeared to have minimal effect, but as little as 1 wt.% Nb addition was sufficient to prevent Te intergranular attack without affecting the material's resistance to corrosion. Additionally, Keiser et al. [1977a] found that keeping the U(IV)/U(III) ratio below 60, though the use of Be additions effectively prevented Te-embrittlement from occurring in the standard Alloy N composition.

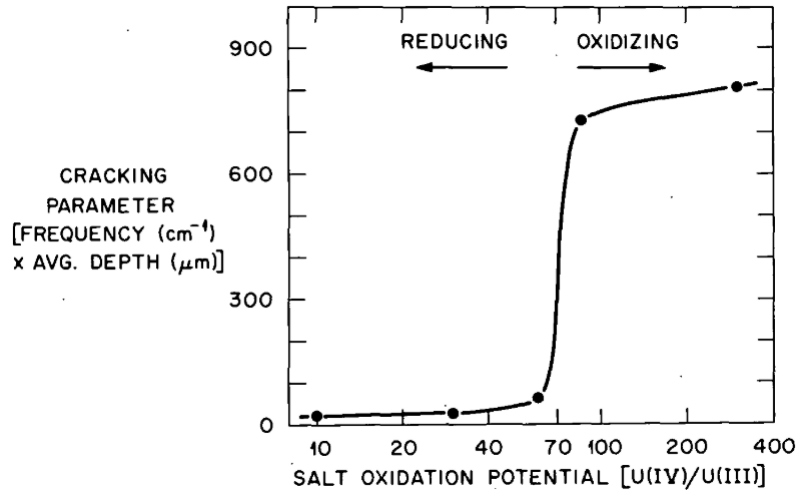


Figure 16. Cracking behavior of Alloy-N exposed 260 h at 700°C to MSBR Fuel Salt Containing CrTe1.266.
Reproduced from Keiser. [Keiser 1977a]

Ignat'ev et al. [2016] observed similar effects when exposing modified Alloy-N to fluoride salt loaded with Te fission product simulants. However, they observed that adding ~1wt% Nb to the alloy did not negate the effects of Te in the salt, contrary to the findings of Keiser et al. [1977a]. The discrepancy may be explained by a few experimental differences between the experiments run by Keiser and Ignat'ev. Ignat'ev et al. added elemental Te to the salt, while Keiser added Te as CrTe. Also, the experiments run by Ignat'ev were conducted at temperatures ~100°C hotter. It is unclear which was the cause of the discrepancy, or which result is the correct one. Additionally, Ignat'ev exposed non-modified alloy N and KhN80MTYu, a Ni-based alloy lower in Mo, Fe, and Si with more Ti and Al (Table 1). They found KhN80MTYu withstood Te embrittlement at higher U(IV)/U(III) ratios better than alloy N or an alloy N variant with ~1% Nb addition. However, the ultimate tensile strength of KhN80MTYu was ~15% lower than the other alloys.

Fabre et al. [2013] exposed the Ni-based alloy C22 to $\text{LiF-CaF}_2\text{-MgF}_2\text{-ZrF}_4$ and varied the fluorine potential using an electrochemical cell to observe the effect on Te embrittlement. They found significant grain boundary embrittlement when a C22 specimen was exposed to Te vapor while immersed in salt. Fabre proposed that this effect was due to formation of brittle metal telluride compounds that form along the grain boundaries of salt-facing surfaces. The phase diagram of Zr-Te-F-O was calculated to determine how the fluorine potential affects telluride compound formation (Figure 17). From the diagram, a potential of -3.1V with respect to $\text{F}^-/\text{F}_2(\text{gas})$ is below the region of stability for Ni_2Te_3 or Mo_3Te_4 . When Fabre exposed a C22 specimen to salt with Te vapor at a potential of -3.4V, minimal signs of Te embrittlement were observed. This is consistent with the observation by Keiser et al. [1977a] that maintaining more reducing conditions in the salt minimizes grain-boundary embrittlement due to Te. Note that the redox control methods employed by Keiser and Fabre were different (Be addition and electrochemical control, respectively) but the outcome was similar.

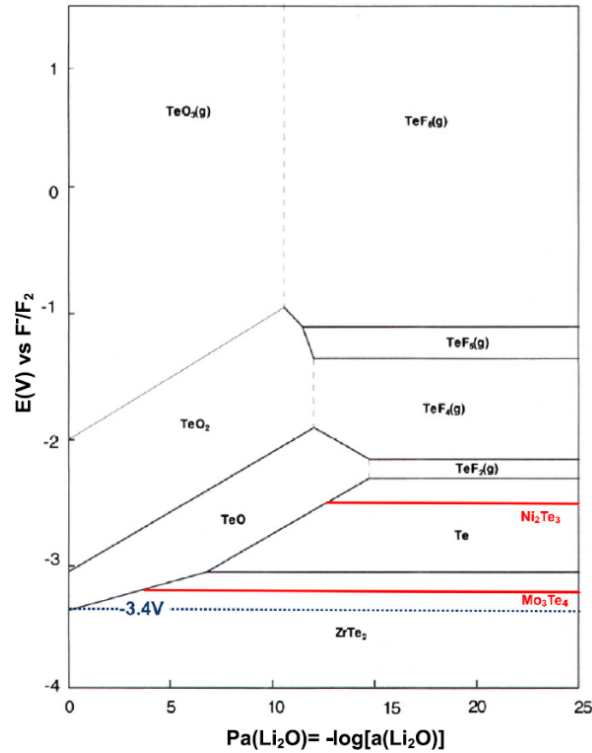


Figure 17. Phase diagram at 953 K in the system Zr–Te–F–O with lines from the diagrams for Ni–Te–F–O and Mo–Te–F–O made using Outotec HSC Chemistry v5.1. Reproduced from Fabre et al. [2013]

6.3 ENVIRONMENTALLY ASSISTED CRACKING

Environmentally assisted cracking (EAC), in which a combination of environmental attack and mechanical stress leads to crack formation, can be a lifetime limiting failure mode in some systems. For ceramics, high temperature mechanisms are a concern [Evans 1996]. However, for structural alloys in general, EAC tends to be a concern at temperatures lower than those at which molten salt systems generally operate [Lynch 2013]. Partially for this reason, limited data on EAC in molten salts are available. Rhodes [1969] compared EAC of 304 stainless steel in aqueous salt solutions vs. a non-aqueous salt melt of KCl:ZnCl₂ (36:64) to observe the effect of cations and determine how water concentration affects crack propagation. Rhodes observed EAC of the stainless steel U-bend samples in the ZnCl₂-based mixture heated to 250°C above a critical level of H₂O, ~2.6%. Additionally, Rhodes measured EAC in aqueous solutions with LiCl, MgCl₂ or MgBr₂ and found that the degree of EAC varied with MgBr₂>MgCl₂>LiCl. The differences were attributed to an increase in hydrolysis that effectively increased the acid content in the solution. Similar comparisons were not made in the salt melt because the melting temperature of MgCl₂-based salt mixtures is ~200°C hotter than their ZnCl₂ counterparts.

Atmani et al. [1984] performed in-situ tensile experiments on 304H exposed to NaCl:CaCl₂ (48:52) at 570°C. Their results are limited and lacking in detail, but they did observe intergranular fracture consistent with EAC at a strain rate of 10⁻⁵ mm/s. This result requires replication to be truly useful, but does show an instance of EAC in a molten halide.

Smyrl et al. [1975] studied crack growth of Ti-8Al-1Mo-1V in LiCl:KCl (58:42) at 375° to 475°C. Using direct cantilever beam (DCB) specimens, they observed crack growth, with a rate that increased as stress intensity increased. This result was expected, because the alloy was chosen for its known EAC susceptibility in this environment. More interestingly, they found that adding water to the melt did not

affect the crack growth rate. This is especially interesting because the introduction of water might affect crack growth by two mechanisms: an increase in the Cl potential of the melt, and hydrogen embrittlement at the crack tip. The result shows that neither was active in this experiment. Note that Smyrl et al. only varied the water content from 10 to 50 ppm, well below the ~2.6% H₂O threshold for crack formation established by Rhodes. Additionally, MgCl₂-based salt melts can dissolve MgOH⁺ into the melt in relatively large quantities (~1%) at temperatures relevant to reactor operation. [Ding 2019] It is unclear if the large amounts of MgOH⁺ would cause more corrosion by reacting with the most reactive elements or by EAC.

6.4 POST-CORROSION MECHANICAL TESTING AND MICROSTRUCTURE ANALYSIS

Little data on the mechanical properties after molten salt exposure is reported in literature. [Jordan 1957, Li 2020, Rhodes, 1969] As noted earlier, Ignat'ev et al. [2016] used tensile properties to evaluate Te embrittlement in Ni alloys. They used the results to supplement depth of attack measurements to evaluate overall strength of the alloy. While there are a few reports on molten salt corrosion that include mechanical testing, there are even fewer that report on *in-situ* mechanical testing. A study by Li et al. [2020] reported increased susceptibility and propagation of cracks when a constant stress was applied in the presence of molten salts. They exposed 304H stainless steel to KNO₃:NaNO₃ and compared the results to air. They found exposure to salt decreased the onset time of crack initiation and the ductility of the alloy. Crack initiated and propagated along the grain boundaries, exposing fresh material to the salt. The salt oxidized the freshly exposed surface along the grain boundaries and decreased the binding between grains further. It should be noted that these tests were in nitrate salts, and many corrosion mechanisms are different when compared to exposures in halide salts. It is unclear if similar phenomena will occur in salts without an oxidizing anion.

6.5 CONCLUSIONS

Tellurium embrittlement remains a concern for low-Cr Ni-based alloys in fueled fluoride salts. Te-cracking can be effectively mitigated by maintaining a low fluoride potential through the use of redox control additives. It is not clear how severe Te induced-cracking may be in other alloys. Limited data on EAC data suggests cracking may only be a problem in melts with high moisture content, but it is not clear if this finding applies to all salts and materials.

6.6 KNOWLEDGE GAPS

6.6.1 Effects of Te embrittlement

Good data exists on effects of Te embrittlement in alloy N and similar low Cr alloys. However, data is not available for other alloys, and it is not clear if intergranular Te might affect Ni-based alloys with higher Cr content, or Fe-based stainless steels (beyond the limited data provided by McCoy [1978]).

6.6.2 Environmentally assisted cracking

Limited data suggests EAC may occur in chloride salts with very high moisture contents. Although nothing suggests that EAC should be a primary concern, data on materials strained *in-situ* in fluoride melts is not available. The lack of EAC data for several material-salt combinations is a knowledge gap

7. RADIATION EFFECTS

Irradiation may affect corrosion by several mechanisms. First, radiation enhanced diffusion may affect the diffusion of species to the salt-material interface [Sizmann 1978]. This is especially important if diffusion

of Cr is the rate-controlling mechanism, as asserted by Evans et al. [1961]. Second, radiation may create oxidizing or reducing species in the salt melt. One concern in Li-containing salts is the production of tritium. The chemical behavior of tritium is similar to hydrogen, and therefore tritium is expected to form corrosive TF in fluoride melts. From a corrosion perspective, tritium can be managed by appropriate redox control methods.

Another concern is radiolysis of the salts. Prior works have shown radiolytic production of fluorine [Briggs 1964] or chlorine [Tandon 2000] gas in low temperature solidified fluoride and chloride salt melts, respectively. Investigations during the MSRE concluded that radiolysis occurred in solid fluoride fuel salts, but was not significant at operating temperatures [Briggs 1964, Icenhour 2001]. This assertion, however, was based on the lack of fluorine gas production from the melt, and the possibility exists (although unlikely) that in-track radiolysis effects may affect material degradation. Lastly, electronic excitation of material surfaces may affect the rate of chemical reactions between the salt melt and the material. This effect has not been shown to affect corrosion in any condition, but Petrik et al. [2001] has shown excess hydrogen production during irradiation of materials in water, but no effects have been shown in molten salts, so any effect on corrosion in salts is not established.

Static and flowing in-pile experiments in molten salts were conducted at ORNL as part of the MSRE and ARE program [Keilholtz 1959][Trauger 1961]. McDuffee et al. [2018] summarized flowing experiments from these eras. Keilholtz asserted that in all static and flowing experiments conducted for the ARE, no acceleration of corrosion due to irradiation was reported.

Sisman et al. [1957] reported on an in-pile experiment conducted for 645h (475 at full power) with flowing NaF-ZrF₄-UF₄ in contact with Ni-based alloy 600. No acceleration of corrosion was observed due to irradiation when comparing specimens taken from the irradiated and unirradiated zones, and no significant mass transfer was found. The experimenters did note a decrease in corrosion when compared to out of pile loops, but attributed the decrease to a lower overall temperature, and a lessened temperature difference between the hot and cold zones of the in-pile loop.

If any corrosion data from flowing in-pile loops conducted for the MSRE program is available, the authors of this report were not able to find it. In-pile TCLs were also operated [Savage 1967], although no corrosion data is available from them either. A diagram of the ORNL in-pile TCL is shown in Figure 18. Examination of salt-facing alloy-N components and surveillance coupons from the MSRE was reported by McCoy et al. [1972b]. The report revealed very low rates of corrosion throughout the loop (aside from Te-induced cracking, discussed elsewhere), so it appears likely that radiation did not significantly accelerate corrosion, consistent with in-pile loop testing for the ARE.

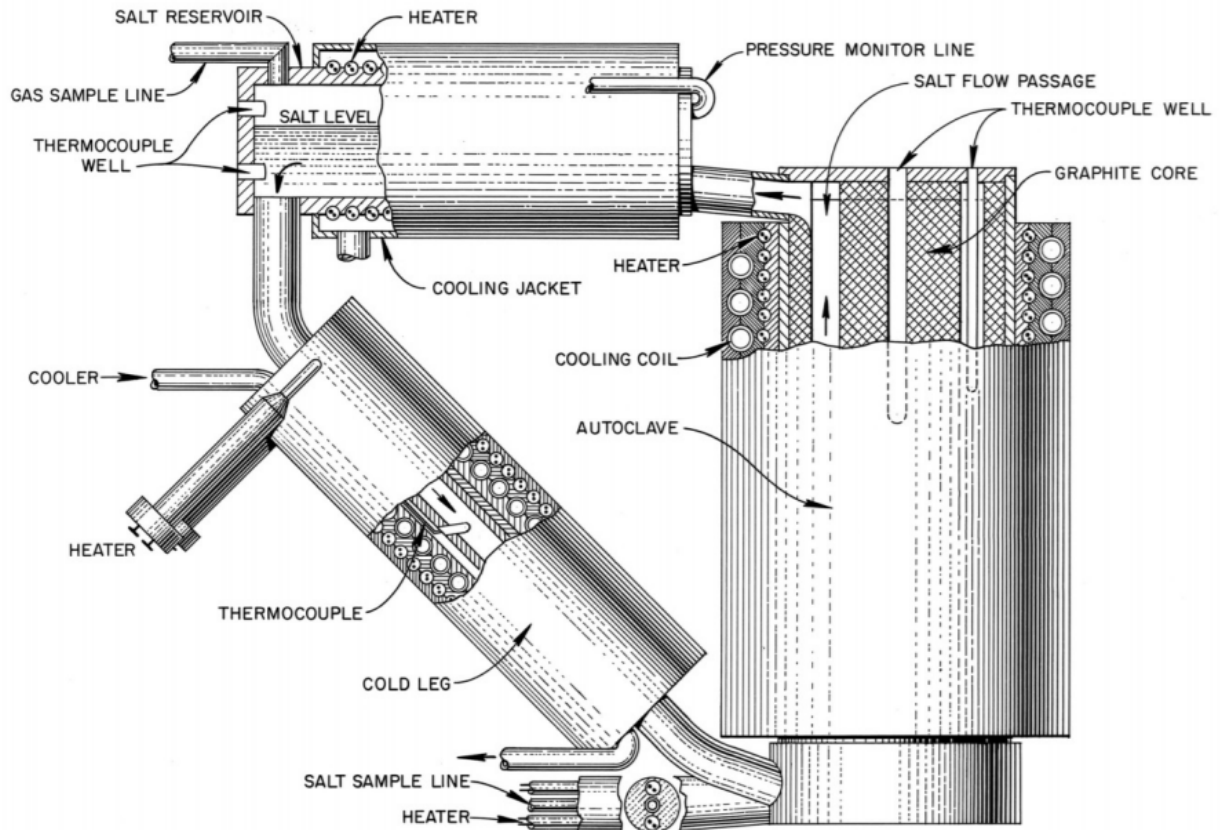


Figure 18. Drawing of a thermal convection loop that was operated in the ORR. Reproduced from Savage et al. [1967]

Zhou et al. [2020] conducted experiments in which Ni-Cr alloys were exposed to FLiNaK salt while simultaneously irradiated with a proton beam, and found that irradiation decelerated corrosion of the alloy. They attributed this deceleration to grain boundary self-healing due to the abundance of irradiation-produced interstitials in the irradiated alloy.

Zheng et al. [2016b] compared corrosion of alloy N and type 316H SS exposed in FLiBe at 700°C both with and without neutron irradiation. Zheng's results showed a dramatic increase in the rate of corrosion due to irradiation. However, despite the use of the same alloys and same salt, there were some differences in the experimental procedure between the irradiated and the unirradiated experiments. The capsules exposed in-pile had a flowing inert cover gas, while the out-of-pile samples were exposed with a stagnant inert glovebox atmosphere as a cover gas. Also, the out of pile samples were heated by a furnace, while the in-pile samples were heated by gamma heating with temperature controlled by the sweep gas. Impurities in the sweep gas or convective currents imposed by non-uniform gamma heating may have accounted for the observed acceleration in corrosion rate.

Bull Ezell et al. [2020] exposed type 316L SS and alloy N samples to NaCl-MgCl₂ for 21 h at 800°C with and without neutron irradiation. They found less attack on the irradiated stainless steel samples when compared to the unirradiated samples, and no difference on an alloy N sample. Ezell only exposed a total of 3 samples. While the experimental setup was the same for both irradiated and unirradiated experiments, the high variability inherent to molten salt experiments suggests that these results be considered preliminary.

7.1 OTHER FISSION PRODUCT EFFECTS

As discussed in chapter 5, the fission product tellurium led to cracking of alloy N in the MSRE. However, Te is not the only potential fission product of concern in MSR. Fission products may be either oxidizing or reducing, depending on their oxidation state, the number of available oxidation states, and on the original oxidation state of the parent fissile element. Figure 19 shows the periodic table with fission products highlighted, reproduced from (Aufiero et al.). Green and yellow highlighting are used to represent fission products that are soluble and insoluble, respectively, in fluoride salts.

hydrogen 1 H 1.00794																	helium 2 He 4.002602						
lithium 3 Li 6.941	beryllium 4 Be 9.0122																	boron 5 B 10.811	carbon 6 C 12.011	nitrogen 7 N 14.007	oxygen 8 O 15.999	fluorine 9 F 18.998	neon 10 Ne 20.180
sodium 11 Na 22.990	magnesium 12 Mg 24.305																	aluminum 13 Al 26.982	silicon 14 Si 28.086	phosphorus 15 P 30.974	sulfur 16 S 32.065	chlorine 17 Cl 35.453	argon 18 Ar 39.948
potassium 19 K 39.098	calcium 20 Ca 40.078	scandium 21 Sc 44.956	titanium 22 Ti 47.867	vanadium 23 V 50.942	chromium 24 Cr 51.996	manganese 25 Mn 54.938	iron 26 Fe 55.845	cobalt 27 Co 58.933	nickel 28 Ni 58.693	copper 29 Cu 63.546	zinc 30 Zn 65.38	gallium 31 Ga 69.723	germanium 32 Ge 72.61	arsenic 33 As 74.922	selecnium 34 Se 78.96	bromine 35 Br 79.904	krypton 36 Kr 83.80						
rubidium 37 Rb 85.468	strontium 38 Sr 87.62	yttrium 39 Y 88.906	zirconium 40 Zr 91.224	niobium 41 Nb 92.906	molybdenum 42 Mo 95.94	technetium 43 Tc [98]	ruthenium 44 Ru 101.07	rhodium 45 Rh 102.91	palladium 46 Pd 106.42	silver 47 Ag 107.87	cadmium 48 Cd 112.41	indium 49 In 114.82	tin 50 Sn 118.71	antimony 51 Sb 121.76	tellurium 52 Te 127.60	iodine 53 I 126.90	xenon 54 Xe 131.29						
cesium 55 Cs 132.91	barium 56 Ba 137.33	* 57-70	lutetium 71 Lu 174.97	hafnium 72 Hf 178.49	tantalum 73 Ta 180.95	tungsten 74 W 183.84	rhenium 75 Re 186.21	osmium 76 Os 190.23	iridium 77 Ir 192.22	platinum 78 Pt 195.08	gold 79 Au 196.97	mercury 80 Hg 200.59	thallium 81 Tl 204.38	lead 82 Pb 207.2	bismuth 83 Bi 208.98	polonium 84 Po [203]	astatine 85 At [210]	radon 86 Rn [222]					
francium 87 Fr [223]	radium 88 Ra [226]	* *	actinium 89 Ac [227]	thorium 90 Th 232.04	protactinium 91 Pa 231.04	uranium 92 U 238.03	neptunium 93 Np [237]	plutonium 94 Pu [244]	americium 95 Am [243]	curium 96 Cm [247]	berkelium 97 Bk [247]	californium 98 Cf [251]	einsteinium 99 Es [252]	fermium 100 Fm [257]	mendelevium 101 Md [258]	nobelium 102 No [259]							
		* Lanthanide series		lanthanum 57 La 138.91	cerium 58 Ce 140.12	praseodymium 59 Pr 140.91	neodymium 60 Nd 144.24	promethium 61 Pm [145]	samarium 62 Sm 150.36	europium 63 Eu 151.96	gadolinium 64 Gd 157.25	terbium 65 Tb 158.93	dysprosium 66 Dy 162.50	holmium 67 Ho 164.93	erbium 68 Er 167.26	thulium 69 Tm 168.93	ytterbium 70 Yb 173.05						
		** Actinide series		actinium 89 Ac [227]	thorium 90 Th 232.04	protactinium 91 Pa 231.04	uranium 92 U 238.03	neptunium 93 Np [237]	plutonium 94 Pu [244]	americium 95 Am [243]	curium 96 Cm [247]	berkelium 97 Bk [247]	californium 98 Cf [251]	einsteinium 99 Es [252]	fermium 100 Fm [257]	mendelevium 101 Md [258]	nobelium 102 No [259]						

Figure 19. Periodic table with fission products that are soluble in fluoride salts highlighted in green, and fission products that are insoluble in fluoride salts highlighted in yellow. Reproduced from Aufiero

Chasanov [1965] mentioned the possibility of plating the more noble fission products onto the walls of the vessel and this was also addressed by Robinson [1958b]. The lanthanides are major fission products. While minimal research in molten salt corrosion focuses on fission products, the pyroprocessing community studies how the actinides and lanthanides behave in molten salts. [Guo 2018, Zhang 2014] Pyroprocessing separates the actinides and lanthanides using electrochemistry. The elements are separable by the different potentials needed to reduce them to the metallic state. Those potentials are a useful guide to determining the level of corrosivity resulting from fission products. Guo et al. [2020] exposed Ni-based alloy 718 and Fe-based NF709 SS (Table 1) to LiCl:KCl pyroprocessing salt with and without EuCl_3 , a possible fission product, added to the salt. They found significant intergranular attack with all elements in the alloy being dissolved in short periods of time (<48 h). Longer exposures lead to an enriched Ni layer on the surface of the alloy. It is unclear if the Ni layer was redeposition of dissolved Ni or after some time the salt was no longer dissolving Ni.

7.1.1 Knowledge gaps

7.1.1.1 Effect of irradiation on corrosion

Little data exists on samples irradiated while exposed to molten salts. What little data exists is often contradictory, with some studies showing accelerated corrosion and others showing decelerated corrosion due to irradiation. There is a need for high-quality in-pile studies of material corrosion in molten salts to study the effects of radiation enhanced diffusion, salt radiolysis, and irradiation-induced microstructural changes. This is especially important for chloride salts, where containment vessels can be expected to receive higher fluences. In thermal reactors, the highest neutron fluences are expected in moderator materials.

7.1.1.2 Effects of fission products

The effect of tellurium on cracking of Alloy-N has been well studied, but little data exists on the effects of other fission products. Some work exists on europium in chloride salt melts, but without knowledge of the oxidation state of europium after transmutation, its effect on corrosion cannot be fully understood. Due to the sheer number of fission products, measuring the effect of each individually may not be feasible, and their effect on corrosion may be best controlled through general control of redox. It is possible that deposited layers of insoluble materials [Kedl 1972] may have a beneficial effect and this needs to be further explored.

8. GRAPHITE & NON-METALS

Graphite is the most commonly proposed moderator material for thermal reactors and is generally understood to have good compatibility with fluoride salts, exhibiting minimal mass loss [Lee 2019]. However, fluorination is a concern because it can lead to chemical changes in the graphite [Tang 2017]. Additionally, formation of uranium carbide is possible at low redox potential. Tang et al. [2017] exposed several grades of graphite to molten FLiBe and observed that graphite grades with higher porosity experienced greater fluorine penetration than grades with lower porosity. Evans et al. [1969] also performed similar studies. This is especially concerning for fuel salts, as infiltration of fissile isotopes may affect core neutronics. DiStefano et al. [1995] asserted that graphite with pore sizes of $<1 \mu\text{m}$ should resist salt intrusion; however, the research that led to this conclusion is not well documented. Accordingly, more data are needed on effects of graphite in fluoride salts building on the work of Compere et al. [1975]. Chloride salt data are not needed at this time, as chloride reactors are generally fast spectrum reactors that do not require moderation.

Most of this report has focused on metals, as metals will very likely be used for containment structures and salt-facing structural components. However, the most abundant material inside the cores of most thermal reactor designs is the graphite moderator. Additionally, some designers may propose the use of ceramics for structural or functional components. This section surveys the corrosion behavior of graphite and ceramic materials in molten salt reactor systems. Graphite has been used as moderator in over 100 nuclear reactors, some of which are still producing power in the UK (15 reactors) and Russia (11 reactors) [Marsden 2016]. Graphite is arguably one of the most well-understood materials in nuclear systems; its radiation response is reasonably well known. Graphite is composed of pure carbon with a complex microstructure with various filler grain sizes and shape distributions, grain orientations, pore size and shape distributions and a proportion of less-graphitic carbon binder [Blackstone 1977]. Its microstructural evolution in a neutron flux typically requires finite element analysis. Many different grades of graphite are available, and each one is different in several important aspects, requiring extensive billet to billet testing of key properties. These often involve independent tests with several specimens from each grade,

often cut in different directions (axial or transverse), leading to large experimental matrices and expensive irradiation campaigns. The response of one grade of graphite should not be extrapolated to another.

Potential corrosion issues related to graphite have been reported as early as the MSRE demonstration of the 1960s and during MSBR conceptualization at ORNL [McCoy 1970, Scott 1969]. Based on some limited compatibility tests, the corrosion behavior of graphite in molten salt was deemed “acceptable” at the time. Because of the void volume of graphite (16 to 20%) with potentially large accessible surface area in voids, its corrosion behavior is further complicated by salt and noble gas permeation (particularly Xe, $\sigma_{th} \sim 2$ million barns) as well as noble metal plate-out on surfaces for liquid fueled reactors. The MSRE graphite was tested and reported elsewhere [Briggs 1964, 1965], providing porosity and permeability data directly related to the Xe problem.

Notably the graphite for MSBR was originally envisioned to last less than 4 years in a service environment as a single fluid reactor [Scott 1969]. Since corrosion behavior is linked to the salt and gas permeation issues, extending graphite lifetime likely involves considerations for protecting the surface in addition to stripping or sparging Xe from the salt, off gas entrainment systems as well as coolant chemistry monitoring of tritium [Engel 1971]. The tritium levels in the coolant have been previously correlated with the corrosion of metallic alloys in these nuclear systems.

Graphite can be used as a moderator material in both salt-fueled and salt-cooled designs. In the MSRE, a salt-fueled design, graphite acted as core structural and moderator material. Salt-cooled designs, such as the Fluoride Salt-Cooled High Temperature Reactor (FHR), typically employ a graphite moderated core with solid-fuel and molten fluoride coolant. The pebble-bed FHR concept [Forsberg 2003] employs ceramic fuel similar to the Very High Temperature Gas-Cooled Reactor (VHTR) concept, strong analogies can be drawn between the two systems. Solid fuel reactors have the advantage of not having to dissolve actinides into the salt. Thus, actinide solubility and fuel reprocessing are not needed. Noble metal plate-out is not expected in FHR compared to a liquid fueled MSR where fissions are occurring in the salt.

For the FHR concept several refractory ceramics are candidate materials to be employed alongside the graphite core and metallic components, such as fiber-woven SiC/SiC composites or C/C composites as shown in Table 6. The ceramic composite candidates are intended for areas of higher neutron fluxes, such as control rod liners and guide channels, core support structures and other core internals. Table 7 displays estimates of typical FHR neutron flux and damage rates for various reactor components based on the pebble-bed Advanced High Temperature Reactor (PB-AHTR) neutronic model for flux called BEAU, developed by University of California-Berkeley [Allen 2013b].

Silicon carbide (SiC) is well known for radiation tolerance, high temperature strength, and its applicability to fuel particles and core internals of nuclear reactors. Silicon carbide fiber-reinforced ceramic matrix composites (SiC_f/SiC composites) could be an attractive option for shutdown rod guide channels, which would eliminate the need for a graphite center reflector column in an annular core [Allen 2013a]. Unlike its behavior in air or moisture-based environments, SiC does not form a protective oxide layer in molten fluoride salt [Yang 2016a, Xue 2018, Xi 2019].

C/C composites are known for their high tensile strength [Snead 2008]. Compared to SiC/SiC composites, C/C composites have a more established market and maturity as a commercial material, with many available options on the market from ordinary to special architectures. One clear disadvantage compared to SiC_f/SiC composites is that C/C composites are far more susceptible to radiation anisotropy [Bonal 1996]. Their corrosion behavior is not well-studied for molten salt reactors but it is reasonably expected to exhibit a similar corrosion behavior to other C-based materials like graphite.

Table 6. Candidate ceramics and metals considered for reactor components of a pebble-bed FHR.

Ceramics	Component	Qualifications
^a CVD SiC	TRISO fuel particles	Up to 1600 °C and stringent failure fractions (<10 ⁻⁴)
^b SiC _f /SiC composites	Core barrel, core internals, control rod guide channels and sleeves	No upper temperature limit specified
^b C/C composites	Core barrel, fuel plates	-
^b Nuclear graphite	Core internals, reflectors, moderator	No upper temperature limit specified
Matrix carbon	Fuel	-
Metals	Component	Qualifications
Nb-1Zr	Control rods and internals	-
^c Alloy N	Reactor vessel and internals PRACS and DRACS heat exchangers	Up to 704 °C
^b 316H stainless steel	Reactor vessel and internals PRACS and DRACS heat exchangers	Up to 816 °C
^b Alloy 800H with Ni-base alloys	Intermediate heat exchangers (salt to gas)	Up to 800 °C

^aDemonstrated by Advanced Gas Reactor TRISO Fuels Qualification Program, AGR-1 [Petti 2012].

^bASME Section III Division 5 code-qualified [ASME 2015].

^cDemonstrated during MSRE by ORNL [Koger, 1972b, 1972c] but only codified in ASME Section VIII. Not codified in ASME Section III Division 5.

Table 7. Calculated maximum flux and radiation damage estimates for PB-AHTR using an MCNP5-based neutronic model BEAU [Allen 2013b].

Reactor component	Fast Flux (> 0.1 MeV) [n/cm² · sec]^c	Temperature [°C]	Damage rate [dpa/year]
^a Inner graphite reflector	1.22 x 10 ¹³	600	15.7
Shutdown rod liners	1.03 x 10 ¹³	600	0.24
Outer graphite reflector	3.55 x 10 ¹¹	700	0.96
Core barrel	1.99 x 10 ⁹	600	4.27 x 10 ⁻⁵
^b Reactor vessel	1.99 x 10 ⁹	600	3.52 x 10 ⁻⁵

^aReplaceable when radiation damage limit is reached.

^bReactor vessel flux assumed to be roughly comparable to the fast flux rate in the core barrel.

8.1 GRAPHITE CORROSION IN MOLTEN SALT REACTORS (STRUCTURAL GRAPHITE ONLY)

Early work from the MSRE reported good compatibility of graphite with fluoride salt. Recent work has shown that structural metals can be attacked more severely in the presence of graphite [Olson 2009] because of a dissimilar materials effect (see Section 2.6.3). In a typical thermal reactor design, graphite comprises a large fraction of the core volume so these interactions warrant further investigation. Graphite, because of its significant open porosity (~18 to 20% for nuclear grades) provides ample surface area for salt and gas permeation and fission products deposition, especially in unclad liquid fuel systems. Some radioisotopes are a much higher-level concern because of the potential for them to disrupt power operations (like Xe) or because of their high mobility through and chemical interactions with structural materials (like tritium). Thus, barrier coatings or seal technologies to lower the open porosity of graphites are an attractive option. In terms of radiation effects, prolonged exposure to a neutron flux causes dimensional property change in graphite [Marsden 2016, Blackstone 1977]. A combination of these degradation processes and thermal aging result in internal stresses. Over time, these stresses can initiate and propagate cracks (allowing salt ingress). The main properties of concern are Young's modulus (elasticity or stiffness of a material), strength, coefficient of thermal expansion (CTE) and irradiation creep. The material performance challenges for graphite in MSRs are interrelated. Graphite component lifetime assessments should include test reactor irradiation data as well as corrosion behavior in the molten salt system of interest.

8.2 SALT AND GAS PERMEATION OF POROUS GRAPHITE

ASTM D8075-16 provides standard guidelines for characterizing graphite grain-sizes by diameter: microfine $\sim < 2 \mu\text{m}$, ultrafine $\sim < 10 \mu\text{m}$, superfine $\sim 50 \mu\text{m}$, fine $\sim 100 \mu\text{m}$ and medium fine $< 1 \text{mm}$, etc. Figure 20 shows a type of ultrafine grained POCO® graphite called ZXF-5Q that has a distribution of pore sizes on the order of a few microns to several hundred nanometers. It is compared with a historical and current isotropic nuclear-grade graphite IG-110 with superfine filler grains. IG-110 has a long operational history in past (DRAGON) and current gas reactors (HTR-10, THTR).

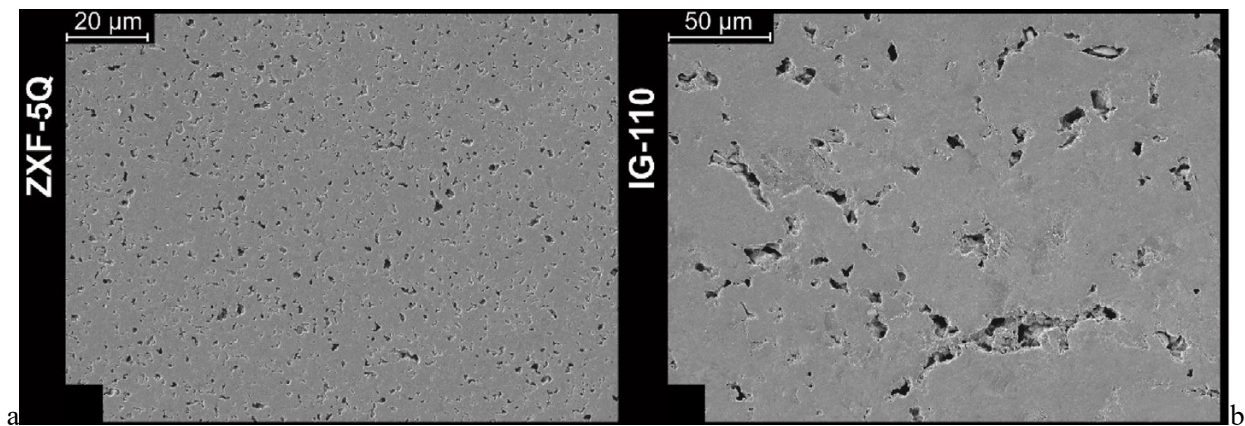


Figure 20. (a) ZXF-5Q low porosity industrial, non-nuclear grade graphite with ultra-fine pores. (b) IG-110 super fine grained nuclear-grade graphite. Note the difference in scale.

To minimize gas permeation, seal coatings of graphite and very low porosity industrial grades of graphite were early considerations during MSBR conceptualization [Scott 1969, Kasten 1969]. Graphite corrosion was studied less than salt and gas permeation behavior and radiation anisotropy [DeVan 1962, Kasten 1969, Engel 1971, Thoma 1971]. In any salt-fueled design, the coolant chemistry will surely consist of some level of fission product gases and volatile species, dependent on the particular reactor design. A

solid fueled molten salt reactor will contain some measurable level of fission product gases and volatiles associated with a UCO matrix and TRISO layer failures. ^{135}Xe is an unfavorable gaseous fission product and powerful neutron poison. Xe and Kr are two major noble fission gases associated with the UO_2 matrix of TRISO fuel and are two higher-yield fission product gases [Bailly 1999]. Volatile species include I, Te, Cs and Rb, with I the most volatile. Partial condensation also affects the gas phase composition, e.g. plating out of fission products on cooler surfaces. Salt sparging removes most volatile species from the salt [Scott 1969], however, the two major noble gasses (Xe and Kr) persist in measurable quantities. If graphite is unclad in an MSR, the xenon that becomes trapped in the porous volume of graphite cannot be stripped and has to be dealt with separately [Engel 1971].

The resistance of graphite to salt penetration is well-described by the Washburn relation,

$$\Delta p = -\frac{4\gamma\cos\theta}{\delta} \quad (1)$$

where δ is the entrance pore diameter of penetrated pores, Δp is the pressure difference, γ is the surface tension, and the θ is the contact angle [He 2015]. Graphite does not exhibit wettability with molten fluoride salts due to the high surface tensions of the salt (about 0.23 N/m and contact angle of 150° with graphite in MSRE) [Kasten 1969].

The graphite entrance pore diameter and applied pressure were deemed to be important factors in salt permeation experiments [McCoy 1970]. The average entrance pores of graphite are recommended to be in the nm-range for low gas permeability and in the $<1 \mu\text{m}$ range for low salt permeability. Because the technology for multiple impregnation processes were not widely available to reduce graphite porosity, post fabrication seal coating of graphite was deemed the “more reasonable” route to achieving $<0.5\%$ retention of ^{135}Xe in the moderator graphite. An experimentally observed helium diffusivity of about $D_{\text{He}} < 10^{-8} \text{ cm}^2/\text{s}$ was deemed representative of the Xe diffusivity in graphite to mitigate Xe retention to acceptable levels [Haubenreich 1970].

The MSRE graphite, deemed CBG, was specially developed by Union Carbide Company and ORNL to have very low salt and gas permeability [MacPherson 1960, Kasten 1969]. The small entrance pore size of CBG was effective in resisting molten salt infiltration. Since graphite is not wetted by the salt, salt and gas intrusion of CBG would require significant pressure differentials but the grade was deemed unsuitable overall because of its high irradiation anisotropy. Table 8 from Haubenreich [1970] shows the major reactor components of MSRE.

Table 8. MSRE materials of construction. Reproduced from Haubenreich [1970].

Fuel Salt	⁷ LiF-BeF ₂ -ZrF ₄ -UF ₄ (65.0-29.1-5.0-0.9 mole%)	
Composition:		
Properties at 1200°F (650°C)		
Density	141 lb/ft ³	2.3 g/cm ³
Specific heat	0.47 Btu/lb-°F	2.0 × 10 ³ J/kg-°C
Thermal conductivity	0.83 Btu/h-ft-°F	1.43 W/m-°C
Viscosity	19 lb/h-ft	29 kg/h-m
Vapor pressure	<0.1 mm Hg	<1 × 10 ⁻⁴ bar
Liquidus temperature	813°F	434°C
Coolant salt ^a	⁷ LiF-BeF ₂ (66-34 mole%)	
Moderator	Grade CGB graphite	
Salt containers	Hastelloy-N (68 Ni-17 Mo-7 Cr-5 Fe)	
Cover gas	Helium	

^aAnother batch of salt of this composition is used to flush the fuel system before it is opened to minimize fission product escape and again after it is resealed to pick up moisture that may have entered.

Coatings and resin impregnation methods to protect MSR graphite are being developed by several groups. [Bernardet 2009, He 2013, 2014, 2018a, 2018b, 2019, Song 2015]. SEM was used to image the microstructure of CBG graphite, shown in Figure 21 [Lee 2020]. Randomly distributed clusters of foam-like pore structures around 20 μm or less were observed.

IG-110 is an isostatically pressed super fine-grained nuclear-grade graphite, a common grade of nuclear graphite used worldwide and produced in multi-ton quantities [Atkinson 2018]. It is still in use today for gas reactors, such as the experimental pebble-bed reactor HTR-10 [Wu 2002] at Tsinghua University in China, the High Temperature engineering Test Reactor (HTTR) in Japan [Shiozawa 2004]. It is also proposed for the prototype Thorium Molten Salt Reactor (TMSR) at Shanghai Institute of Applied Physics (SINAP) [Zhou 2015, 2018]. The average filler grain size of IG-110 is about 20 μm (40 μm maximum grain size) with about 18 to 20% open porosity [Wen 2008]. IG-110 is highly graphitized, produced from petroleum coke by isostatic pressing and complies with standard guidelines for nuclear-grade graphites defined in ASTM D7219-08. Furthermore, because it is a historic grade, its radiation behavior is better understood and databased than many other modern grades of graphite.

Gilsocarbon is a semi-isotropic grade with long operational history in 15 advanced gas-cooled reactors (AGR) in the UK and Russia. Gilsocarbon tends to have pores over very wide range of sizes [Laudone 2014].

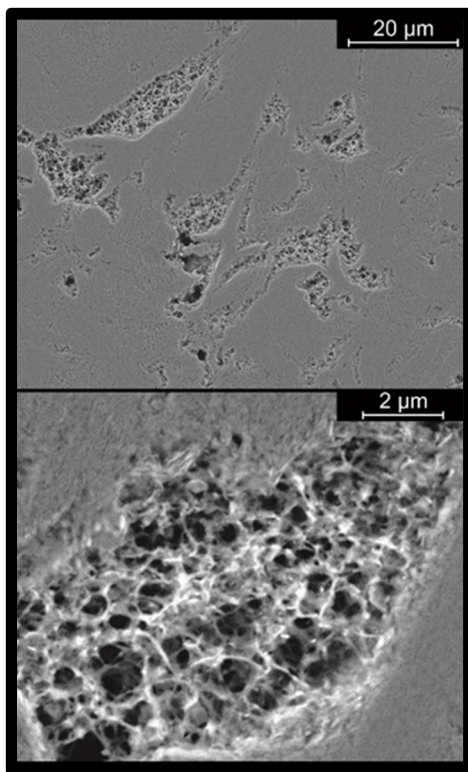


Figure 21. MSRE low porosity graphite CBG [Lee 2020].

8.3 INFILTRATION MITIGATION STRATEGIES

In order to seal nuclear-grades of graphite, one strategy is to apply an outer layer with smaller entrance pores. Thus, many recent studies focus on sealing and otherwise modifying this grade. The CTE change of graphite and coating candidates do not allow many viable options but they are briefly reviewed here. The radiation response of these coated systems is a technical gap.

Pyrolytic Carbon (PyC) coatings were considered during the MSRE demonstration and are promising technological solutions based on experimental phenomena [McCoy 1970, Kasten 1969]. Glassy carbon and PyC/glassy carbon protection layers were studied in LiF-NaF-ZrF₄ (27.0-36.5-36.5 mol%) salt [Bernardet 2009]. Graphite disks were dipped in precursor phenolic resin until covered and then pyrolyzed. A simple glassy carbon layer only showed slight improvement of the graphite surface to salt permeation, but a double coating layer consisting of PyC layer and subsequent glassy carbon layer showed good protection of the graphite discs.

SiC coatings on graphite for MSR applications have been explored in unfueled salts. He et al. [2018b] studied nuclear graphite with SiC seal coatings fabricated via impregnation and pyrolysis of polycarbosilane to produce modified IG-110 (M-IG-110). X-ray diffraction (XRD) was used to confirm that polycarbosilane had successfully converted to β -SiC phase. SiC had a filling effect on the pores, taking the initially measured median pore diameter of 2.06 μm in uncoated IG-110 down to about 0.01 μm in M-IG-110. Further, the open porosity reduced from 18% to about 10% in the coated graphite. The salt infiltration was less than 1.1 wt.% in FLiNaK for 24 h at 650 $^{\circ}\text{C}$ at 5 atm.

He et al. investigated the salt permeability of IG-110 coated with CVD SiC [He 2014]. Uncoated and CVD PyC coated IG-110 were heated to 650 $^{\circ}\text{C}$ in FLiNaK for 12 h at 5 atm. They found that the uncoated graphite exhibited over 12x the salt uptake as the SiC-coated graphite.

Resin impregnation can block the graphite pore structure from fluid permeation. Zhao et al. prepared densified IG-110 (D-IG-110) by impregnating IG-110 with phenolic resin which decreased the pore diameter to nearly 11 nm [He 2018a]. The resin had a filling-effect on the pores and cracks of D-IG-110, which exhibited significantly reduced open porosity (from 18.4% to 2.8%), higher density, and increased thermal conductivity. Graphite samples were immersed in LiF-NaF-KF (46.5-11.5-42.0 mol%) salt at 650 °C for 12 h. Mercury intrusion was used to measure permeability at various pressures from 0 to 10 atm. For unimpregnated IG-110, samples were found to gain mass up to a maximum saturation at ~14 wt.% at 2 to 3 atm. No infiltration was detected for the impregnated D-IG-110.

8.4 METALLIC ALLOY-GRAPHITE COMPATIBILITY

Enhanced degradation of structural alloys has been observed in the presence of graphite [Olson 2009]. Depending on the electrochemical balance of the system as well as the impurity levels, graphite can participate in several corrosion reactions [Guo 2018] including reacting with Cr dissolved in the salt to form Cr-rich carbides. This is a typical dissimilar material reaction as noted earlier (Section 2.6.3).

Interaction between graphite and metals was observed during the MSRE [Lane 1958, Grimes 1967, Thoma 1971]. Graphite was once believed to be “noble” enough capsule material for testing metal coupons in fluoride salt. In many short-term exposures, graphite seemed resistant to corrosion, but longer tests revealed more salt penetration with exposure time [Lane 1958].

Grimes [1967] studied corrosion of Ni-based alloys N, X, 230 and 617 (see Table 1), and Fe-based alloy 800H in FLiNaK at 850 °C in Ar-sealed graphite capsules. Significant corrosion was observed at the grain boundaries of the alloys tested, and Cr carbide phases formed on the graphite crucible internal walls. The formation of carbides is believed to accelerate corrosion, because when Cr in solution reacts with the carbon to form carbides, it decreases the activity of Cr in the melt, presumably increasing the thermodynamic favorability for Cr to move from the alloys to the melt. Carbide formation was not observed when nickel crucibles were used in place of the graphite crucibles.

Olson et al. observed an increase in the mass loss of alloys N, X, 230, 617 and 800H in FLiNaK at 850 °C when tested in graphite containers, when compared to metal containers [Olson 2009, 2015]. Consistent with the increase in metal corrosion, the graphite containers also showed accelerated corrosion. Chromium carbide phases were identified on the crucible interior walls, and the formation of chromium carbides appears to be the driver of corrosion in both the alloy and the graphite container. The formation of carbides would reduce the activity of Cr in the melt and possibly accelerated Cr dissolution from the specimen. The graphite and alloys were in electrical contact, and Olson postulated that a galvanic couple between the graphite and alloys were responsible for the increased attack. As of this report, there is a debate in the molten salt corrosion community regarding whether galvanic corrosion can be a significant driver of corrosion in molten salts.

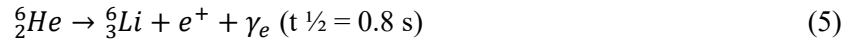
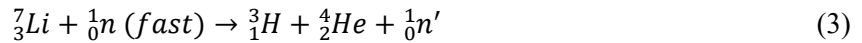
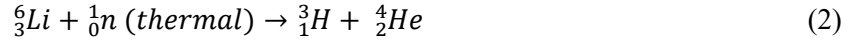
Sellers et al. [2014] exposed type 316L SS and alloy N in Zr-reduced FLiNaK. Non-nuclear grade, low porosity graphite from POCO®, AXF-5Q was added to 316L crucibles with alloy N and 316L coupons at 850 °C for 1000h. Some of the static tests included graphite coupons. In the crucibles with graphite, the alloy N and 316L exhibited distinct corrosion behaviors. The accelerated corrosion of 316L in the presence of graphite (twice as much weight loss and void formation) was attributed to a “nonelectric transfer” of Cr, Fe and Mo from the steel to the graphite surface to form carbides of Cr, Fe and Mo. Alloy N gained weight and had a layer rich in Fe and Cr plated on its surface.

Chan et al. [2018] demonstrated the stability of chromium carbide phases in FLiNaK. They studied graphite interaction with pure elements Cr, Fe, Ni, W and Mo in FLiNaK at 700 °C for 100h. Cr, Mo and W samples formed surface carbides in their respective graphite crucibles. A graphitic peak was identified

using GAXRD. The corrosion resistance of elements from most corrosive to least corrosive were Cr<Fe<W<Mo<Ni. The Ni and Mo weight losses were similar, but the Mo lost more due to carbide formation. Pre-carburized chromium samples were then compared in FLiNaK tests at 700°C for 100h and the chromium carbide layer was shown to decelerate the corrosion of the bulk Cr.

8.5 TRITIUM, FISSION PRODUCTS REACTIVITIES AND OTHER IMPURITIES

Tritium is an internal radiation hazard that can be inhaled or ingested. It has a half-life of 12.3years and is generated from ${}^6\text{Li}$, ${}^7\text{Li}$ and ${}^9\text{Be}$ [Briggs 1971, Stempien 2016, Forsberg 2017a] according to the reactions



Tritium can increase the corrosivity of salt [Forsberg 2017]. Tritium likely exists as tritium fluoride, known to be corrosive to metallic alloys [Grimes 1967, Rosenthal 1971]. Uptake of tritium may affect the balance of tritium in the primary salt melt. The predicted the tritium levels in the primary coolant at the beginning of life will approach that of a heavy water reactor, and exceed that at equilibrium conditions [Stempien 2016, Forsberg 2017]. Table 9 from Forsberg et al. [2017a] shows that tritium production in FLiBe-cooled FHRs (considering ${}^7\text{Li}$ enrichment) is expected to exceed production in LWRs by ~3 orders of magnitude. Direct, in-situ measurements of tritium are scarce. One study involved measurements of tritium concentration to determine the amount of T and H in the MSRE pump-bowl gas [Briggs 1975].

Table 9. Tritium production rates in different reactors compared to FHRs [Forsberg 2017a].

	Tritium production rates		
	(Bq/GWd)	(Ci/GWd)	(g/GWd)
BWR ^a	4.6E+11	12.3	1.27E-3
PWR ^a	5.1E+11	13.9	1.43E-3
HTGR ^a	6.8E+11	18.5	1.91E-3
Fast Reactor ^a	9.2E+11	24.9	2.57E-3
Heavy Water Reactor ^a	4.4E+13	1176	0.12
FHR	BOL: 3.7E+14 EQ: 1.1E+14	BOL: 10129 EQ: 2931	BOL: 1.04 EQ: 0.30

^a from IAEA [2004]

Thoma [1971] examined and tested graphite stringers from the MSRE. The results showed that about 15% of the tritium produced from the fuel salt in MSRE had adsorbed on to the moderator graphite. The tritium concentration in “thin” (unspecified thickness) surface samples was as high as 10^{11} dis/min·g (1.67×10^{10} Bq/g) decreasing to about 10^9 dis/min·g (1.67×10^8 Bq/g) for about 60 mm depth and 6×10^8 dis/min·g for 800 mm depth.

The retention behavior of tritium in graphite is expected to involve chemisorption (formation of new C-H bonds), and tritium retention tends to increase with neutron fluence due to the increase in trapping sites developed by neutron damage [Yaita 1995, Atsumi 2009, 2011]. This is one basis for which graphite is deemed a “tritium sink” for the FHR [Forsberg 2017b]. However, because the expected surface area of graphite or fuel matrix carbon is limited (in the range of 1-2 m²/g), trapping tritium by in-core carbon components may not be sufficient by itself [Grabaskas 2020]

8.6 FLUORINATION

Several studies have shown etching of graphite surface and edge planes exposed to fluoride salt. Wu et al. [2018] studied graphite fluorination in FLiBe and FLiNaK. Using XPS and Raman, Wu found an increase in sp^3 hybridized carbon correlated to graphite fluorination immersion of IG-110 in FLiBe in glassy carbon crucibles at 700 °C. Graphite is a typical sp^2 -hybridized crystal structure, and nuclear-grade graphite is especially highly graphitized. An increase in sp^3 hybridization could indicate a reduction in graphitization. GDMS analysis uncovered evidence of bulk fluorination of graphite.

Qiu et al. [2014] tested graphite crucibles in FLiNaK with and without Cr added. IG-110 fine-grained nuclear-grade graphite was immersed in molten FLiNaK for 16 h at 500 °C. C-F bonding was detected via XPS high resolution scan of the C_{1s} peak and using C K-edge X-ray Absorption Near-Edge Structure (XANES) technique. It was shown that F- ions can substitute for residual H atoms (from the graphitization process between petroleum coke and binder pitch) on the edge sites of graphene layers.

Yang et al. [2012] studied the reactivity of C-H due to residual H from the graphitization (breakdown of structure) process of IG-110 in FLiNaK at 500 °C. Yang showed that the H bonded to C atoms on graphite edge planes were available for substitution with F. XRD indicated that the interlayer spacing in graphite increases upon fluorination. K-edge XANES was used to also confirm that C-F bonds formed after the salt immersion test as shown in Figure 22 [Yang 2012].

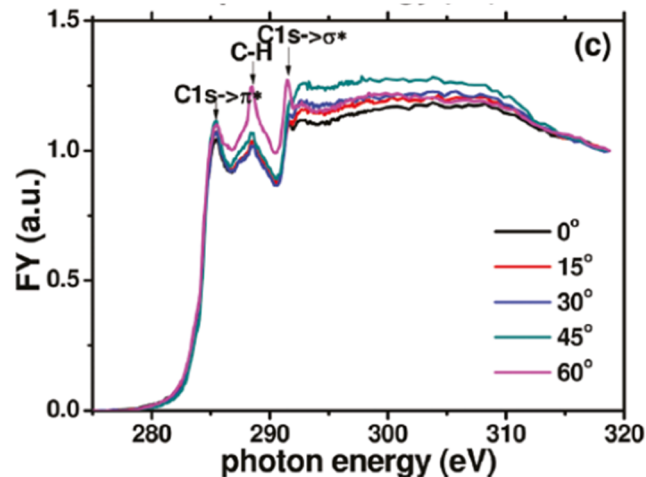


Figure 22. FY (fluorescence yield) spectra of IG-110 graphite. Reproduced from Yang et al. [2012].

8.7 RADIATION EFFECTS IN GRAPHITE

It is prudent to be aware of radiation effects in graphite that may affect corrosion and salt infiltration. Porosity and pore evolution of graphite certainly produces some challenges in modeling graphite behavior but so does fracture, induced by dimensional change in graphite due to neutron damage.

Neutron irradiation causes individual crystallites in graphite to swell along the c -axis and shrink along the a -axis [Blackstone 1977, Snead 2008, Marsden 2016], increasing the distance between the graphene sheets resulting in anisotropic crystallite growth. Over time, shrinkage and thermal stresses are generated. Most of the stress is thankfully relieved by radiation creep (inelastic strain). Graphite undergoes inelastic strain during neutron irradiation under stress at temperatures where thermal creep is considered negligible [Snead 2008, Marsden 2016]. The stress-strain relationship for graphite is non-linear and a permanent set (residual strains) can be produced even at very low stresses. Because of the significance of irradiation

induced creep in graphite core components, robust creep models (especially to resolve the high dose and high temperature tensile creep data) have long been sought. As graphite ages in service, it forms cracks [Freeman 2016, Marsden 2016]; micro and nano-cracks have been discovered in present UK gas reactors. Cracks can eventually allow ingress of molten salt.

The radiation response of Gilsocarbon grade graphite used in 14 of the UK’s current generation graphite reactors, shown in Figure 23. The temperature-dependent transition from shrinking to swelling, known as “turnaround,” is commonly observed in irradiated graphite.

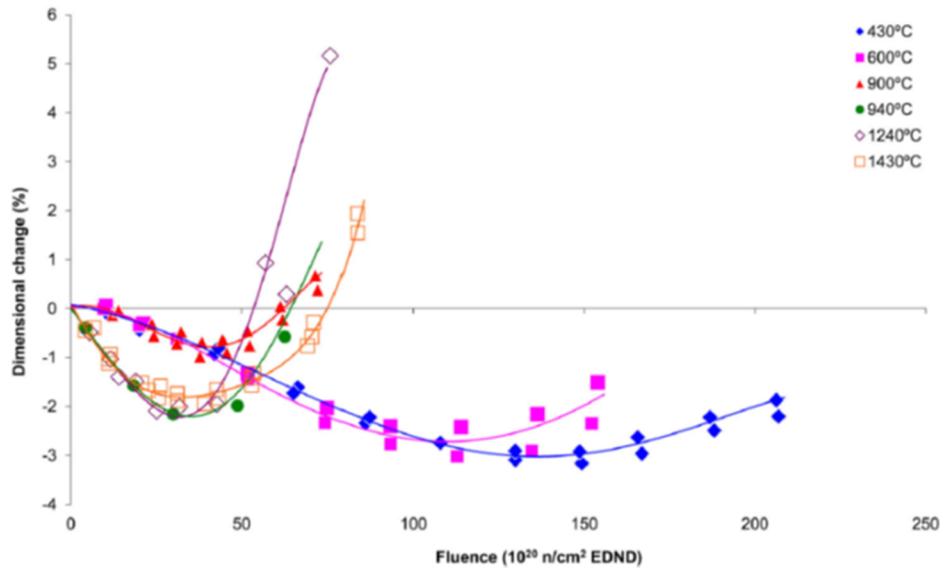


Figure 23. Dimensional change of in neutron irradiated semi-isotropic Gilsocarbon grade graphite, from Marsden [2016].

8.8 SiC_F/SiC AND C/C COMPOSITES FOR CORE STRUCTURAL COMPONENTS OF FHR

SiC is well-known for its radiation tolerance and stability in aggressive environments [Koyanagi 2014, Perez-Bergquist 2015, Deck 2015, Li 2018]. Because monolithic SiC is too brittle to be used in most structural applications, SiC/SiC ceramic matrix composite materials are typically used in engineering applications. SiC composites are produced by several fabrication routes, including chemical vapor infiltration (CVI), polymer impregnation and pyrolysis (PIP), reaction sintering (RS) and Nano-Infiltration and Transient Eutectic phase processing (NITE) [Igawa 2005, Koyanagi 2014, Park 2016]. However, the third-generation, nuclear-grade SiC/SiC composites are most often fabricated through CVI due to the highly crystalline, near stoichiometric SiC matrix yields and minimal fiber damage during processing [Li 2018]. Further, the CVI process is well-established and advancing due to its application for SiC/SiC composites for accident tolerant fuel cladding for Light Water Reactors [Deck 2015, Kim 2016, Li 2018]. SiC is less susceptible to dimensional change than graphite or C/C composites. An electron micrograph of SiC_F/SiC composite with exposed fiber bundles are shown in Figure 24.

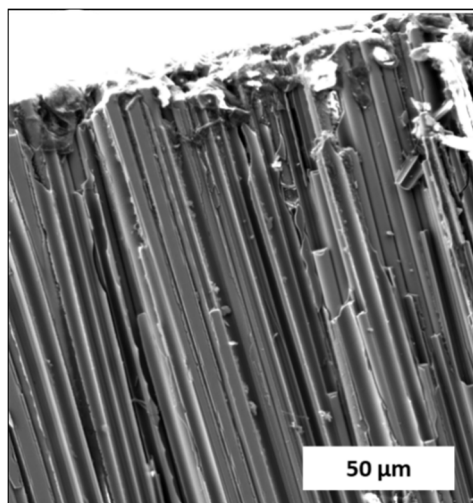


Figure 24. Secondary electron image of exposed fiber region of Rolls Royce® CVI SiC/SiC composite with 2D satin weave SA3 fiber reinforcement (silica polished).

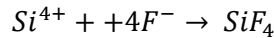
Xue et al. [2017, 2018] found that Cr^{3+} from alloy N accelerated corrosion of SiC due to the preferential formation of chromium carbides. CVD SiC samples were dipped in FLiNaK in sintered SiC capsules at 700 °C for 15 days, then SiC with alloy N, and finally SiC with CrF_3 to study Cr^{3+} . For CVD SiC in purified FLiNaK, cross-sectional Energy Dispersive X-ray Spectroscopy (EDS) spectra showed that corrosion resulted in the loss of elemental Si and the formation of a C-rich and O-rich surface. Slight corrosion of CVD SiC was observed in purified FLiNaK with a corrosion depth around 2.5 μm . For CVD SiC samples corroded in molten FLiNaK salt with CrF_3 , cross-sectional Scanning Electron Microscopy (SEM) showed that the corrosion depth was > 12.5 μm . Xue et al. also conducted a SiC capsule study with additions of 400, 800, 1200, and 2000 ppm CrF_3 in FLiNaK at 700 °C for 400 h to study the deposition/depletion corrosion of SiC. These tests further show that FLiNaK with Cr^{3+} is more aggressive toward SiC when compared to FLiNaK without Cr^{3+} addition.

Zaykov et al. [2014] shows that the solubility of silica in a fluoride-chloride melt depends on the melt composition. High resolution XPS scans of the O_{1s} peak before and after CrF_3 -SiC corrosion showed that peaks corresponding to Si-O disappeared after corrosion tests [Xue 2017]. High resolution Cr_{2p} scan showed the corresponding Cr-O interactions and Cr-C bonds of Cr_7C_3 and Cr_3C_2 . Results of Grazing Incidence X-ray Diffraction (GI-XRD) analysis were consistent with the XPS results for chromium carbides, and demonstrated that the CrF_3 formed carbides, mainly Cr_7C_3 and Cr_3C_2 , as corrosion products for Cr^{3+} reaction with SiC.

Yang et al. [2016b] studied the effects of Cr^{2+} and Ni^{2+} from Alloy N and its corrosion products CrF_2 and NiF_2 on SiC corrosion in FLiNaK at 700 °C. The capsule material was sintered SiC and the exposures lasted for 15 or 45 days. It was shown NiF_2 accelerated SiC corrosion. Potential reactivity between SiC and metal fluorides that form chromium carbides (e.g. Cr_7C_3) and nickel silicides (NiSi , $\text{Ni}_{31}\text{Si}_{12}$) is a possible explanation. Raman Spectroscopy before and after corrosion of CVD SiC (without Alloy N present) in pure FLiNaK at 700 °C for 15 days showed a disorder peak (D peak) and a graphitic peak (G peak) consistent with those of a graphite-rich layer. These tests were followed by exposure of Alloy N and SiC samples together in capsules containing FLiNaK. Cross-sectional EDS line-scans showed that Ni, Cr, Fe and Mo diffused outward to the alloy surface, but Fe and Mo accumulated near the surface while Ni and Cr dissolved into the salt. Glow Discharge Mass Spectroscopy (GD-MS) of FLiNaK after corrosion showed the Si content in FLiNaK increased. To study the effect of Cr^{2+} and Ni^{2+} on SiC corrosion, CrF_2 and NiF_2 were immersed with SiC in FLiNaK in the same SiC capsules. Cr^{3+} accelerated SiC corrosion by forming chromium carbides. It was found that Si leached preferentially into the melt

forming SiF_6^{2-} , and leaving behind a graphitic layer [Yang 2016b]. For Ni^{2+} corrosion, GI-XRD patterns revealed that the CVD SiC surface coating composed of β -SiC of about 50 μm disappeared after about 45 days, but the corrosion of simultaneously immersed alloy N and SiC were not as severe.

Si in SiC has been shown to preferentially dissolve into FLiNaK by a mechanism in which SiF_4 goes into the salt and a C-rich overlayer remains on SiC with chromium carbides.



Thermodynamic assessments suggest that chromium carbides will be favored over the carbides of other major alloying elements in molten FLiNaK. These reactions were shown to accelerate with added impurities of CrF_2 [Yang 2016b]. Overall, the corrosion behavior of SiC seemed favorable in purified FLiNaK tests around 700 °C with minimal weight change from Si-loss among similar capsule experiments [Xue 2018].

For the SiC_f/SiC composite, Yang [2016b] and Wang [2017a, 2017b] showed preferential corrosion of the SiC matrix when compared to the composite fibers in molten FLiNaK at 700 °C, due to the slightly higher oxygen content of this matrix phase. Micrographs in Figure 25 showed exfoliation of the composite surface. However, it is not clear what composite was being used in these studies and whether they were nuclear-grade. There are several manufacturing methods for SiC/SiC composites including chemical vapor infiltration (CVI), liquid silicon infiltration (LSI), melt infiltration (MI), polymer impregnation and pyrolysis (PIP), and transient eutectic phase (TEP) processes, and it is not yet clear how the manufacturing method affects corrosion behavior in molten salts.

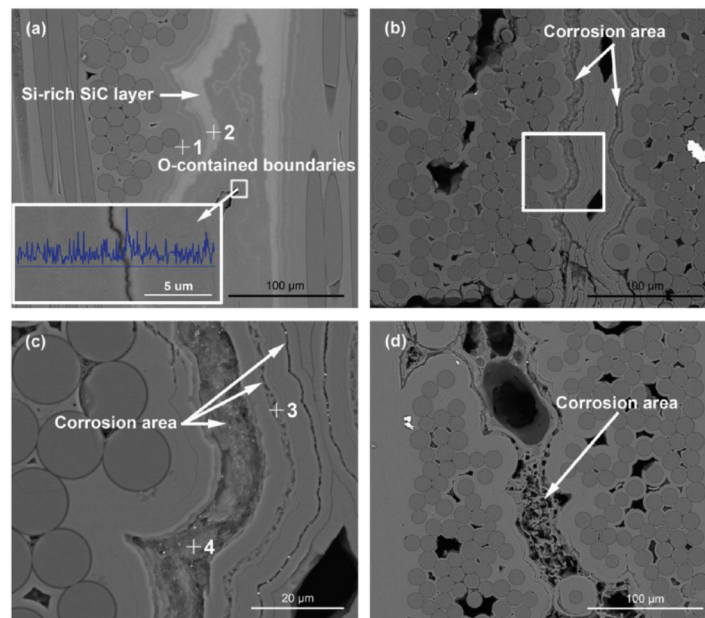


Figure 25. Corrosion of exposed matrix regions around fiber bundles of SiC_f/SiC composite in FLiNaK at 700 °C. Reproduced from Wang [2017b].

8.9 C/C COMPOSITES

The MSR compatibility of C/C composites has not been conclusively shown. C/C composites are a high strength material consisting of a carbon or graphite matrix with carbon reinforcing fibers. Like SiC_f/SiC composites, C/C composites are being considered in both fusion and fission reactors [Sauder 2015]. C/C

composites are potential candidates for MSR components because of their superior thermal shock resistance, high strength and low activation. Zhang et al. [2016] exposed C/C composites at 650 °C in FLiNaK at different pressures. The composites gained weight with increasing infiltration pressure and duration of exposure to molten FLiNaK. Mercury intrusion showed that the porosity of the composites was around 11% and 20 to 30 µm diameter pore sizes. The high temperature mechanical properties, such as interlaminar shear strength, compressive strength and flexural strength increased with weight gain from salt infiltration.

8.10 KNOWLEDGE GAPS

8.10.1 Salt penetration of medium and large grained graphite grades

A fine -grained graphite was used for the MSRE to prevent infiltration of salt into the graphite, but it is no longer available. While several graphite grades have been explored for use in gas reactors, these are generally medium to large-grained grades, as these exhibit superior radiation tolerance. The salt permeability of these larger-granted grades is a knowledge gap. This is a larger concern for salt-fueled concepts, as permeability of fuel into the graphite may have reactivity effects.

8.10.2 Effects of graphite on metal corrosion and vice versa

Available data show that graphite can accelerate corrosion of metals and vice versa. The most likely cause is formation of chromium carbides, which precipitate from the melt and decrease the activity of Cr and C in the melt, accelerating further corrosion. The effects are not yet well quantified, especially in flowing systems. The impact of galvanic effects between dissimilar materials in molten salts is also not yet well known. Corrosion testing with both graphite and containment materials can resolve this knowledge gap.

8.10.3 Degradation of structural SiC/SiC and C/C composites

While interactions with moderator and matrix graphite are the most pressing compatibility concern among non-metals, there may be interest in studying salt compatibility with SiC/SiC and C/C composite materials. These materials have favorable mechanical properties and radiation tolerance, and may be proposed as structural components in MSRs. Currently, the work on these materials has focused on bulk SiC and C, and knowledge of the behavior of the structural composite forms of these materials remains a knowledge gap.

9. CONCLUSIONS

This document has provided relevant background in the major technical areas related to corrosion in MSRs. Specific recommendations on materials have not been given, and instead the focus has been on general knowledge for informed regulatory decisions. Knowledge gaps have been identified at the end of each chapter, and the most important gaps have been synthesized (to avoid repetition) and are summarized below.

9.1 KNOWLEDGE GAPS

9.1.1 Standards for molten salt corrosion experiments

There is a shortage of quality data on corrosion of materials in molten salts. To enable understanding and quantification of materials degradation in molten salt environments, data need to be collected in a systematic fashion, using proper experimental controls. Data are also needed for purified salts that have

been verified using high-quality analytic chemistry before exposure. Experimental data are especially needed for salts with different impurity levels to understand the realistic limits that must be met for salt purification to enable acceptable material performance

Studies of alloy corrosion in molten salts are not standardized. Different labs have historically conducted tests with varied conditions, salt chemistries, and experimental methods, leading to difficulty comparing results across different efforts [Raiman 2018]. Reliable data on molten fluorides from the 1960s–1970s exist [Manly 1957, Koger 1972a, 1972b, Keiser 1977a, 1977b, 1977c], but they cover a limited range of fluoride salts and alloys and often lack complete salt chemistry analysis. Reliable data for chloride salts are particularly lacking.

Recognizing the need for regulators to analyze and assess data presented by diverse stakeholders, there is a need for standard methods for conducting corrosion experiments in molten salts. Creating these standards is not easy, as there is insufficient data to make evidence-based decisions regarding optimal experimental methods. Standards for salt purity are required, along with generally accepted best practices for salt handling, container materials, and corrosion testing procedures.

9.1.2 Effect of salt impurities and fission products

Oxidizing impurities in salt are a strong driver of corrosion. Since most salts proposed for use in MSRs are quite hygroscopic, moisture-based impurities are always present in salts to some degree, and removing them (and keeping them out) may be difficult. Total removal is not required, as MSRE ran successfully with little corrosion despite the certain presence of some level of impurities, but control of impurity levels within some yet-to-be-defined bounds is desirable for long-term operation.

There are currently no standards for salt purity or purification when conducting experiments in molten salt. Most available studies report the purification routines used for their salt, but they do not commonly report any analysis of the metal or oxide content of the salt after purification. Thus, there is no strong metric of the quality or effectiveness of the salt purification and no indication of the redox potential of the salt. This lack of standardization has led to extreme variability in data across studies [Raiman 2018]. Because of this variability, it is difficult to compare results to obtain data on the corrosion properties of alloys, container materials, and salt types.

Further, recent studies have been unable to replicate the very low corrosion rates reported by the ORNL experiments in the 1960s and 1970s [Koger 1972a, 1972b, Keiser 1977b, 1977c, DiStefano 1995]. While a number of factors may contribute to this, a likely contributing issue is the lack of effective salt purification. The ORNL experimenters used highly pure salts, but they released little data on purification techniques or Be additives in the starting salt. The lack of knowledge transfer has resulted in the current generation of molten salt experimenters using less pure, more aggressive salts for corrosion testing, and reported corrosion rates in the last several decades have yet to consistently match the low corrosion rates reported by the early ORNL experimenters.

It is therefore recommended that a greater emphasis be placed on understanding the effect of salt impurities on corrosion. Further, standards for salt purity need to be developed so data can be compared across studies. Two suggested metrics for salt purity are maximum oxygen content and maximum metallic impurity content. Engagement with a standards development organization such as ASTM International also is recommended.

The effect of fission products on corrosion is another area that is not well understood. Although past work has studied the effect of Te induced cracking [Keiser 1977a, Ignat'ev 2016], a significant knowledge gap exists regarding the effects of other fission products that may affect corrosion, among other materials

issues. Among them, tritium is believed to be a potential corrodent, as it readily forms an oxidizing halide.

9.1.3 Effectiveness of redox control additives

Even if salts can be cleaned of impurities during initial loading, it is unrealistic to assume that salts will remain pure during operation because fission products are being created during operation. Moisture, oxygen, and metallic impurities will inevitably get into salt melts, rendering the coolant more corrosive. Additionally, as fission products accumulate, they will likely affect salt corrosivity. For these reasons, it is likely necessary to use salt additives to control redox during operation. Metallic Be has been shown to be an effective redox control additive in FLiBe [Thoma 1971, Keiser 1979, Olander 2002]. In chloride salts, contact with reactive metals such as Mg has been shown to reduce corrosivity [Susskind 1960, Olson 2015, Pint 2019], although the studies have been more limited. One concern with Mg additives is that excessive additions result in the formation of Mg-rich compounds on alloys surfaces [Pint 2019]. Other negative consequences are possible with excessive Be additions in FLiBe, such as attack of graphite in fuel salts.

Assessment and qualification of redox control additives is an important knowledge gap. An assessment of redox control schemes would be needed to determine their effectiveness in managing corrosion, and to determine their viability in-service by demonstrating acceptable mass transport behavior in flowing systems.

9.1.4 Graphite compatibility and infiltration

Graphite is the most commonly proposed moderator material for thermal reactors. Carbon also is a proposed outer-layer material for fuel pebbles in the solid-fueled FHR design [Allen 2013, Scarlet 2014, Qualls 2017]. Structural graphite is generally understood to have good compatibility with fluoride salts, exhibiting minimal mass loss. However, fluorination is a concern because it can lead to chemical changes in the graphite [Tang 2017]. Tang et al. [2017] exposed several grades of graphite to molten FLiBe and observed that graphite grades with higher porosity experienced greater fluorine penetration than grades with lower porosity. This is especially concerning for fuel salts, as infiltration of fissile isotopes may affect core neutronics. DiStefano et al. [1995] asserted that graphite with pore sizes of $<1 \mu\text{m}$ should resist salt intrusion; however, the research that led to this conclusion is not well documented. Further, the fine-grained graphite grade used in the MSRE is no longer available. Most current research on graphite focuses on grades proposed for HTGR, which tend to be larger grained grades with larger pores, which have better dimensional stability under irradiation.

Selection and testing of graphite grades for MSRs is a knowledge gap. Research on graphite infiltration as a function of pressure and pore size is required to properly assess graphite behavior and to select and approve a graphite grade that balances fluoride salt hermeticity with radiation stability. Chloride salt data are not needed at this time, as chloride reactors are generally fast spectrum reactors that do not require moderation.

9.1.5 Corrosion sensors

In-service feedback on corrosion and salt chemistry is desired for safe and effective reactor operation. Electro-chemistry in molten salts has been used in pyro-metallurgy [Zhang 2014], but a reliable method for in-service redox monitoring has not yet been developed, although this is an active area of research [Carotti 2017, Zhang 2018]. The MSRE successfully employed offline measurement of dissolved Cr as a corrosion indicator [McCoy 1970]. Spectroscopic methods have been proposed [e.g. Young 1967, Toth

1973], but are not yet mature. The development and qualification of a reliable, preferably commercial method for measuring salt and material conditions is a knowledge gap.

9.1.6 SiC and ceramic components

Little data exists on the compatibility of SiC and other ceramics with molten salts. Ceramic materials have not been widely adopted for use in MSRs, but limited data suggests they may have merit in some applications but may not be compatible with all salts. Ceramic matrix composite (CMC) materials may be proposed as structural materials, and ceramic components have been explored in a limited capacity for pump components, sealing components, and heat exchangers. For a system with both ceramic and metal components, the potential for dissimilar material corrosion also should be evaluated. The performance of ceramic materials in molten salts is a knowledge gap.

9.1.7 Irradiation-corrosion

There presently are few data on the effects of radiation on corrosion. There are gaps in the current understanding of the effect of irradiation on salt properties, and of how irradiating salt might affect its corrosive properties. Further, understanding of the effect of radiation on salt-material interfaces is incomplete for both structural alloys and moderator materials. The effect of irradiation on corrosion in molten salts is a knowledge gap as it may have a significant impact on reactor performance.

9.1.8 Chloride Salts

Substantial knowledge of molten fluoride chemistry and material compatibility was gained during the MSRE and MSBR days in the 1950s to the 70s. Even after those years, fluoride salts were explored substantially more compared to their chloride salt counterparts. While chloride salts have received attention from the pyroprocessing and CSP communities in recent years, the available data are far less comprehensive. With several vendors pursuing chloride-salt-based fast reactors, there is little data available on corrosion in chloride salts, especially fuel salts. Also, purification techniques used with chloride salts are less mature than techniques used with fluoride salts [Ambrosek 2011].

10. REFERENCES

- Afonichkin, V., Bovet, A., Shishkin, V. (2011) "Salts purification and voltametric study of the electroreduction of U(IV) to U(III) in molten LiF–ThF₄," *Journal of Nuclear Materials*, 419, 347-352.
- Allen, T., et al. (2013a) "Integrated Research Project Workshop 1: Fluoride-Salt-Cooled, High-Temperature Reactor (FHR) Subsystems Definition, Functional Requirement Definition, and Licensing Basis Event (LBE) Identification White Paper." INL NEUP report.
- Allen, T., et al. (2013b) "FHR Materials, Fuels and Components White Paper Integrated Research Project Workshop 3 Fluoride-Salt-Cooled High Temperature Reactor (FHR) Materials, Fuels and Components White Paper." INL NEUP report.
- Ambrosek, J. (2011) "Doctoral Dissertation: Molten Chloride Salts for Heat Transfer in Nuclear Systems," University of Wisconsin, Madison, WI.
- ASME (2015) ASME Boiler and Pressure Vessel Code Division 5 High Temperature Reactors, III Rules for Construction of Nuclear Facility Components, 2015.
- Atkinson, S., Abram, T. J., Litskevich, D., Merk, B. (2019) "Small modular high temperature reactor optimisation – Part 1: A comparison between beryllium oxide and nuclear graphite in a small scale high temperature reactor," *Progress in Nuclear Energy* 111, 223-232.

- Atmani, H., Rameau, J. J. (1984) "Environmentally assisted cracking of 304L stainless steel in molten salts media," *Corrosion Science*, 24(4), 279-285.
- Atsumi, H., Muhaimin, A., Tanabe, T., Shikama, T. (2009) "Hydrogen trapping in neutron-irradiated graphite," *Journal of Nuclear Materials* 386-388, 379-382.
- Atsumi, H., Tanabe, T., Shikama, T. (2011) "Hydrogen behavior in carbon and graphite before and after neutron irradiation – Trapping, diffusion and the simulation of bulk retention," *Journal of Nuclear Materials* 417, 633-636.
- Aufiero, M., et al. (2013) "An Extended Version of the SERPENT-2 Code to Investigate Fuel Burn-up and Core Material Evolution of the Molten Salt Fast Reactor." *Journal of Nuclear Materials*, 441, 473–86, doi:10.1016/j.jnucmat.2013.06.026.
- Baes, C. F. (1974). The chemistry and thermodynamics of molten salt reactor fuels," *Journal of Nuclear Materials*, 51(1), 149-162.
- Bailly, H., Prunier, C., Ménessier, D. (1999) "The Nuclear Fuel of Pressurized Water Reactors and Fast Neutron Reactors: Design and Behaviour," Intercept Limited.
- Bamberger, C. (1975) "Experimental Techniques in Molten Fluoride Chemistry." *Advances in Molten Salt Chemistry*, vol. 3.
- Benes, O., Konings, R.J.M., (2009) Thermodynamic properties and phase diagrams of fluoride salts for nuclear applications," *J. Fluorine Chem.* 130 (1), 22-29.
- Bernardet, V., S. Gomes, S. Delpoux, M. Dubois, K. Guérin, D. Avignant, G. Renaudin, L. Duclaux, (2009) "Protection of nuclear graphite toward fluoride molten salt by glassy carbon deposit," *J. Nucl. Mater.* 384, 292-302.
- Bettis, E. S., et al. (1957) "The Aircraft Reactor Experiment-Operation 1." *Nuclear Science and Engineering*, 2, 841–53.
- Blackstone, R. (1977) "Radiation creep of graphite. An introduction," *Journal of Nuclear Materials* 65, 72-78.
- Bonal, J. P., Wu, C. H. (1996) "Neutron induced thermal properties changes in carbon fiber composites irradiated from 600 to 1000°C," *Journal of Nuclear Materials* 230, 271-279.
- Briggs, R. B. (1964) "Molten-Salt Reactor Program Semiannual Progress Report for Period Ending July 31, 1964," ORNL Report ORNL-3708, Oak Ridge, TN.
- Briggs, R. B. (1965) "Molten-Salt Reactor Program Semiannual Progress Report for Period Ending February 28, 1965," ORNL Report ORNL-3872, Oak Ridge, TN.
- Briggs, R.B. (1971) "Tritium in molten-salt reactors," *React. Technol.* 14, 335.
- Briggs, R. B., Nestor, C. W. (1975) "A method for calculating the steady-state distribution of tritium in a molten-salt breeder reactor plant," ORNL Report ORNL-TM-4804, Oak Ridge, TN.
- Bull Ezell, N. D., Raiman, S. S., Kurley, J. M., McDuffee, J. (2020) "Neutron irradiation of alloy N and 316L stainless steel in contact with a molten chloride salt," *Nuclear Engineering and Technology* (2020) in press. doi.org/10.1016/j.net.2020.07.042.
- Bulmer, J. J., et al. (1956) "Fused Salt Fast Breeder Reactor Design and Feasibility Study," ORNL report ORNL-CF-56-8-204, Oak Ridge, TN.
- Carling, R.W., Mar, R.W. (1981) "Industrial Use of Molten Nitrate/Nitrite Salts," SNL Report SAND-81-8020, Albuquerque, NM.

- Carotti, F., et al. (2017) “Characterization of a Thermodynamic Reference Electrode for Molten LiF-BeF₂ (FLiBe).” *Journal of The Electrochemical Society*, 164, 854–61, doi:10.1149/2.1591712jes.
- Chan, K. J., Ambrecht, R. J., Luong, J. M., Choi, W. T., Singh, P. M. (2018) “Carburization effects on the corrosion of Cr, Fe, Ni, W and Mo in Fluoride-salt cooled high temperature reactor,” *Annals of Nuclear Energy* 120, 279-285.
- Chasanov, M. G. (1965) “Fission-Product Effects in Molten Chloride Fast-Reactor Fuels,” *Nuclear Science and Engineering*, 23(2), 189-190.
- Chase M.W., Davies, C.A., Downey, J.R., Frurip, D.J., McDonald, R.A., and Syverud, A.N., (1985) *JANAF Thermochemical Tables, Third Edition, J. Phys. Chem. Ref. Data, Vol. 14, Suppl. 1.*
- Cheng, W.-J., R. S. Sellers, M. H. Anderson, K. Sridharan, C.-J. Wang, and T. R. Allen, (2017) “Zirconium Effect on the Corrosion Behavior of 316L Stainless Steel Alloy and Hastelloy-N Superalloy in Molten Fluoride Salt,” *Nucl. Technol.*, 183 (2), 248–259.
- Cherginets, V. L., Rebrova, T. P., & Naumenko, V. A. (2015). Oxoacidity scale of molten ionic chlorides and bromide. *Fluid Phase Equilibria*, 401, 77-81.
- Cohen, S I, Jones, T N. (19570 “Viscosity Measurements on Molten Fluoride Mixtures,” ORNL report ORNL-2278, Oak Ridge, TN.
- Compere, E. L., Kirslis, S. S., Bohlmann, E. G., Blankenship, F. F., Grimes, W. R. (1975) “Fission product behavior in the Molten Salt Reactor Experiment,” ORNL report ORNL-4865, Oak Ridge, TN. doi:10.2172/4077644.
- Danon, A. E., Muránsky, O., Karatchevtseva, I., Zhang, Z., Li, Z. J., Scales, N., . . . Edwards, L. (2020). Molten salt corrosion (FLiNaK) of a Ni–Mo–Cr alloy and its welds for application in energy-generation and energy-storage systems. *Corrosion Science*, 164, 108306.
- Deck, C. P., Jacobsen, G. M., Sheeder, J., Gutierrez, O., Zhang, J., Stone, J., Khalifa, H. E., Back, C. A. (2015) “Characterization of SiC–SiC composites for accident tolerant fuel cladding,” *Journal of Nuclear Materials* 466, 667-681.
- DeVan, J. H., and R. B. Evans, III (1962) “Corrosion Behavior of Reactor Materials in Fluoride Salt Mixtures,” ORNL report ORNL-TM-328, 4774669, Oak Ridge, TN. doi:[10.2172/4774669](https://doi.org/10.2172/4774669).
- Ding, W., Bonk, A., Bauer, T. (2018a) “Corrosion behavior of metallic alloys in molten chloride salts for thermal energy storage in concentrated solar power plants: A review,” *Frontiers of Chemical Science and Engineering*, 12(3), 564-576.
- Ding, W., Shi, H., Xiu, Y., Bonk, A., Weisenburger, A., Jianu, A., & Bauer, T. (2018b). Hot corrosion behavior of commercial alloys in thermal energy storage material of molten MgCl₂/KCl/NaCl under inert atmosphere. *Solar Energy Materials and Solar Cells*, 184, 22-30.
- Ding, W. Shi, H., Jianu, A., Xiu, Y., Bonk, A., Weisenburger, A., Bauer, T. (2019) “Molten chloride salts for next generation concentrated solar power plants: Mitigation strategies against corrosion of structural materials,” *Solar Energy Materials and Solar Cells* 193 (2019) 298–313
- DiStefano, J. R., Devan, J. H., Keiser, J. R., Klueh, R. L., Eatherly, W. P. (1995) *Materials Considerations for Molten Salt Accelerator Based Plutonium Conversion Systems*,” ORNL Report ORNL/TM/12925/R1, Oak Ridge, TN.
- Edeleanu, C., & Littlewood, R. (1960). Thermodynamics of corrosion in fused chlorides. *Electrochimica Acta*, 3(3), 195-207.

- Elbakhshwan, M., Doniger, W., Falconer, C., Moorehead, M., Parkin, C., Zhang, C., Sridharan, K., Couet, A. (2019) "Corrosion and Thermal Stability of CrMnFeNi High Entropy Alloy in Molten FLiBe Salt," *Scientific Reports* 9, 18993.
- Engel, J. R., Steffy, R. C. (1971) "Xenon behavior in the molten salt reactor experiment," ORNL Report ORNL-TM-3464, Oak Ridge, TN.
- Evans, A. G., Zok, F. W., McMeeking, R. M., Du, Z. Z. (1996) "Models of high-temperature, environmentally assisted embrittlement in ceramic-matrix composites," *Journal of the American Ceramic Society* 79, 2345-2352.
- Evans, R. B., et al. (1961) "Self-Diffusion of Chromium in Nickel-Base Alloys," ORNL Report ORNL-2982, Oak Ridge, TN.
- Evans, R. B., Rutherford, J. L., Malinauskas, A. P. (1969) "Gas Transport in MSRE Moderator Graphite. II Effects of Impregnation III. Variation of Flow Properties," ORNL Report ORNL-4389, Oak Ridge, TN, doi:10.2172/4788362.
- Fabre, S., Cabet, C., Cassayre, L., Chamelot, P., Delepech, S., Finne, J., . . . Noel, D. (2013) "Use of electrochemical techniques to study the corrosion of metals in model fluoride melts," *Journal of Nuclear Materials*, 441, 583-591.
- Feng, X. K., C. A. Melendres, (1982) "Anodic Corrosion and Passivation Behavior of Some Metals in Molten LiCl-KCl Containing Oxide Ions," *J. Electrochem. Soc.*, 129, 1245.
- Forsberg, C. W., Peterson, P. F., Pickard, P. S. (2003) "Molten-Salt-Cooled Advanced High-Temperature Reactor for Production of Hydrogen Electricity," *Nuclear Technology* 144, 289-302, DOI: 10.13182/NT03-1.
- Forsberg, C.W. (2004) "Reactors with molten salts: options and missions," in Frederick Joliot and Otto Hahn Summer School on Nuclear Reactors, Physics and Fuels Systems, Cadarache, France, held Aug. 25 – Sept. 3, 2004.
- Forsberg, C. W., Lam, S., Carpenter, D. M., Whyte, D. G., Scarlet, R., Contescu, C., Wei, L., Stempien, J., Blandford, E. (2017a) "Tritium Control and Capture in Salt-Cooled Fission and Fusion Reactors: Status, Challenges, and Path Forward," *Nuclear Technology* 197, 119-139.
- Forsberg, C. W., Carpenter, D. M., Whyte, D. G., Scarlet, R., Wei, L. (2017b) "Tritium Control and Capture in Salt-Cooled Fission and Fusion Reactors," *Fusion Science and Technology* 71, 584-589.
- Freeman, H. M., Jones, A. N., Ward, M. B., Hage, F. S., Tzelepi, N., Ramasse, Q. M., Scott, A. J., Brydson, R. M. D. (2016) "On the nature of cracks and voids in nuclear graphite," *Carbon* 103, 45-55.
- Friedman, H. A., et al. (1963) "Thermal Analysis and Gradient Quenching Apparatus and Techniques for the Investigation of Fused Salt Phase Equilibria," ORNL Report ORNL-3373, Oak Ridge, TN.
- Gibilaro, M., Massot, L., & Chamelot, P. (2015). A way to limit the corrosion in the Molten Salt Reactor concept: the salt redox potential control. *Electrochimica Acta*, 160, 209-213.
- Glassner, A. (1957) "The Thermochemical Properties of the oxides, fluorides and chlorides to 2500 K," ANL report ANL-5750. Lemont, IL.
- Goldberg, G., Meyer Jr., A. S., White, J. C. (1960) "Determination of oxides in fluoride salts by high-temperature fluorination with potassium bromotetrafluoride," *Analytical Chemistry* 32 (3) 314-317.
- Gomez-Vidal, J. C., Tirawat, R. (2016) "Corrosion of alloys in a chloride molten salt (NaCl-LiCl) for solar thermal technologies," *Sol. Energy Mater. Sol. Cells*, 157, 234-244

- Gomez-Vidal, J. C., A. G. G. Fernandez, R. Tirawat, C. Turchi, and W. Huddleston, (2017) "Corrosion resistance of alumina-forming alloys against molten chlorides for energy production. I: Pre-oxidation treatment and isothermal corrosion tests," *Sol. Energy Mater. Sol. Cells*, 166, 222–233.
- Grabaskas, D. Fei, T., Jerden, J. (2020) "Technical Letter Report on The Assessment of Tritium Detection and Control in Molten Salt Reactors: Final Report," Argonne National Laboratory, ANL/NSE-20-15, Argonne, IL.
- Grimes, W.R. (1967) "Chemical research and development for the molten-salt breeder reactor," ORNL report ORNL/TM-1853, Oak Ridge, TN.
- Guo, S., Zhang, J., Wu, W., & Zhou, W. (2018) "Corrosion in the Molten Fluoride and Chloride Salts and Materials Development for Nuclear Applications." *Progress in Materials Science*, 97, 448–487. doi:[10.1016/j.pmatsci.2018.05.003](https://doi.org/10.1016/j.pmatsci.2018.05.003).
- Guo, S., Zhuo, W., Wang, Y., & Zhang, J. (2020). Europium induced alloy corrosion and cracking in molten chloride media for nuclear applications. *Corrosion Science*, 163, 108279.
- Gurvich, L.V., Veyts, I.V., and Alcock, C.B., (1994) "Thermodynamic Properties of Individual Substances," Fourth Edition, Vol. 3, CRC Press, Boca Raton, FL, 1994.
- Harder, B. R., Long, G., and Stanaway, W. P. (1969) "Compatibility and Processing Problems in the Use of Molten Uranium Chloride–Alkali Chloride Mixtures as Reactor Fuels," *Nucl. Met., Met. Soc. AIME*, 15, 405-432.
- Haubenreich, P. N. and J. R. Engel, J. R. (1970) "Experience with the Molten-Salt Reactor Experiment," *Nuclear Applications and Technology*, 8(2), 118-136, DOI: 10.13182/NT8-2-118.
- He, X., J. Song, L. Xu, J. Tan, H. Xia, B. Zhang, Z. He, L. Gao, X. Zhou, M. Zhao, Z. Zhu, S. Bai, (2013) "Protection of nuclear graphite toward liquid fluoride salt by isotropic pyrolytic carbon coating," *J. Nucl. Mater.* 442 (1-3) (2013) 306-308.
- He, X., J. Song, J. Tan, B. Zhang, H. Xia, Z. He, X. Zhou, M. Zhao, X. Liu, L. Xu, S. Bai, (2014) "SiC coating: an alternative for the protection of nuclear graphite from liquid fluoride salt," *J. Nucl. Mater.* 448, 1-3.
- He, Z., Gao, L., Qi, W., Zhang, B., Wang, X., Song, J., He, X., Zhang, C., Tang, H., Holmes, R., Xia, H., Zhou, X. (2015) "Molten FLiNaK salt infiltration into degassed nuclear graphite under inert gas pressure," *Carbon* 84, 511-518.
- He, Z., P. Lian, Y. Song, Z. Liu, J. Song, J. Zhang, J. Feng, X. Yan, Q. Guo, (2018a) "Improving molten fluoride salt and Xe 135 barrier property of nuclear graphite by phenolic resin impregnation process," *J. Nucl. Mater.* 499, 79-87.
- He, Z., P. Lian, Y. Song, Z. Liu, J. Song, J. Zhang, X. Ren, J. Feng, X. Yan, Q. Guo, W. Liu, (2018b) "Protecting nuclear graphite from liquid fluoride salt and oxidation by SiC coating derived from polycarbosilane," *J. Eur. Ceram. Soc.* 38, 453-462.
- He, Z., J. Song, P. Lian, D. Zhang, Z. Liu, (2019) "Excluding molten fluoride salt from nuclear graphite by SiC/glassy carbon composite coating," *Nucl. Eng. Technol.* 51 (5) (2019) 1390-1397.
- Hou, J., et al., (2016) "Effects of exposing duration on corrosion performance in weld joint of Ni-Mo-Cr alloy in FLiNaK molten salt," *J. Fluor. Chem.*, 191, 110–119.
- Hyland, R. F. (1962) Tests of a Resistance-Type High-Temperature Sensor for the Continuous Measurement of Salt Level in Molten Salt Fueled Reactors," ORNL report ORNL-TM-331, 4776622. doi:[10.2172/4776622](https://doi.org/10.2172/4776622).

- IAEA (2004) "Management of Waste Containing Tritium and Carbon-14," Technical Reports Series No. 421, Vienna.
- Icenhour, A.S., Williams, D.F., Trowbridge, L.D., Toth, L.M., & Del Cul, G.D. (2001) "An overview of radiolysis studies for the molten salt reactor remediation project," in Proceedings of the Global 2001 International Conference on Back-end of the fuel cycle: from research to solutions, Paris, France.
- Igawa, N., Taguchi, T., Nozawa, T., Snead, L. L., Hinoki, T., McLaughlin, J. C., Katoh, Y., Jitsukawa, S., Kohyama, A. (2005) Fabrication of SiC fiber reinforced SiC composite by chemical vapor infiltration for excellent mechanical properties," *Journal of Physics and Chemistry of Solids* 66, 551-554.
- Ignatiev, V., et al., (2008) "Compatibility of Selected Ni-Based Alloys in Molten Li,Na,Be/F Salts with PuF₃ and Tellurium Additions," *Nucl. Technol.* 164 (1), 130–142.
- Ignatiev V., Surenkov, A. (2013a) "Alloys compatibility in molten salt fluorides: Kurchatov Institute related experience," *J. Nucl. Mater.*, 441, 592–603.
- Ignatiev, V., et al., (2013b) "Intergranular tellurium cracking of nickel-based alloys in molten Li, Be, Th, U/F salt mixture," *J. Nucl. Mater.*, 440, 243–249.
- Ignat'ev, V. V., Surenkov, A. I., Gnidoi, I. P., Uglov, V. S., & Konakov, S. A. (2016) "Experimental Investigation of Tellurium Corrosion of Nickel-Molybdenum Alloys in Molten Lithium-, Beryllium-, and Uranium-Fluoride Salts," *Atomic Energy*, 120(6), 397-402.
- Ingersoll, D. T., Forsberg, C. W., MacDonald, P. E. (2006) "Trade Studies on the Liquid-Salt-Cooled Very High-Temperature Reactor: Fiscal Year 2006 Progress Report," ORNL Report ORNL/TM-2006/140, Oak Ridge, TN.
- Jenkins, H. W. (1969) "Electrochemical Measurements in Molten Fluorides," University of Tennessee, 1969. https://trace.tennessee.edu/utk_graddiss/3072.
- Jordan, W. H. (1957) "Aircraft Nuclear Propulsion Project Quarterly Progress Report for Period Ending December 31, 1956," ORNL Report ORNL-1170, Oak Ridge, TN.
- Kasten, P. R., Bettis, E. S., Cook, W. H., Eatherly, W. P., Holmes, D. K., Kedl, R. J., Kennedy, C. R., Kirslis, S. S., McCoy, H. E., Perry, A. M., Robertson, R. C., Scott, D., Strehlow, R. A. (1969) "Graphite behavior and its effects on MSBR performance," *Nuclear Engineering and Design* 9, 157-195.
- Kato, Y., Furukawa, K., Araki, N., Kobayasi, K. (1983) "Thermal diffusivity measurement of molten salts by use of a simple ceramic cell," *High Temperature High Pressure* 15, 191 (1983).
- Kedl, R. J. (1972) "Migration of a class of fission products (noble metals) in the Molten-Salt Reactor Experiment," ORNL report ORNL-TM-3884, Oak Ridge, TN, doi:10.2172/4471292.
- Keilholtz, G. W., et al. (1959) "Effect of Radiation on Corrosion of Structural Materials by Molten Fluorides." *Nuclear Science and Engineering*, vol. 5, no. 1, pp. 15–20. doi:10.13182/NSE59-A27323.
- Keiser, J. R., Manning, D. L., Clausing, R. E. (1976) "Corrosion resistance of some Nickel-Base Alloys to Molten Fluoride Salts Containing UF₄ and Tellurium," in *Molten Salts*, ECS Proceedings Vol. 1976-6, Electrochemical Society, Pennington, NJ, pp. 315–328.
- Keiser, J. R. (1977a). "Status of Tellurium-Hastelloy N Studies in Molten Fluoride Salts," ORNL report ORNL/TM-6002, Oak Ridge, TN.
- Keiser, J. R., DeVan, J. H., & Manning, D. L. (1977b). The Corrosion Resistance of Type 316 Stainless Steel to Li₂BeF₄," ORNL report ORNL/TM/5782, Oak Ridge, TN.
- Keiser, J. R. (1977c) "Compatibility Studies of Potential Molten Salt Breeder Reactor Materials in Molten Fluoride Salts," ORNL report ORNL/TM/5783, Oak Ridge, TN.

- Keiser, J. R., DeVan, J. H., Lawrence, E. J. (1979) "Compatibility of molten salts with type 316 stainless steel and lithium," *J. Nucl. Mater.*, 85–86, 295–298.
- Kim, H.-G., Yang, J.-H., Kim, W.-J., Koo, Y.-H. (2016) "Development Status of Accident-tolerant Fuel for Light Water Reactors in Korea," *Nuclear Engineering and Technology* 48, 1-15.
- Kipouros, G. J., Sadoway, D. R. (2001) "A thermochemical analysis of the production of anhydrous $MgCl_2$," *Journal of Light Metals* 1, 111-117.
- Kirtchik, H., Culp, S. (1965) "Bromine trifluoride method for oxygen in liquid alkali metals," NASA Report NASw-882.
- Koger, J. W., Litman, A. P. (1970) "Catastrophic Corrosion of Type 304 Stainless Steel in a System Circulating Fused Sodium Fluoroborate. ORNL-TM-2741, Oak Ridge, TN.
- Koger, J. W. (1972a) "Alloy Compatibility with LiF--BeF Salts Containing ThF and UF," ORNL Report ORNL/TM/4286, Oak Ridge, TN.
- Koger, J.W. (1972b) "Evaluation of Hastelloy N Alloy After Nine Years Exposure to Both a Molten Fluoride Salt and At at Temperatures from 700 to 560C," ORNL Report ORNL TM 4189, Oak Ridge, TN.
- Koger, J. W. (1972c) "Effect of FeF_2 addition on mass transfer in a Hastelloy N-LiF-BeF₂-UF₄ thermal convection loop system," ORNL Report ORNL-TM-4188, Oak Ridge, TN.
- Köhler, J. (2014). Halides: Solid-State Chemistry. In *Encyclopedia of Inorganic and Bioinorganic Chemistry*, R.A. Scott (Ed.). doi:[10.1002/9781119951438.eibc0078.pub2](https://doi.org/10.1002/9781119951438.eibc0078.pub2)
- Koyanagi, T., Ozawa, K., Hinoki, T., Shimoda, K., Y. Katoh, Y., (2014) "Effects of neutron irradiation on mechanical properties of silicon carbide composites fabricated by nano-infiltration and transient eutectic-phase process," *Journal of Nuclear Materials* 448, 478-486.
- Kurley, J. M., Halstenberg, P. W., McAlister, A., Raiman, S., Dai, S., Mayes, R. T. (2019) "Enabling Chloride Salts for Thermal Energy Storage: Implications of Salt Purity." *RSC Advances*, 9, 25602–25608, doi:[10.1039/C9RA03133B](https://doi.org/10.1039/C9RA03133B).
- Lane, J. A., MacPherson, H. G., Maslan, F. (1958) "Fluid Fuel Reactors," Addison-Wesley,
- Laudone, G. M., Gribble, C. M., Matthews, G. P. (2014) "Characterisation of the porous structure of Gilsocarbon graphite using pycnometry, cyclic porosimetry and void-network modeling," *Carbon* 73, 61-70.
- Lee, J. J., Raiman, S. S., Katoh, Y., Koyanagi, T., Contescu, C. I., Hu, X., Yang, Y. (2019) "Chemical compatibility of silicon carbide in molten fluoride salts for the fluoride salt-cooled high temperature reactor," *Journal of Nuclear Materials* 524, 119–134.
- Lee, J. J., Arregui-Mena, J. D., Contescu, C. I., Burchell, T. D., Katoh, Y., Loyalka, S. K. (2020) "Protection of graphite from salt and gas permeation in molten salt reactors," *Journal of Nuclear Materials* 534, 152119.
- Lewis, D. (1971). Some aspects of electrochemical thermodynamics and equilibrium diagrams for aqueous systems at elevated temperatures and for simple molten salt systems. *Journal of Inorganic and Nuclear Chemistry*, 33(7), 2121-2140.
- Li, H., Yang, X., Yin, X., Tang, J., Gong, J., Fuyang, C. (2020) "Effects of constant load on corrosion cracking of 304 ASS at 600°C in molten salts," *Materials and Corrosion* 71, 938-948.
- Li, M., Zhou, X., Yang, H., Du, S., Huang, Q. (2018) "The critical issues of SiC materials for future nuclear systems," *Scripta Materialia* 143, 149-153.

- Liu, M., et al., (2013) "Investigation on corrosion behavior of Ni-based alloys in molten fluoride salt using synchrotron radiation techniques," *J. Nucl. Mater.*, 440, 124–128.
- Long, J. R. (1948) "The Use of Ammonium Bifluoride in the Preparation of Fluorides from Oxides." U.S. Atomic Energy Commission. Technical Information Service, 1948.
- Lynch, S. P. (2013) "Mechanisms and Kinetics of Environmentally Assisted Cracking: Current Status, Issues, and Suggestions for Further Work," *Metallurgical and Materials Transactions A* 44, 1209-1229.
- MacPherson, H. G., Alexander, L. G., Carrison, D. A., Estabrook, J. Y., Kinyon, B. W., Mann, L. A., Roberts, J. T., Romie, E. F., VonderLage, F. C. (1957). "A Preliminary Study of Molten Salt Power Reactors," ORNL Report CF-57-4-27, Oak Ridge, TN.
- MacPherson, H. G. (1959) "Molten Salt Reactor Project Quarterly Project Report for Period Ending January 31, 1959," ORNL Report ORNL-2684, Oak Ridge, TN.
- MacPherson, H. G. (1960) "Molten-salt reactor program quarterly progress report for periods ending January 31 and April 30, 1960," ORNL Report ORNL-2973, Oak Ridge, TN.
- Mamantov, G., Manning, D. L. (1966) "Voltammetry and Related Studies of Uranium in Molten Lithium Fluoride-Beryllium Fluoride-Zirconium Fluoride." *Analytical Chemistry*, 38, 1494–98.
doi:[10.1021/ac60243a010](https://doi.org/10.1021/ac60243a010).
- Manly, W. D., et al. (1957) "Aircraft Reactor Experiment-Metallurgical Aspects," ORNL Report ORNL-2349, Oak Ridge, TN.
- Marsden, B. J., Haverty, M., Bodel, W., Hall, G N., Jones, A. N., Mummery, P. M., Treifi, M. (2016) "Dimensional change, irradiation creep and thermal/mechanical property changes in nuclear graphite," *International Materials Reviews* 61, 155-182.
- Martínez, A. M., Castrillejo, Y., Børresen, B., Bermejo, M. R., & Vega, M. (2000). Chemical and electrochemical behaviour of chromium in molten chlorides. *Journal of Electroanalytical Chemistry*, 493(1), 1-14.
- Mathews, A. L., Baes Jr., C. F. (1968) "Oxide chemistry and thermodynamics of molten LiF-BeF₂ solutions," *Inorganic Chemistry* 7 (2), 373-382.
- Mayes, R. T., Kurley III, J. M., Halstenberg, P. W., McAlister, A., Sulejmanovic, D., Raiman, S. S., Dai, S. Pint, B. A. (2018) "Purification of Chloride Salts for Concentrated Solar Power Applications." ORNL Report ORNL LTR-2018/1052, Oak Ridge, TN.
- McCoy, H. E., Beatty, R. L., Cook, W. H., Gehlbach, R. E., Kennedy, C. R., Koger, J. W., Litman, A. P., Sessions, C. E., Weir, J. R. (1970) "New developments in materials for molten-salt reactors," *Nuclear Applications & Technology* 8, 156-169.
- McCoy, H. E., McNabb, B. (1972a) "Intergranular Cracking of INOR-8 in the MSRE," ORNL Report ORNL-4829, Oak Ridge, TN.
- McCoy, H. E., and B. McNabb, B. (1972b) "Post-irradiation Examination of Materials from the MSRE," ORNL Report ORNL-TM--4174, 4468053, Oak Ridge, TN, doi:10.2172/4468053.
- McCoy, H. E. (1978) "Status of materials development for molten salt reactors," ORNL report ORNL-TM-5920, Oak Ridge, TN. doi:10.2172/5195742.
- McDuffee, J. L., et al. (2018) "Evaluation of Flowing Salt Irradiation Facilities with High Neutron Flux," ORNL report ORNL/TM-2018/954, Oak Ridge, TN. doi:10.2172/1474548.
- Mehos, M.; Turchi, C.; Vidal, J.; Wagner, M.; Ma, Z.; Ho, C.; Kolb, W.; Andraka, C.; Kruiuzenga, A. (2017) *Concentrating Solar Power Gen3 Demonstration Roadmap*: Golden, CO.

- O'Hara, Matthew J., et al. (2017) "Decomposition of Diverse Solid Inorganic Matrices with Molten Ammonium Bifluoride Salt for Constituent Elemental Analysis." *Chemical Geology*, 466, 341–351. doi:10.1016/j.chemgeo.2017.06.023.
- Olander, D. (2002) "Redox condition in molten fluoride salts: Definition and control," *Journal of Nuclear Materials*, 300, 270-272.
- Olson, L.C. Ambrosek, J.W., Sridharan, K., Anderson, M.H., Allen, T.R. (2009) "Materials corrosion in molten LiF-NaF-KF salt," *Journal of Fluorine Chemistry*, 130, 67-73.
- Olson, L. C. (2009b) "Material corrosion in molten LiF-NaF-KF eutectic salt," Ph.D. dissertation, University of Wisconsin, Madison, WI.
- Olson, L. C., Fuentes, R. E., Martinez-Rodriguez, M. J., Ambrosek, J. W., Sridharan, K., Anderson, M. H., Garcia-Diaz, B. L., Gray, J., Allen, T. R. (2015) "Impact of Corrosion Test Container Material in Molten Fluorides." *Journal of Solar Energy Engineering*, 137, 061007, doi:10.1115/1.4031682.
- Park, J.-S., Nishimura, H., Hayasaka, D., Yu, J.-H., Kishimoto, H., Kohyama, A. (2016) "Fabrication of short SiC fiber reinforced SiC matrix composites with high fiber volume fraction," *Fusion Engineering and Design* 109-111, 1174-1178.
- Perez-Bergquist, A. G., Nozawa, T., Shih, C., Leonard, K. J., Snead, L. L. Katoh, Y. (2015) "High dose neutron irradiation of Hi-Nicalon Type S silicon carbide composites, Part 1: Microstructural evaluations," *Journal of Nuclear Materials* 462, 443-449.
- Petrik, N. G., et al. (2001) "Interfacial Energy Transfer during Gamma Radiolysis of Water on the Surface of ZrO₂ and Some Other Oxides." *The Journal of Physical Chemistry B*, 105, 5935–5944, doi:10.1021/jp004440o.
- Petti, D. A., Demkowicz, P. A. Maki, J. T., Hobbins, R. R. (2012) "TRISO-Coated Particle Fuel Performance," in: R.J.M. Konings (Ed.), *Comprehensive Nuclear Materials*, Elsevier, Oxford, pp. 151-213.
- Pint, B. A., McMurray, J. W., Willoughby, A. W., Kurley, J. M., Pearson, S. R., Lance, M. J., . . . Mayes, R. T. (2019). Re-establishing the paradigm for evaluating halide salt compatibility to study commercial chloride salts at 600°C–800°C. *Materials and Corrosion* 70, 1439-1449.
- Punwani, D., Chi, C. W., Wasan, D. T. (1968) "Dynamic sorption by hygroscopic salts," *I&EC Process Design and Development* 7(3), 410-415.
- Qiu, J., Zou, Y., Yu, G., Liu, H., Jia, Y., Li, Z., Huai, P., Zhou, X., Xu, H. (2014) "Compatibility of container materials with Cr in molten FLiNaK salt," *J. Fluor. Chem.*, 168, 69–74.
- Qualls, A. L., et al. (2017) "Preconceptual Design of a Fluoride High Temperature Salt-Cooled Engineering Demonstration Reactor: Motivation and Overview," *Annals of Nuclear Energy* 107, 144-155. doi:10.1016/j.anucene.2016.11.021.
- Raiman, S. S., Lee, S. (2018) "Aggregation and Data Analysis of Corrosion Studies in Molten Chloride and Fluoride Salts." *Journal of Nuclear Materials*, 511, 523–535. doi:10.1016/J.JNUCMAT.2018.07.036.
- Raiman, S. S., et al. (2019) "Amorphous and Partially-Amorphous Metal Coatings for Corrosion Resistance in Molten Chloride Salt." *Solar Energy Materials and Solar Cells*, 201, 110028, doi:10.1016/j.solmat.2019.110028.
- Rhodes, P. R. (1969) "Mechanism of Chloride Environmentally Assisted Cracking of Austenitic Stainless Steels," *Corrosion* 25(11), 462-472.

- Robinson, M. T. (1958a). On the Chemistry of the Fission Process in Reactor Fuels Containing UF₄ and UO₂. *Nuclear Science and Engineering*, 4, 263-269.
- Robinson, M. T., Brooksbank Jr., W. A., Reynolds, S. A., Wright, H. W., Handley, T. H. (1958b) "The Behavior of Fission Products in Molten Fluoride Reactor Fuels," *Nuclear Science and Engineering*, 4, 288-296. DOI: 10.13182/NSE58-A25529.
- Rosenthal, M. W., et al. (1969) "Molten-Salt Reactor Program Semiannual Progress Report for Period Ending February 28, 1969. ORNL report ORNL-4396, Oak Ridge, TN, p. 331.
- Rosenthal, M. W., et al. (1970a) "Molten-Salt Reactor Program Semiannual Progress Report for Period Ending February 28, 1970." ORNL report ORNL-4548, Oak Ridge, TN, p. 364.
- Rosenthal, M. W., Kasten, P. R. and Briggs, R. B. (1970b) "Molten-Salt Reactors—History, Status, and Potential," *Nuclear Applications and Technology*, 8:2, 107-117, DOI:10.13182/NT70-A28619.
- Rosenthal, R. W., Briggs, R. B., Haubenreich, P. N. (1971) "Molten-Salt Reactor Program Semiannual Progress Report," ORNL Report ORNL-4676, Oak Ridge, TN.
- Rosenthal, M. W., et al. (1972) "The Development Status of Molten-Salt Breeder Reactors," ORNL report ORNL-4812, Oak Ridge, TN, p. 434.
- Sabharwall, P., et al., (2010) "Molten Salts for High Temperature Reactors: University of Wisconsin Molten Salt Corrosion and Flow Loop Experiments – Issues Identified and Path Forward," INL Report INL/EXT-10-18090.
- Sauder, C. (2015) "Ceramic Matrix Composites: Nuclear Applications," in *Ceramic Matrix Composites: Materials, Modeling and Technology*, N. P. Bansal and J. Lamon, ed., Wiley, New York, pp. 609-646.
- Savage, H. C., et al. (1967) "Operation of Molten Salt Convection Loops In The ORR," ORNL Report ORNL-TM-1960, Oak Ridge, TN.
- Scarlat, R. O., Peterson, P. F. (2014) "The Current Status of Fluoride Salt Cooled High Temperature Reactor (FHR) Technology and Its Overlap with HIF Target Chamber Concepts." *Nuclear Instruments and Methods in Physics Research Section A: Accelerators, Spectrometers, Detectors and Associated Equipment*, 733, 57–64, doi:10.1016/J.NIMA.2013.05.094.
- Scott, D., Eatherly, W. P. (1969) "Graphite and xenon behavior and their influence on molten-salt reactor design," *Nuclear Applications & Technology* 8, 179-189.
- Sellers, R. S., Cheng, W.-J., Kelleher, B. C., Anderson, M. H., Sridharan, K., Wang, C.-J., Allen, T. R. (2014) "Corrosion of 316L stainless steel alloy and Hastelloy-N superalloy in molten eutectic LiF-NaF-KF salt and interaction with graphite," *Nuclear Technology* 188, 192-199.
- Serp, J., Allibert, M., Beneš, O., Delpech, S., Feynberg, O., Ghetta, V., . . . Zhimin, D. (2014). The molten salt reactor (MSR) in generation IV: Overview and perspectives. *Progress in Nuclear Energy*, 77, 308-319.
- Shaffer, J. H. (1971) "Preparation and Handling of Salt Mixtures for the Molten Salt Reactor Experiment," ORNL report ORNL-4616, Oak Ridge, TN. doi:10.2172/4074869.
- Scheele, R. D., Casella, A. M. (2010) "Assessment of the Use of Nitrogen Trifluoride for Purifying Coolant and Heat Transfer Salts in the Fluoride Salt-Cooled High-Temperature Reactor," PNNL Report PNNL-19793. doi:10.2172/1017120.
- Sheil, B. J., Evans, R. B. (1959) "Molten Salt-Graphite Compatibility Test. Results of Physical and Chemical Measurements," ORNL Report CF-59-8-133, Oak Ridge, TN. www.osti.gov/servlets/purl/4098729.

- Shiozawa, S., Fujikawa, S., Iyoku, T., Kunitomi, K., Tachibana, Y. (2004) "Overview of HTTR design features," *Nuclear Engineering and Design* 233, 11-21.
- Sisman, O., et al. (1957) "A Fluoride Fuel In-Pile Loop Experiment," ORNL report ORNL-1965, Oak Ridge, TN.
- Sizmann, R. (1978) "The Effect of Radiation upon Diffusion in Metals," *Journal of Nuclear Materials* 69–70, 386–412. doi: 10.1016/0022-3115(78)90256-8.
- Smyrl, W. H., Blackburn, M. J. (1975) "Environmentally assisted cracking of Ti-8Al-1Mo-1 V in Molten Salts," *Corrosion* 31(10), 370-375.
- Snead, L. L., Burchell, T. D., Katoh, Y. (2008) "Swelling of nuclear graphite and high quality carbon fiber composite under very high irradiation temperature," *Journal of Nuclear Materials* 381, 55-61.
- Sohal, M.S., Ebner, M.A., Sabharwall, P., Sharpe, P. (2010) "Engineering database of liquid salt thermophysical and thermochemical properties," INL report INL/EXT-10-18297.
- Song, J., Y. Zhao, X. He, B. Zhang, L. Xu, Z. He, D. Zhang, L. Gao, H. Xia, X. Zhou, P. Huai, S. Bai, (2015) "Preparation of pyrolytic carbon coating on graphite for inhibiting liquid fluoride salt and Xe135 penetration for molten salt breeder reactor," *J. Nucl. Mater.* 456, 33-40.
- Sridharan, K. Allen, T. R. R., (2013) *Corrosion in Molten Salts*. Elsevier Inc..
- Stempien, J. D., Ballinger, R. G., Forsberg, C. W. (2016) "An integrated model of tritium transport and corrosion in Fluoride Salt-Cooled High-Temperature Reactors (FHRs) – Part I: Theory and benchmarking," *Nuclear Engineering and Design* 310, 258-272.
- Suski, L. (1991). 4 - Corrosion in Molten Salts—A Thermodynamic Approach. In J. Flis (Ed.), *Materials Science Monographs* (Vol. 59, pp. 124-151): Elsevier, Oxford, UK.
- Susskind, H., et al., (1960) "Corrosion studies for a fused salt-liquid metal extraction process for the liquid metal fuel reactor," BNL report BNL 585 (T-146), Upton, NY. doi:10.2172/4023508.
- Tandon, L. (2000) "Radiolysis of Salts and Long-Term Storage Issues for Both Pure and Impure PuO₂ Materials in Plutonium Storage Containers," LANL Report LA-13725-MS, Los Alamos, NM.
- Tang, H, et al. (2017) Infiltration of Graphite by Molten 2LiF–BeF₂ Salt," *Journal of Materials Science* 52, 11346–11359. doi:10.1007/s10853-017-1310-4.
- Thoma, R. E. (1971) "Chemical Aspects of MSRE Operations," ORNL Report ORNL-4658, Oak Ridge, TN. doi:10.2172/4675946.
- Toth, L. M., Gilpatrick, L. O. (1973) "Temperature and solvent effects on the equilibrium of dilute uranium trifluoride solutions contained in graphite," *J. Phys. Chem.* 77, 2799–2803.
- Trauger, D. B., and J. A. Conlin, J. A. (1961) "Circulating Fused-Salt Fuel Irradiation Test Loop," *Nuclear Science and Engineering*, 9, 346-356. doi:10.13182/NSE61-A25886.
- Tylka, M. M., et al. (2015a) "Application of Voltammetry for Quantitative Analysis of Actinides in Molten Salts." *Journal of The Electrochemical Society*, vol. 162, no. 12, pp. H852–59. doi:[10.1149/2.0281512jes](https://doi.org/10.1149/2.0281512jes).
- Tylka, M. M., et al. (2015b) "Method Development for Quantitative Analysis of Actinides in Molten Salts." *Journal of The Electrochemical Society*, vol. 162, no. 9, pp. H625–33. doi:[10.1149/2.0401509jes](https://doi.org/10.1149/2.0401509jes).
- Vignarooban, K., P. Pugazhendhi, C. Tucker, D. Gervasio, and A. M. M. Kannan, (2014) "Corrosion resistance of Hastelloys in molten metal-chloride heat-transfer fluids for concentrating solar power applications," *Sol. Energy*, 103, 62–69.

- Vignarooban, K.; Xu, X. H.; Arvay, A.; Hsu, K.; Kannan, A. M. (2015) "Heat transfer fluids for concentrating solar power systems - A review.," *Appl. Energy* 146, 383-396.
- Vignarooban, K., et al., (2015) "Vapor pressure and corrosivity of ternary metal-chloride molten-salt based heat transfer fluids for use in concentrating solar power systems," *Appl. Energy*, 159, 206–213.
- Wang, H., Feng, Q., Wang, Z., Zhou, H., Kan, Y., Hu, J., Dong, S. (2017a) "Microstructure evolution and high-temperature mechanical properties of SiCf/SiC composites in liquid fluoride salt environment," *Corrosion Science* 124, 131-137.
- Wang, H., Feng, Q., Wang, Z., Zhou, H., Kan, Y., Hu, J., Dong, S. (2017b) "The corrosion behavior of CVI SiC matrix in SiCf/SiC composites under molten fluoride salt environment," *Journal of Nuclear Materials* 487, 43-49
- Wen, K., Marrow, J., Marsden, B. (2008) "Microcracks in nuclear graphite and highly oriented pyrolytic graphite (HOPG)," *Journal of Nuclear Materials* 381, 199-203.
- White, S.H. (1983) "Halides," D.G. Lovering and R.J. Gale, editors, *Molten Salt Techniques*, Vol 1, Chapter 2, Plenum Press, New York, 1983.
- Williams, D.F., Toth, L.M., Clarno, K.T., (2006) "Assessment of Candidate Molten Salt Coolants for the Advanced High-Temperature Reactor (AHTR)," ORNL Report ORNL/TM-2006/12, Oak Ridge, TN.
- Williams, D. F., Clarno, K. T. (2008) "Evaluation of Salt Coolants for Reactor Applications," *Nuclear Technology*, 163:3, 330-343, DOI: 10.13182/NT08-A3992
- Wu, Z., Lin, D., Zhong, D. (2002) "The design features of the HTR-10," *Nuclear Engineering and Design* 218, 25-32.
- Wu, B., Li, Y., Zhao, H.-S., Liu, S., Liu, B., Wang, J.-H. (2018) "Wear behavior of graphitic matrix of fuel elements used in pebble-bed high-temperature gas-cooled reactors against steel," *Nuclear Engineering and Design* 328, 353-358.
- Xi, J., Jiang, H., Liu, C., Morgan, D., Szlufarska, I. (2019) "Corrosion of Si, C, and SiC in molten salt," *Corrosion Science* 146, 1-9.
- Xue, W., Yang, X., Qiu, J., Liu, H., Zhao, B., Xia, H., Zhou, X., Huai, P., Liu, H., Wang, J. (2017) "Effects of Cr^{3+} on the corrosion of SiC in LiF–NaF–KF molten salt," *Corrosion Science* 114, 96-101.
- Xue, W., Yang, X., Zhou, X., Liu, H., Han, L., Zhang, X., Wang, J. (2018) "Effect of concentration of Cr^{3+} in LiF–NaF–KF salt on the corrosion of SiC," *Journal of Nuclear Materials* 509, 527-531.
- Yaita, Y., O'hira, S., Okuno, K. (1995) "Study of Tritium Retention in Graphite by Simulating First Wall Circumstances," *Fusion Technology* 28, 1294-1298.
- Yang, X., Feng, S., Zhou, X., Xu, H., Sham, T. K. (2012) "Interaction between nuclear graphite and molten fluoride salts: a synchrotron radiation study of the substitution of graphitic hydrogen by fluoride ion," *J. Phys. Chem. A*, 116, 985-989.
- Yang, X., Liu, M., Gao, Y., Zhang, D., Feng, S., Liu, H., Yu, G., Wu, G., Wang, M., Zhou, X., Xia, H., Huai, P., Sham, T. K., Wang, J., Guo, J. (2016a) "Effect of oxygen on the corrosion of SiC in LiF–NaF–KF molten salt," *Corrosion Science* 103, 165-172.
- Yang, X., Zhang, D., Liu, M., Feng, S., Xue, W., Liu, H., Yu, G., Zhou, X., Xia, H., Huai, P., Li, Z., Lu, Y., Zhou, H., Dong, S. (2016b) "Corrosion of SiC induced by Hastelloy N alloy and its corrosion products in LiF–NaF–KF molten salt," *Corrosion Science* 109, 62-67.
- Young, J. P. (1967) "Spectra of uranium(IV) and uranium(III) in molten fluoride solvents," *Inorg. Chem.* 6, 1486–1488.

- Zaykov, Y. P., Isakov, A. V., Zakiryanova, I. D., Reznitskikh, O. G., Chemezov, O. V., Redkin, A. A. (2014) "Interaction between SiO₂ and a KF-KCl-K₂SiF₆ Melt," *Journal of Physical Chemistry B* 118, 1584-1588.
- Zhang, J. (2014) "Electrochemistry of Actinides and Fission Products in Molten Salts -Data Review." *Journal of Nuclear Materials*, 447, 271–284. doi:10.1016/j.jnucmat.2013.12.017.
- Zhang, W.-T., B.-L. Zhang, J.-L. Song, W. Qi, X.-J. He, Z.-J. Liu, P.-F. Lian, Z.-T. He, L.-N. Gao, H.-H. Xia, X.-D. Liu, X.-T. Zhou, L.-B. Sun, X.-X. Wu, (2016) "Microstructure and molten salt impregnation characteristics of a micro-fine grain graphite for use in molten salt reactors," *New Carbon Materials* 31(6) (2016) 585-593.
- Zhang, C., Wallace, J., & Simpson, M. F. (2018a). Electrochemical measurement of high concentrations of UCl₃ and GdCl₃ in molten LiCl-KCl eutectic," *Electrochimica Acta*, 290, 429-439.
- Zhang, J., Forsberg, C. W., Simpson, M. F., Guo, S., Lam, S. T., Scarlat, R. O., . . . Keiser, J. R. (2018b). Redox potential control in molten salt systems for corrosion mitigation. *Corrosion Science*, 144, 44-53.
- Zheng, G., L. He, D. Carpenter, and K. Sridharan, (2016a) "Corrosion-induced microstructural developments in 316 stainless steel during exposure to molten Li₂BeF₄ (FLiBe) salt," *J. Nucl. Mater.*, vol. 482, pp. 147–155, 2016.
- Zheng, G., et al. (2016b) "High Temperature Corrosion of Structural Alloys in Molten Li₂BeF₄ (FLiBe) Salt." *Advances in Materials Science for Environmental and Energy Technologies V: Ceramic Transactions*, John Wiley & Sons, Inc., pp. 93–101, doi:10.1002/9781119323624.ch9.
- Zhou, W., et al. (2020) "Proton Irradiation-Decelerated Intergranular Corrosion of Ni-Cr Alloys in Molten Salt," *Nature Communications* 11, 3430.
- Zou, C. Y., Cai, X. Z., Jiang, D. Z., Yu, C. G., Li, X. X., Ma, Y. W., Han, J. L., Chen, J. G. (2015) "Optimization of temperature coefficient and breeding ratio for a graphite-moderated molten salt reactor, *Nuclear Engineering and Design* 281, 114-120.
- Zou, C. Y., Cai, C. Z., Yu, C. G., Wu, J. H., Chen, J. G. (2018) "Transition to thorium fuel cycle for TMSR," *Nuclear Engineering and Design* 330, 420-428.